A New Efficient Formulation of the HLLEM Riemann Solver for General Conservative and Non-Conservative Hyperbolic Systems

Michael Dumbser*[a], Dinshaw S. Balsara[b]

[a] *Laboratory of Applied Mathematics, Department of Civil, Environmental and Mechanical Engineering University of Trento, Via Mesiano 77, I-38123 Trento, Italy*
[b] *Physics Department, University of Notre Dame du Lac, 225 Nieuwland Science Hall, Notre Dame, IN 46556, USA*

Abstract

In this paper a new, *simple* and *universal* formulation of the HLLEM Riemann solver (RS) is proposed that works for general conservative and non-conservative systems of hyperbolic equations. For non-conservative PDE, a path-conservative formulation of the HLLEM RS is presented for the first time in this paper. The HLLEM Riemann solver is built on top of a novel and very robust path-conservative HLL method. It thus naturally inherits the positivity properties and the entropy enforcement of the underlying HLL scheme. However, with just the slight additional cost of evaluating eigenvectors and eigenvalues of intermediate characteristic fields, we can represent linearly degenerate intermediate waves with a minimum of smearing.

For conservative systems, our paper provides the easiest and most seamless path for taking a pre-existing HLL RS and quickly and effortlessly converting it to a RS that provides improved results, comparable with those of an HLLC, HLLD, Osher or Roe-type RS. This is done with minimal additional computational complexity, making our variant of the HLLEM RS also a very fast RS that can accurately represent linearly degenerate discontinuities. Our present HLLEM RS also transparently extends these advantages to non-conservative systems. For shallow water-type systems, the resulting method is proven to be well-balanced.

Several test problems are presented for shallow water-type equations and two-phase flow models, as well as for gas dynamics with real equation of state, magnetohydrodynamics (MHD & RMHD), and nonlinear elasticity.

Since our new formulation accommodates multiple intermediate waves and has a broader applicability than the original HLLEM method, it could alternatively be called the HLLI Riemann solver, where the "I" stands for the intermediate characteristic fields that can be accounted for.

Keywords: path-conservative HLLEM Riemann solver, resolution of linearly degenerate intermediate waves, conservation laws and general hyperbolic PDE with non-conservative terms, well-balanced scheme for single and two-layer shallow water equations, Euler equations with real equation of state and multiphase flows, RMHD/MHD equations and nonlinear elasticity

1. Introduction

Riemann solvers are an important building block of modern numerical schemes for hyperbolic systems. For hyperbolic systems in conservation form, a large number of Riemann solvers (RS) are available. For exact Riemann solvers, see Godunov [51] and van Leer [94]. Approximate RS based on the two-shock formulation are presented in Colella [29], Colella & Woodward [30], Chorin [28]. In [76] Roe presented a very popular Riemann solver that is based on a special linearization of the nonlinear system of governing PDE. It was later reformulated by Toumi in [93] using a weak integral form, which also allows for an extension to non-conservative hyperbolic systems and which can be seen as a predecessor of the family of path-conservative schemes introduced by Parés and Castro in the seminal papers [70] and [25]. Riemann solvers whose numerical dissipation term is based on a path integral in

*Corresponding author
Email addresses: michael.dumbser@unitn.it (Michael Dumbser*), dbalsara@nd.edu (Dinshaw S. Balsara)

phase space were first proposed by Osher and Solomon in [69] and have been recently generalized by Dumbser & Toro to general nonlinear hyperbolic conservation laws and to non-conservative hyperbolic systems in [45, 44]. In this context, we also would like to point out the recent reformulation of the Osher-type solver [45] in the context of polynomial viscosity methods (PVM) [34] by Castro et al., see [24]. The HLL/HLLE/HLLEM/HLLC Riemann solver (Harten, Lax & van Leer [57], Einfeldt [46], Einfeldt et al. [47], Toro, Spruce and Speares [88], Batten et al. [16], Billett & Toro [19]) have gained considerable popularity owing to their simplicity. The local Lax-Friedrichs (LLF) method (Rusanov [78]) is even simpler, but often carries the penalty of a high level of numerical dissipation, as well as centered fluxes, like the FORCE method of Toro and Billet [91].

Out of all these methods, the HLLEM Riemann solver of Einfeldt [46] and Einfeldt et al. [47] has seen the least further development and extensions to more general nonlinear systems of conservation laws. Yet, it has some very desirable features that have gone unappreciated. Like HLLC, it can be built on top of an existing HLL Riemann solver, thereby ensuring that it has a positivity preserving property and that it is entropy enforcing. Only the intermediate eigenvalues and the associated left and right eigenvectors need to be evaluated in order to implement an HLLEM RS. Since these are usually easier to compute analytically, the HLLEM RS has the additional advantage over the Riemann solvers of Roe [76] and Osher [69, 45, 44] that it is *not* necessary to know the *entire* eigenstructure of the hyperbolic system. It nevertheless produces solutions that are competitive with Roe-type, Osher-type and HLLC/HLLD-type RS. It furthermore does not require an entropy fix, unlike the original Riemann solver of Roe [76]. A first goal of this paper is therefore to bring these features to the forefront by showing that the HLLEM RS accommodates very well to general nonlinear hyperbolic conservation laws, for example the MHD system or the Euler system of compressible gas dynamics with general equation of state (EOS), or the Godunov-Romenski model for nonlinear elasticity [52, 53, 54].

Extensive recent progress has been made on path-conservative methods for treating non-conservative hyperbolic systems, see for example the following list of references, which does not pretend to be complete: Parés et al. [70, 66], Castro et al. [25, 49, 23, 27, 21, 22], Morales de Luna et al. [32], Dumbser et al. [37, 40, 44]. The progress has been made within the context of the DLM theory for non-conservative systems (Dal Maso, LeFloch & Murat [63]). Therefore, when a conservation form exists, the family of path-conservative schemes reproduces well-known Riemann solvers like the Roe RS, HLL, HLLC, FORCE, GFORCE, Osher, and so on. However, the optimal choice of the path that needs to be defined in order to connect the two states of the RP is still to a certain extent ambiguous. Usually, the path is chosen in such a way that other important properties are ensured, like the well-balancedness of the scheme, see [25, 67]. For a detailed discussion of open problems related to path-conservative methods, see [26, 2]. However, most physical systems of interest, like shallow water-type systems and multiphase flow models, tend to be in quasi-conservative form, where the non-conservative terms act only on linearly degenerate fields. This fact makes the choice of a particular path less delicate.

The study of one-dimensional Riemann solvers for non-conservative hyperbolic systems has, by now, reached a high level of sophistication. Even so, to the best of our knowledge, the HLLEM RS has never been adapted to non-conservative systems. The second goal of this paper is therefore to show that the HLLEM scheme can be easily adapted to hyperbolic systems with non-conservative products. For shallow water-type equations, the HLLEM RS is also shown to be well-balanced, owing to the fact that it resolves the intermediate waves associated with the bottom jump exactly.

The rest of this paper is organized as follows: Section 2 presents the new formulation of the HLLEM scheme in similarity variables. Since all Riemann problems have a self-similar structure, we show the utility of similarity variables in formulating the one-dimensional HLLEM RS by following Balsara [9, 10, 11, 12], Balsara, Dumbser & Abgrall [14] and Balsara & Dumbser [13]. In Section 3 we present computational results for a large set of different conservative and non-conservative hyperbolic systems, in particular for the single and two-layer shallow water equations; the multi-phase debris flow model of Pitman and Le [72], the Baer-Nunziato model of compressible multi-phase flows [6], the Euler equations of compressible gas dynamics with ideal and real equation of state, the magnetohydrodynamics system (MHD & RMHD) and finally the nonlinear elasticity equations according to Godunov and Romenski [52]. Section 4 contains conclusions and an outlook to future developments. Several FORTRAN sample codes are given in the appendix, to show the simplicity of the proposed algorithm and to facilitate the practical implementation of the HLLEM Riemann solver.

For the reader who is only interested in the purely *conservative* case, an explicit expression of the HLLEM flux is given in Eqn. (30) of Section 2.3, together with a detailed FORTRAN sample code in Appendix C.

2. Self-similar formulation of the HLLEM Riemann solver for conservative and non-conservative systems

We consider nonlinear hyperbolic systems of the form

$$\frac{\partial \mathbf{Q}}{\partial t} + \frac{\partial \mathbf{f}}{\partial x} + \mathbf{B}(\mathbf{Q})\frac{\partial \mathbf{Q}}{\partial x} = 0, \qquad x \in \Omega \subset \mathbb{R}, \quad t \in \mathbb{R}_0^+, \tag{1}$$

where $\mathbf{Q} \in \Omega_q \subset \mathbb{R}^{n_q}$ is the state vector and Ω_q is the state-space or phase-space. The conservative part of the system is contained in the nonlinear flux vector $\mathbf{f} = \mathbf{f}(\mathbf{Q})$ and the non-conservative terms are grouped together in the non-conservative product $\mathbf{B}(\mathbf{Q})\frac{\partial \mathbf{Q}}{\partial x}$. The computational domain is denoted by $\Omega = [x_L, x_R]$. The above PDE can also be cast into the following alternative quasi-linear form,

$$\frac{\partial \mathbf{Q}}{\partial t} + \mathbf{A}(\mathbf{Q})\frac{\partial \mathbf{Q}}{\partial x} = 0, \tag{2}$$

where the matrix $\mathbf{A}(\mathbf{Q}) = \frac{\partial \mathbf{f}}{\partial \mathbf{Q}} + \mathbf{B}(\mathbf{Q})$ includes the Jacobian of the flux $\frac{\partial \mathbf{f}}{\partial \mathbf{Q}}$, as well as the genuinely non-conservative part of the system contained in $\mathbf{B}(\mathbf{Q})$. The system is hyperbolic if $\mathbf{A}(\mathbf{Q})$ has only real eigenvalues and if a full set of linearly independent eigenvectors exists. In the case $\mathbf{B}(\mathbf{Q}) = 0$, the PDE (1) reduces to a flux form and is hence called a system of conservation laws. In the following we will denote the matrix of eigenvalues of $\mathbf{A}(\mathbf{Q})$ with $\mathbf{\Lambda}(\mathbf{Q}) = \text{diag}\left(\lambda_1, \lambda_2, ..., \lambda_{n_q}\right)$, where the eigenvalues are ordered as $\lambda_1 \leq \lambda_2, ..., \leq \lambda_{n_q}$. The matrix of left eigenvectors of $\mathbf{A}(\mathbf{Q})$ associated with the eigenvalues will be denoted by $\mathbf{L}(\mathbf{Q}) = \left(\mathbf{l}_1^T, \mathbf{l}_2^T, ..., \mathbf{l}_{n_q}^T\right)^T$ and the matrix of right eigenvectors of $\mathbf{A}(\mathbf{Q})$ with $\mathbf{R}(\mathbf{Q}) = \left(\mathbf{r}_1, \mathbf{r}_2, ..., \mathbf{r}_{n_q}\right)$. We furthermore assume that the left and right eigenvectors are orthonormal, i.e. $\mathbf{L} \cdot \mathbf{R} = \mathbf{I}$, where $\mathbf{I}$ is the identity matrix. When the system (1) is hyperbolic, the matrix $\mathbf{A}(\mathbf{Q})$ can be diagonalized, hence $\mathbf{A}(\mathbf{Q}) = \mathbf{R}(\mathbf{Q})\,\mathbf{\Lambda}(\mathbf{Q})\,\mathbf{L}(\mathbf{Q})$. In the following two sections we will extend the HLLEM-type Riemann solver [46, 47] to general hyperbolic systems with non-conservative products of the type (1). For that purpose, we will make use of the self-similarity of the solution of the Riemann problem and subsequently will derive the scheme based on similarity variables. This follows the ideas of Balsara [11] for the construction of genuinely multi-dimensional Riemann solvers using similarity variables in the conservative case. In other words, the similarity variable becomes a single variable that parametrizes the evolution of the resolved state of the RS. We further show that for $\mathbf{B}(\mathbf{Q}) = 0$, the conservative HLL/HLLEM Riemann solvers are retrieved. We first start with a derivation of a path-conservative HLL scheme in similarity variables.

2.1. Derivation of path-conservative HLL schemes in similarity variables

Using the classical similarity variable of the Riemann problem $\xi = x/t$ and assuming thus that $\mathbf{Q}(x,t) = \mathbf{Q}(\xi)$, the system (1) can be rewritten as

$$-\xi\frac{\partial \mathbf{Q}}{\partial \xi} + \frac{\partial \mathbf{f}}{\partial \xi} + \mathbf{B}(\mathbf{Q})\frac{\partial \mathbf{Q}}{\partial \xi} = 0, \tag{3}$$

or, equivalently, as

$$\mathbf{Q} - \frac{\partial(\xi\mathbf{Q})}{\partial \xi} + \frac{\partial \mathbf{f}}{\partial \xi} + \mathbf{B}(\mathbf{Q})\frac{\partial \mathbf{Q}}{\partial \xi} = 0. \tag{4}$$

The solution strategy for the HLL class of Riemann solvers consists of first finding the constant, resolved state $\mathbf{Q}_*$ that lies between the left state $\mathbf{Q}_L$ and the right state $\mathbf{Q}_R$. We focus on that task in the next paragraph. The resolved state propagates into the left and right states with speeds $s_L \leq 0$ and $s_R \geq 0$. However, entropy enforcement might call for further expansion of the Riemann fan consistent with the physics of the hyperbolic system; see [46, 47]. The speeds s_L and s_R with the constant intermediate state $\mathbf{Q}_*$ constitute a self-similarly evolving wave model for the one-dimensional HLL Riemann solver, where the exact solution of the original Riemann problem has been significantly simplified. In the HLL method, the entire wave structure of the Riemann problem is only approximated by the two fastest outward-moving waves and one single intermediate state. In this paper, we choose the following simple wave speed estimates for s_L and s_R:

$$s_L = \min\left(0, \mathbf{\Lambda}(\mathbf{Q}_L), \mathbf{\Lambda}(\bar{\mathbf{Q}})\right), \qquad s_R = \max\left(0, \mathbf{\Lambda}(\mathbf{Q}_R), \mathbf{\Lambda}(\bar{\mathbf{Q}})\right), \tag{5}$$

with the intermediate state $\bar{\mathbf{Q}}$ simply being the arithmetic average $\bar{\mathbf{Q}} = \frac{1}{2}(\mathbf{Q}_L + \mathbf{Q}_R)$. One could also use the Roe-average for $\bar{\mathbf{Q}}$, as suggested in [46, 47]. The approximate solution of the Riemann problem is therefore given by

$$\mathbf{Q}(\xi) = \begin{cases} \mathbf{Q}_L, & \text{if} \quad \xi \leq s_L, \\ \mathbf{Q}_*, & \text{if} \quad s_L < \xi < s_R, \\ \mathbf{Q}_R, & \text{if} \quad \xi \geq s_R. \end{cases} \tag{6}$$

As a consequence, the jumps in the states that occur at the two extremal speeds s_L and s_R will lead to Borel measures in the non-conservative product contained in (4). Integrating (4) over $\xi \in [s_L, s_R]$ yields

$$\int_{s_L}^{s_R} \left(\mathbf{Q}(\xi) - \frac{\partial(\xi \mathbf{Q})}{\partial \xi} \right) d\xi + \int_{s_L}^{s_R} \left(\frac{\partial \mathbf{f}}{\partial \xi} + \mathbf{B}(\mathbf{Q}) \frac{\partial \mathbf{Q}}{\partial \xi} \right) d\xi = 0. \tag{7}$$

Using (6), one obtains the condition

$$\mathbf{Q}_* \left(s_R - s_L \right) - \left(\mathbf{Q}_R s_R - \mathbf{Q}_L s_L \right) + \left(\mathbf{f}_R - \mathbf{f}_L \right) + \int_{\mathbf{Q}_L}^{\mathbf{Q}_R} \mathbf{B}(\mathbf{Q}) \, d\mathbf{Q} = 0, \tag{8}$$

with $\mathbf{f}_L = \mathbf{f}(\mathbf{Q}_L)$ and $\mathbf{f}_R = \mathbf{f}(\mathbf{Q}_R)$. Eqn. (8) is the particular case of a path-conservative approximate Riemann solver based on only two waves, while a more general definition for path-conservative approximate Riemann solvers that admit a more general wave structure has been detailed in [70] and [22]. In principle, we could use the above expression to compute the resolved state $\mathbf{Q}_*$ directly, if the path-integral is assumed to be only a function of the left and right states $\mathbf{Q}_L$ and $\mathbf{Q}_R$. However, note that the path from $\mathbf{Q}_L$ to $\mathbf{Q}_R$ should also pass through $\mathbf{Q}_*$, to be consistent with the assumed structure of the approximate solution of the Riemann problem (6), hence we have

$$\int_{\mathbf{Q}_L}^{\mathbf{Q}_R} \mathbf{B}(\mathbf{Q}) \, d\mathbf{Q} = \int_{\mathbf{Q}_L}^{\mathbf{Q}_*} \mathbf{B}(\mathbf{Q}) \, d\mathbf{Q} + \int_{\mathbf{Q}_*}^{\mathbf{Q}_R} \mathbf{B}(\mathbf{Q}) \, d\mathbf{Q} = \int_0^1 \mathbf{B}\left(\psi(\mathbf{Q}_L, \mathbf{Q}_*, s) \right) \frac{\partial \psi}{\partial s} \, ds + \int_0^1 \mathbf{B}\left(\psi(\mathbf{Q}_*, \mathbf{Q}_R, s) \right) \frac{\partial \psi}{\partial s} \, ds, \tag{9}$$

so that the above equation (8) with (9) actually describes an *implicit* relation for $\mathbf{Q}_*$, similar to what one would also have for the Godunov method based on the exact Riemann solver or based on a two-shock approximate state Riemann solver, see [90] for more details. However, we would like to point out that relations (8) and (9) can not yet be interpreted as a two-shock approximate state Riemann solver, since the bounding wave speeds s_L and s_R are *a priori* fixed, while the true wave speeds in the two-shock approximate state Riemann solver also depend on $\mathbf{Q}_*$, see [90].

In (9) the path $\psi(\mathbf{Q}_a, \mathbf{Q}_b, s)$ between two generic states $\mathbf{Q}_a$ and $\mathbf{Q}_b$ is a Lipschitz continuous function that satisfies $\psi(\mathbf{Q}_a, \mathbf{Q}_b, 0) = \mathbf{Q}_a$ and $\psi(\mathbf{Q}_a, \mathbf{Q}_b, 1) = \mathbf{Q}_b$ The present scheme is to some extent *different* from existing path-conservative HLL and Lax-Friedrichs-type methods, see e.g. [79, 20, 27], where the path has usually been prescribed *a priori* as a given function of $\mathbf{Q}_L$ and $\mathbf{Q}_R$, i.e. in the form $\psi(\mathbf{Q}_L, \mathbf{Q}_R, s)$, without taking into account $\mathbf{Q}_*$. In the method proposed here, the PDE system has a certain influence on the choice of the path via the implicit relations (8) and (9). This means that the present path-conservative HLL Riemann solver incorporates the property of an iterative computation of $\mathbf{Q}_*$ from the Godunov method with two-shock approximate state Riemann solver, but with signal speeds s_L and s_R that have been fixed *a priori*. In the rest of this paper, we will now assume a piecewise linear segment path from $\mathbf{Q}_L$ to $\mathbf{Q}_*$ and from $\mathbf{Q}_*$ to $\mathbf{Q}_R$. More precisely, we choose the straight line segment between two arbitrary states $\mathbf{Q}_a$ and $\mathbf{Q}_b$ as

$$\psi(\mathbf{Q}_a, \mathbf{Q}_b, s) = \mathbf{Q}_a + (\mathbf{Q}_b - \mathbf{Q}_a) \, s, \qquad \text{with} \qquad 0 \leq s \leq 1, \tag{10}$$

hence obtaining

$$\int_{\mathbf{Q}_L}^{\mathbf{Q}_R} \mathbf{B}(\mathbf{Q}) \, d\mathbf{Q} = \left(\int_0^1 \mathbf{B}\left(\psi(\mathbf{Q}_L, \mathbf{Q}_*, s) \right) \, ds \right) (\mathbf{Q}_* - \mathbf{Q}_L) + \left(\int_0^1 \mathbf{B}\left(\psi(\mathbf{Q}_*, \mathbf{Q}_R, s) \right) \, ds \right) (\mathbf{Q}_R - \mathbf{Q}_*) \, . \tag{11}$$

If a Roe-type linearization is available we can write the previous equation more compactly as

$$\int_{\mathbf{Q}_L}^{\mathbf{Q}_R} \mathbf{B}(\mathbf{Q})\, d\mathbf{Q} = \tilde{\mathbf{B}}\left(\mathbf{Q}_L, \mathbf{Q}_*\right)\left(\mathbf{Q}_* - \mathbf{Q}_L\right) + \tilde{\mathbf{B}}\left(\mathbf{Q}_*, \mathbf{Q}_R\right)\left(\mathbf{Q}_R - \mathbf{Q}_*\right). \tag{12}$$

For proper Roe linearizations in the context of path-conservative schemes, see [70, 25, 93]. Here, we compute the matrix $\tilde{\mathbf{B}}$ directly based on the path-integral as

$$\tilde{\mathbf{B}}\left(\mathbf{Q}_a, \mathbf{Q}_b\right) = \int_0^1 \mathbf{B}\left(\psi(\mathbf{Q}_a, \mathbf{Q}_b, s)\right)\, ds. \tag{13}$$

If a Roe linearization is not available for a particular hyperbolic system under consideration, the matrix $\tilde{\mathbf{B}}$ can be simply evaluated numerically using Gaussian quadrature of appropriate order, see for example [40, 44]. The final equation for the intermediate HLL state $\mathbf{Q}_*$ reads

$$\mathbf{Q}_* = \frac{1}{(s_R - s_L)}\left[\left(\mathbf{Q}_R s_R - \mathbf{Q}_L s_L\right) - \left(\mathbf{f}_R - \mathbf{f}_L\right) - \left(\tilde{\mathbf{B}}\left(\mathbf{Q}_L, \mathbf{Q}_*\right)\left(\mathbf{Q}_* - \mathbf{Q}_L\right) + \tilde{\mathbf{B}}\left(\mathbf{Q}_*, \mathbf{Q}_R\right)\left(\mathbf{Q}_R - \mathbf{Q}_*\right)\right)\right]. \tag{14}$$

The above equation is in general non-linear in terms of $\mathbf{Q}_*$ and needs to be iterated to convergence. Fortunately, practical experience shows that the convergence is very rapid. An excellent initial guess for $\mathbf{Q}_*$, denoted by $\mathbf{Q}_*^0$, is provided by approximating the path from $\mathbf{Q}_L$ to $\mathbf{Q}_R$ via only one straight segment, as in a classical path-conservative HLL scheme:

$$\mathbf{Q}_*^0 = \frac{1}{(s_R - s_L)}\left[\left(\mathbf{Q}_R s_R - \mathbf{Q}_L s_L\right) - \left(\mathbf{f}_R - \mathbf{f}_L\right) - \tilde{\mathbf{B}}\left(\mathbf{Q}_L, \mathbf{Q}_R\right)\left(\mathbf{Q}_R - \mathbf{Q}_L\right)\right]. \tag{15}$$

Note that for practical calculations, the simple choice $\mathbf{Q}_* = \mathbf{Q}_*^0$ without any further iteration of the implicit equation (14) and keeping the simple segment path $\psi(\mathbf{Q}_L, \mathbf{Q}_R)$ to connect the left and the right state is indeed possible and leads to a classical path-conservative HLL scheme.

A first and very simple iterative scheme for computing $\mathbf{Q}_*$ can be obtained by using the initial guess (15) and then

$$\mathbf{Q}_*^{r+1} = \frac{1}{(s_R - s_L)}\left[\left(\mathbf{Q}_R s_R - \mathbf{Q}_L s_L\right) - \left(\mathbf{f}_R - \mathbf{f}_L\right) - \left(\tilde{\mathbf{B}}\left(\mathbf{Q}_L, \mathbf{Q}_*\right)\left(\mathbf{Q}_*^r - \mathbf{Q}_L\right) + \tilde{\mathbf{B}}\left(\mathbf{Q}_*, \mathbf{Q}_R\right)\left(\mathbf{Q}_R - \mathbf{Q}_*^r\right)\right)\right]. \tag{16}$$

A second alternative is the following quasi-Newton-type iterative scheme, where the nonlinear function of which we seek the roots is given by

$$\mathbf{g}(\mathbf{Q}_*) = \mathbf{Q}_* - \frac{\left(\mathbf{Q}_R s_R - \mathbf{Q}_L s_L\right) - \left(\mathbf{f}_R - \mathbf{f}_L\right) - \left(\tilde{\mathbf{B}}\left(\mathbf{Q}_L, \mathbf{Q}_*\right)\left(\mathbf{Q}_* - \mathbf{Q}_L\right) + \tilde{\mathbf{B}}\left(\mathbf{Q}_*, \mathbf{Q}_R\right)\left(\mathbf{Q}_R - \mathbf{Q}_*\right)\right)}{(s_R - s_L)} = 0. \tag{17}$$

To keep the RS as simple as possible one can choose to ignore the derivatives of the Roe matrices $\tilde{\mathbf{B}}$ with respect to $\mathbf{Q}_*$. The iteration can then be expressed as

$$\left(\mathbf{I} + \frac{\tilde{\mathbf{B}}\left(\mathbf{Q}_L, \mathbf{Q}_*\right) - \tilde{\mathbf{B}}\left(\mathbf{Q}_*, \mathbf{Q}_R\right)}{s_R - s_L}\right)\Delta\mathbf{Q}_*^r = \mathbf{g}(\mathbf{Q}_*^r), \tag{18}$$

$$\mathbf{Q}_*^{r+1} = \mathbf{Q}_*^r - \Delta\mathbf{Q}_*^r, \tag{19}$$

with the identity matrix $\mathbf{I}$. The reason for the fast convergence of both methods is that $s_R - s_L$ is larger than any of the eigenvalues of $\tilde{\mathbf{B}}\left(\mathbf{Q}_L, \mathbf{Q}_*\right)$ or $\tilde{\mathbf{B}}\left(\mathbf{Q}_*, \mathbf{Q}_R\right)$. Besides, observe that the Roe matrices inside the bracket in eqn. (18) have opposite signs, i.e. for close initial data $\mathbf{Q}_L$ and $\mathbf{Q}_R$, the left hand side of eqn. (18) approaches the identity matrix. Note that for a system in conservation form ($\mathbf{B}(\mathbf{Q}) = 0$), we directly retrieve the familiar form

$$\mathbf{Q}_* = \frac{\left(\mathbf{Q}_R s_R - \mathbf{Q}_L s_L\right) - \left(\mathbf{f}_R - \mathbf{f}_L\right)}{(s_R - s_L)}, \tag{20}$$

which is independent of the path ψ and hence does *not* need any iterations for the computation of $\mathbf{Q}_*$! The corresponding fluctuations of the path-conservative HLL scheme are easily obtained by integrating (4) over ξ in the intervals $[s_L, 0]$ and $[0, s_R]$, respectively:

$$\int_{s_L}^{0} \left(\mathbf{Q}(\xi) - \frac{\partial(\xi \mathbf{Q})}{\partial \xi} \right) d\xi + \overbrace{\int_{s_L}^{0} \left(\frac{\partial \mathbf{f}}{\partial \xi} + \mathbf{B}(\mathbf{Q}) \frac{\partial \mathbf{Q}}{\partial \xi} \right) d\xi}^{:=\mathbf{D}^-_{\mathrm{HLL}}(\mathbf{Q}_L, \mathbf{Q}_R)} = 0, \qquad \int_{0}^{s_R} \left(\mathbf{Q}(\xi) - \frac{\partial(\xi \mathbf{Q})}{\partial \xi} \right) d\xi + \overbrace{\int_{0}^{s_R} \left(\frac{\partial \mathbf{f}}{\partial \xi} + \mathbf{B}(\mathbf{Q}) \frac{\partial \mathbf{Q}}{\partial \xi} \right) d\xi}^{:=\mathbf{D}^+_{\mathrm{HLL}}(\mathbf{Q}_L, \mathbf{Q}_R)} = 0. \quad (21)$$

In Eqn. (21) above, the overbraced terms are the sought fluctuations for the HLL Riemann solver, while the non-overbraced terms are known quantities, since the HLL state $\mathbf{Q}_*$ is known from (14). Hence, we have the following relations to compute the fluctuations from the approximate solution of the Riemann problem $\mathbf{Q}(\xi)$, see Eqn. (6):

$$\int_{s_L}^{0} \left(\mathbf{Q}(\xi) - \frac{\partial(\xi \mathbf{Q})}{\partial \xi} \right) d\xi + \mathbf{D}^-_{\mathrm{HLL}}(\mathbf{Q}_L, \mathbf{Q}_R) = 0, \qquad \int_{0}^{s_R} \left(\mathbf{Q}(\xi) - \frac{\partial(\xi \mathbf{Q})}{\partial \xi} \right) d\xi + \mathbf{D}^+_{\mathrm{HLL}}(\mathbf{Q}_L, \mathbf{Q}_R) = 0. \quad (22)$$

Integrating (22) and inserting the HLL state $\mathbf{Q}_*$ from (14) yields then the final expressions for the HLL fluctuations:

$$\begin{aligned} \mathbf{D}^-_{\mathrm{HLL}}(\mathbf{Q}_L, \mathbf{Q}_R) &= -\frac{s_L}{s_R - s_L} \left[\mathbf{f}_R - \mathbf{f}_L + \tilde{\mathbf{B}}\left(\mathbf{Q}_L, \mathbf{Q}_*\right)(\mathbf{Q}_* - \mathbf{Q}_L) + \tilde{\mathbf{B}}\left(\mathbf{Q}_*, \mathbf{Q}_R\right)(\mathbf{Q}_R - \mathbf{Q}_*) \right] + \frac{s_L s_R}{s_R - s_L} (\mathbf{Q}_R - \mathbf{Q}_L), \\ \mathbf{D}^+_{\mathrm{HLL}}(\mathbf{Q}_L, \mathbf{Q}_R) &= +\frac{s_R}{s_R - s_L} \left[\mathbf{f}_R - \mathbf{f}_L + \tilde{\mathbf{B}}\left(\mathbf{Q}_L, \mathbf{Q}_*\right)(\mathbf{Q}_* - \mathbf{Q}_L) + \tilde{\mathbf{B}}\left(\mathbf{Q}_*, \mathbf{Q}_R\right)(\mathbf{Q}_R - \mathbf{Q}_*) \right] - \frac{s_L s_R}{s_R - s_L} (\mathbf{Q}_R - \mathbf{Q}_L). \end{aligned} \quad (23)$$

Note that the above fluctuations satisfy the consistency conditions

$$\mathbf{D}^- + \mathbf{D}^+ = \mathbf{f}_R - \mathbf{f}_L + \int_{\mathbf{Q}_L}^{\mathbf{Q}_R} \mathbf{B}(\mathbf{Q})\, d\mathbf{Q} = \int_{\mathbf{Q}_L}^{\mathbf{Q}_R} \mathbf{A}(\mathbf{Q})\, d\mathbf{Q} \qquad \text{and} \qquad \mathbf{D}^{\pm}(\mathbf{Q}, \mathbf{Q}) = 0. \quad (24)$$

In the case when (1) is a conservation law, i.e. when $\mathbf{B}(\mathbf{Q}) = 0$, the fluctuations $\mathbf{D}^-_{\mathrm{HLL}}(\mathbf{Q}_L, \mathbf{Q}_R)$ and $\mathbf{D}^+_{\mathrm{HLL}}(\mathbf{Q}_L, \mathbf{Q}_R)$ are related to the numerical flux $\mathbf{f}_{\mathrm{HLL}}(\mathbf{Q}_L, \mathbf{Q}_R)$ by

$$\mathbf{D}^-_{\mathrm{HLL}}(\mathbf{Q}_L, \mathbf{Q}_R) = \mathbf{f}_{\mathrm{HLL}}(\mathbf{Q}_L, \mathbf{Q}_R) - \mathbf{f}_L, \qquad \text{and} \qquad \mathbf{D}^+_{\mathrm{HLL}}(\mathbf{Q}_L, \mathbf{Q}_R) = \mathbf{f}_R - \mathbf{f}_{\mathrm{HLL}}(\mathbf{Q}_L, \mathbf{Q}_R). \quad (25)$$

2.2. Extension from HLL to HLLEM

We describe the extension of the previous HLL Riemann solver to the one-dimensional HLLEM Riemann solver in similarity variables next. Once the HLL state $\mathbf{Q}_*$ is obtained, the HLLEM Riemann solver consists of endowing the intermediate HLL state with a *linear variation*, see [46, 47]. The linear variation is designed to represent the effect of the intermediate waves of the hyperbolic system. In the original papers of Einfeldt et al., where the HLLEM scheme has been developed for the Euler equations in one space dimension, the intermediate wave was the linearly degenerate entropy wave that represents the physics of the contact discontinuity. In the more general setting considered in this paper, we will take into account all linear degenerate fields of the hyperbolic system (1) for which closed analytical expressions for the eigenvalues and eigenvectors are available. Let us in the following denote the matrix of eigenvalues associated with the n_i linearly degenerate intermediate characteristic fields with $\mathbf{\Lambda}_*(\mathbf{Q})$ and the associated matrices of left and right eigenvectors with $\mathbf{L}_*(\mathbf{Q})$ and $\mathbf{R}_*(\mathbf{Q})$, respectively. Please recall that usually one needs to retain substructure in the Riemann problem only for the linearly degenerate intermediate waves, in order to reduce the numerical dissipation exerted on the associated characteristic fields. Then, the linear variation of the inner state can be obtained by projecting the difference $\mathbf{Q}_R - \mathbf{Q}_L$ onto the right eigenvectors $\mathbf{R}_*(\bar{\mathbf{Q}})$ of an intermediate state $\bar{\mathbf{Q}}$ at the aid of the left eigenvectors $\mathbf{L}_*(\bar{\mathbf{Q}})$. In the following, we choose $\bar{\mathbf{Q}} = \frac{1}{2}(\mathbf{Q}_L + \mathbf{Q}_R)$, for simplicity. If exact expressions of Roe

averages are available, one should better use the Roe-averaged state for $\bar{\mathbf{Q}}$, as suggested in [46, 47]. The resulting linear approximation of the inner HLL state reads:

$$\mathbf{Q}(\xi) = \begin{cases} \mathbf{Q}_L, & \text{if} \quad \xi \le s_L, \\ \mathbf{Q}_* + \varphi \mathbf{R}_*(\bar{\mathbf{Q}})\, 2\boldsymbol{\delta}_*(\bar{\mathbf{Q}})\, \mathbf{L}_*(\bar{\mathbf{Q}}) \frac{\mathbf{Q}_R - \mathbf{Q}_L}{s_R - s_L} \left(\xi - \frac{1}{2}(s_L + s_R) \right), & \text{if} \quad s_L < \xi < s_R, \\ \mathbf{Q}_R, & \text{if} \quad \xi \ge s_R, \end{cases} \tag{26}$$

with the diagonal matrix $\boldsymbol{\delta}_*(\bar{\mathbf{Q}})$, which will be explained later in more detail and which generalizes the scalar coefficient δ introduced by Einfeldt et al. in [46, 47]. Furthermore, the scalar $\varphi \in [0, 1]$ is a flattener variable according to [8], that allows to switch smoothly between the HLL RS and the HLLEM RS.

Substituting eqn. (26) and (6) into eqn. (4) we can retrieve eqn. (20) in the conservative case. Hence, for a conservation law, the constant HLL state is not affected by the inclusion of a linear variation. In the following, we will assume this to be valid also for a non-conservative system, i.e. the HLL state $\mathbf{Q}_*$ will be computed according to (14) also in the case of the generalized HLLEM method. This is of course a simplifying assumption, in order to keep the HLLEM scheme simple. For an alternative formulation of the HLLEM scheme that is in the non-conservative case more consistent with the assumed structure of the solution of the Riemann problem (26), see Appendix A. Integrating (4) over $\xi \in [s_L, 0]$ and $\xi \in [0, s_R]$ yields

$$\int_{s_L}^{0} \left(\mathbf{Q}(\xi) - \frac{\partial(\xi \mathbf{Q})}{\partial \xi} \right) d\xi + \overbrace{\int_{s_L}^{0} \left(\frac{\partial \mathbf{f}}{\partial \xi} + \mathbf{B}(\mathbf{Q}) \frac{\partial \mathbf{Q}}{\partial \xi} \right) d\xi}^{:= \mathbf{D}^-_{\text{HLLEM}}(\mathbf{Q}_L, \mathbf{Q}_R)} = 0, \qquad \int_{0}^{s_R} \left(\mathbf{Q}(\xi) - \frac{\partial(\xi \mathbf{Q})}{\partial \xi} \right) d\xi + \overbrace{\int_{0}^{s_R} \left(\frac{\partial \mathbf{f}}{\partial \xi} + \mathbf{B}(\mathbf{Q}) \frac{\partial \mathbf{Q}}{\partial \xi} \right) d\xi}^{:= \mathbf{D}^+_{\text{HLLEM}}(\mathbf{Q}_L, \mathbf{Q}_R)} = 0, \tag{27}$$

where now $\mathbf{Q}(\xi)$ is given by (26). Integrating (27) and simplifying the terms gives us the expression for $\mathbf{D}^-$ and $\mathbf{D}^+$ for the HLLEM RS as follows:

$$\begin{aligned} \mathbf{D}^-_{\text{HLLEM}}(\mathbf{Q}_L, \mathbf{Q}_R) &= \mathbf{D}^-_{\text{HLL}}(\mathbf{Q}_L, \mathbf{Q}_R) - \varphi \frac{s_R s_L}{s_R - s_L} \mathbf{R}_*(\bar{\mathbf{Q}})\, \boldsymbol{\delta}_*(\bar{\mathbf{Q}})\, \mathbf{L}_*(\bar{\mathbf{Q}})\, (\mathbf{Q}_R - \mathbf{Q}_L), \\ \mathbf{D}^+_{\text{HLLEM}}(\mathbf{Q}_L, \mathbf{Q}_R) &= \mathbf{D}^+_{\text{HLL}}(\mathbf{Q}_L, \mathbf{Q}_R) + \varphi \frac{s_R s_L}{s_R - s_L} \mathbf{R}_*(\bar{\mathbf{Q}})\, \boldsymbol{\delta}_*(\bar{\mathbf{Q}})\, \mathbf{L}_*(\bar{\mathbf{Q}})\, (\mathbf{Q}_R - \mathbf{Q}_L), \end{aligned} \tag{28}$$

with the HLL fluctuations defined previously in eqn. (23) and the *anti-diffusive* contributions given by the second terms on the right hand side of (28) that stem from the inclusion of the intermediate waves in the Riemann problem. Obviously, also the HLLEM fluctuations satisfy the consistency conditions (24).

In the case of only one single intermediate field (contact discontinuity in the Euler equations associated with the eigenvalue $\lambda = u$), Einfeldt et al. carried out a stability analysis of the scheme in order to define the scalar $2\delta = (s_R - s_L)/(\bar{c} + |\bar{u}|)$, with $\bar{c} = \frac{1}{2}(s_R - s_L)$, hence $\delta = (s_R - s_L)/(s_R - s_L + 2|\bar{u}|)$. For the more general setting considered here, we repeat the stability analysis of Einfeldt [46] in Appendix B and find the following simple expression for the diagonal matrix $\boldsymbol{\delta}_*(\bar{\mathbf{Q}})$ that controls the amount of anti-diffusion:

$$\boldsymbol{\delta}_*(\bar{\mathbf{Q}}) = \mathbf{I} - \frac{\boldsymbol{\Lambda}^-_*}{s_L} - \frac{\boldsymbol{\Lambda}^+_*}{s_R}, \tag{29}$$

with the identity matrix $\mathbf{I}$ and where all calculations are supposed to be performed componentwise on the diagonal elements of $\boldsymbol{\Lambda}_* = \boldsymbol{\Lambda}_*(\bar{\mathbf{Q}})$. Furthermore, the usual abbreviations $\boldsymbol{\Lambda}^\pm_* = \frac{1}{2}(\boldsymbol{\Lambda}_* \pm |\boldsymbol{\Lambda}_*|)$ are used. The amount of anti-diffusion is therefore controlled by the ratio of the inner eigenvalues and the outer extremal speeds. Please note that for all inner fields we have $|\boldsymbol{\Lambda}^-_*| < |s_L|$ and $\boldsymbol{\Lambda}^+_* < s_R$, hence $0 < \boldsymbol{\delta}_*(\bar{\mathbf{Q}}) \le 1$.

For a full FORTRAN 90 sample code of the path-conservative HLLEM Riemann solver (28) proposed in this paper, please see Appendix C.

Finally, we would like to comment briefly on the problem of *resonance*, see [59]. In that case, some of the eigenvalues of the hyperbolic system coincide and there exists no complete set of linearly independent eigenvectors any more. Furthermore, in this situation the uniqueness of the solution of the PDE can be lost, and thus represents a major difficulty. In that case, we simply drop the anti-diffusive term of the HLLEM scheme, thus reverting back to the classical HLL method, which does not need the eigenstructure of the PDE system, but which requires only an

estimate of the bounding speeds from the left and the right. In practice, this corresponds to setting simply $\mathbf{R}_*(\bar{\mathbf{Q}}) = \mathbf{\Lambda}_*(\bar{\mathbf{Q}}) = \mathbf{L}_*(\bar{\mathbf{Q}}) = 0$ in the resonant case. Of course, this is only a very crude procedure and does not address the issue of the uniqueness of the solution at all. Further research about this rather complex topic is necessary and will be carried out in the future, for example by *smoothly* changing the flattener variable from $\varphi = 0$ at the resonant points to $\varphi = 1$ sufficiently far away from resonance, in order to avoid an abrupt change of the properties of the Riemann solver, see also [8].

2.3. Numerical HLLEM flux for conservation laws

In the case when (1) is a conservation law, i.e. for $\mathbf{B}(\mathbf{Q}) = 0$, the numerical flux associated with the HLLEM Riemann solver [46, 47] using (29) reads:

$$\mathbf{f}_{\text{HLLEM}} = \frac{s_R \mathbf{f}_L - s_L \mathbf{f}_R}{s_R - s_L} + \frac{s_L s_R}{s_R - s_L}(\mathbf{Q}_R - \mathbf{Q}_L) - \varphi \frac{s_R s_L}{s_R - s_L} \mathbf{R}_*(\bar{\mathbf{Q}})\, \delta_*(\bar{\mathbf{Q}})\, \mathbf{L}_*(\bar{\mathbf{Q}})\, (\mathbf{Q}_R - \mathbf{Q}_L). \tag{30}$$

Note that only a few linearly degenerate intermediate eigenvectors $\mathbf{R}_*(\bar{\mathbf{Q}})$ and $\mathbf{L}_*(\bar{\mathbf{Q}})$ need to be evaluated just *once* per call to the one-dimensional Riemann solver. These linearly degenerate intermediate eigenvectors are usually much simpler to evaluate than the entire eigenstructure of the matrix $\mathbf{A}(\mathbf{Q})$, as is the case for the Osher-type RS proposed in [45, 44] (DOT solver). Also note that in the DOT solver, the eigenstructure needed to be evaluated in each Gaussian quadrature point again, hence several times per call to the Riemann solver.

The above HLLEM RS is in general *not* complete, in particular if there are several genuinely nonlinear intermediate characteristic fields. In principle, however, the user can choose to include *all* intermediate characteristic fields in the matrices $\mathbf{R}_*$, $\mathbf{L}_*$ and $\mathbf{\Lambda}_*$, i.e. also the genuinely nonlinear intermediate fields. In that case, the HLLEM RS becomes a *complete* Riemann solver. In practice, however, the most important issue is to resolve *linearly degenerate* intermediate fields, since they are more sensitive to numerical dissipation. In contrast, genuinely nonlinear fields tend to steepen up discontinuities in a natural way, due to the physical compression of the associated characteristic curves. Also note that usually the eigenvectors and eigenvalues of linear degenerate intermediate fields are much simpler to compute than the nonlinear ones, see the two-layer shallow water system and the Pitman and Le model in the following section. For these particular systems, the eigenvalues of the nonlinear characteristic fields are the roots of a fourth degree polynomial, while the eigenvalues and eigenvectors of the linear degenerate fields can be explicitly given and have rather simple expressions.

For a full FORTRAN 90 sample code of the numerical HLLEM flux (30), please see Appendix C.

3. Numerical results

All computational results shown in this section have been produced by using the path-conservative HLLEM scheme inside a standard second order TVD finite volume framework [90], based on the minmod slope limiter. The domain Ω is divided into equidistant control volumes $\Omega_i = [x_{i-\frac{1}{2}}, x_{i+\frac{1}{2}}]$ with mesh spacing $\Delta x = x_{i+\frac{1}{2}} - x_{i-\frac{1}{2}}$. The time step is computed according to the usual CFL condition as

$$\Delta t = \text{CFL} \frac{\Delta x}{\max_i \left| \mathbf{\Lambda}(\mathbf{Q}_i^n) \right|}, \qquad \text{with} \qquad \text{CFL} \leq 1. \tag{31}$$

An explicit second order TVD finite volume discretization of PDE (1) based on the path-conservative HLLEM scheme reads

$$\mathbf{Q}_i^{n+1} = \mathbf{Q}_i^n - \frac{\Delta t}{\Delta x}\left(\mathbf{D}^-_{i+\frac{1}{2}} + \mathbf{D}^+_{i-\frac{1}{2}} \right) - \frac{\Delta t}{\Delta x}\left(\mathbf{f}^-_{i+\frac{1}{2}} - \mathbf{f}^+_{i-\frac{1}{2}} \right) - \frac{\Delta t}{\Delta x} \mathbf{B}(\mathbf{Q}_i^{n+\frac{1}{2}}) \Delta \mathbf{Q}_i^n, \tag{32}$$

with the jump terms and the boundary-extrapolated fluxes evaluated at the half time level $t^{n+\frac{1}{2}}$:

$$\mathbf{D}^-_{i+\frac{1}{2}} = \mathbf{D}^-_{\text{HLLEM}}\left(\mathbf{Q}^{n+\frac{1}{2},-}_{i+\frac{1}{2}}, \mathbf{Q}^{n+\frac{1}{2},+}_{i+\frac{1}{2}} \right), \qquad \mathbf{D}^+_{i-\frac{1}{2}} = \mathbf{D}^+_{\text{HLLEM}}\left(\mathbf{Q}^{n+\frac{1}{2},-}_{i-\frac{1}{2}}, \mathbf{Q}^{n+\frac{1}{2},+}_{i-\frac{1}{2}} \right), \qquad \mathbf{f}^{\pm}_{i+\frac{1}{2}} = \mathbf{f}(\mathbf{Q}^{n+\frac{1}{2},\pm}_{i+\frac{1}{2}}). \tag{33}$$

The slopes and the boundary-extrapolated values of the state vector $\mathbf{Q}$ at time t^n are simply obtained as

$$\Delta \mathbf{Q}_i^n = \text{minmod}\left(\mathbf{Q}_{i+1}^n - \mathbf{Q}_i^n, \mathbf{Q}_i^n - \mathbf{Q}_{i-1}^n \right), \qquad \mathbf{Q}^{n,\mp}_{i\pm\frac{1}{2}} = \mathbf{Q}_i^n \pm \frac{1}{2} \Delta \mathbf{Q}_i^n. \tag{34}$$

The evolution to the half time level needed in (32) and (33) is directly obtained from a discrete form of the PDE (1) *in the small*, without coupling to the neighbor elements:

$$\partial_t \mathbf{Q}_i^n = -\frac{\left(\mathbf{f}(\mathbf{Q}_{i+\frac{1}{2}}^{n,-}) - \mathbf{f}(\mathbf{Q}_{i-\frac{1}{2}}^{n,+})\right)}{\Delta x} - \mathbf{B}(\mathbf{Q}_i^n)\frac{\Delta \mathbf{Q}_i^n}{\Delta x}, \qquad \mathbf{Q}_{i\pm\frac{1}{2}}^{n+\frac{1}{2},\mp} = \mathbf{Q}_i^n \pm \frac{1}{2}\Delta \mathbf{Q}_i^n + \frac{1}{2}\Delta t \partial_t \mathbf{Q}_i^n, \qquad \mathbf{Q}_i^{n+\frac{1}{2}} = \mathbf{Q}_i^n + \frac{1}{2}\Delta t \partial_t \mathbf{Q}_i^n. \tag{35}$$

If not stated otherwise, the flattener variable has been set to $\varphi = 1$ in all cases.

3.1. Single-layer shallow water equations

The augmented shallow water system with transverse flow velocity and time-independent bottom topography read in one space dimension

$$\begin{aligned}
\frac{\partial h}{\partial t} + \frac{\partial}{\partial x}(hu) &= 0, \\
\frac{\partial hu}{\partial t} + \frac{\partial}{\partial x}\left(hu^2 + \frac{1}{2}gh^2\right) + gh\frac{\partial b}{\partial x} &= 0, \qquad (36) \\
\frac{\partial hv}{\partial t} + \frac{\partial}{\partial x}(huv) &= 0, \qquad (37) \\
\frac{\partial b}{\partial t} &= 0,
\end{aligned}$$

where h is the water depth, u is the normal velocity and v is the transverse velocity; $b = b(x)$ is the bottom topography and g denotes the gravity acceleration. The velocity vector is also denoted by $\mathbf{v} = (u, v)$. This system contains two important linearly degenerate fields associated with intermediate eigenvalues that represent i) a stationary wave, associated with the bottom jump, see also [70, 25], and ii) a shear wave associated with the transverse flow velocity v. The eigenvalues of these two linearly degenerate inner fields, together with the associated left and right eigenvectors are given by

$$\mathbf{\Lambda}_* = \begin{pmatrix} 0 & 0 \\ 0 & u \end{pmatrix}, \qquad \mathbf{R}_* = \begin{pmatrix} 1 & 0 \\ 0 & 0 \\ 0 & 1 \\ \frac{u^2-c^2}{c^2} & 0 \end{pmatrix}, \qquad \mathbf{L}_* = \begin{pmatrix} 0 & 0 & 0 & \frac{c^2}{u^2-c^2} \\ -v & 0 & 1 & 0 \end{pmatrix}, \qquad \text{with} \qquad c^2 = gh. \tag{38}$$

3.1.1. Well-balancing / C-property

The path-conservative HLLEM scheme presented in this paper is *well-balanced* in the sense of [62, 55, 56, 17, 70, 25], i.e. the scheme preserves steady state solutions of the form $\eta = const$ and $u = 0$ *exactly*. This feature is also known as the so-called *C*-property.

Proof of the exact C-property. First, we proof the exact C-property for the path-conservative HLLEM scheme for the single-layer shallow water equations. For that purpose, we consider a left state and a right state that satisfy the lake-at-rest condition, $\eta = h + b = const.$ and $u = v = 0$. Hence, the two states can be written as $\mathbf{Q}_L = (h_L, 0, 0, b_L)$ and $\mathbf{Q}_R = (h_R, 0, 0, b_R)$ with $h_L = \eta - b_L$ and $h_R = \eta - b_R$. The fluxes are $\mathbf{f}_L = (0, \frac{1}{2}gh_L^2, 0, 0)$ and $\mathbf{f}_R = (0, \frac{1}{2}gh_R^2, 0, 0)$, and the Roe matrix $\tilde{\mathbf{B}}(\mathbf{Q}_a, \mathbf{Q}_b)$ is simply

$$\tilde{\mathbf{B}}(\mathbf{Q}_a, \mathbf{Q}_b) = \begin{pmatrix} 0 & 0 & 0 & 0 \\ 0 & 0 & 0 & \frac{1}{2}g(h_a + h_b) \\ 0 & 0 & 0 & 0 \\ 0 & 0 & 0 & 0 \end{pmatrix}. \tag{39}$$

The equation (14) for the HLL state $\mathbf{Q}_*$ therefore becomes

$$(s_R - s_L)\begin{pmatrix} h_* \\ h_*u_* \\ h_*v_* \\ b_* \end{pmatrix} = s_R\begin{pmatrix} h_R \\ 0 \\ 0 \\ b_R \end{pmatrix} - s_L\begin{pmatrix} h_L \\ 0 \\ 0 \\ b_L \end{pmatrix} - \begin{pmatrix} 0 \\ \frac{1}{2}gh_R^2 \\ 0 \\ 0 \end{pmatrix} + \begin{pmatrix} 0 \\ \frac{1}{2}gh_L^2 \\ 0 \\ 0 \end{pmatrix} - \begin{pmatrix} 0 \\ \frac{1}{2}g\left((h_L + h_*)(b_* - b_L) + (h_* + h_R)(b_R - b_*)\right) \\ 0 \\ 0 \end{pmatrix}. \tag{40}$$

Using $h_L = \eta - b_L$ and $h_R = \eta - b_R$ we obtain the following solution for $\mathbf{Q}_*$:

$$\mathbf{Q}_* = \begin{pmatrix} \eta - b_* \\ 0 \\ 0 \\ b_* \end{pmatrix}, \qquad \text{with} \qquad b_* = \frac{s_R b_R - s_L b_L}{s_R - s_L}, \tag{41}$$

in other words, the HLL state $\mathbf{Q}_*$ itself preserves the C-property, but not the resulting HLL Riemann solver with the fluctuations given by (23). Since $u = 0$, the matrices $\mathbf{\Lambda}_*$ and $\boldsymbol{\delta}_*$ read in this case simply

$$\mathbf{\Lambda}_* = 0, \qquad \Rightarrow \qquad \boldsymbol{\delta}_* = \mathbf{I}, \tag{42}$$

and thus the HLLEM fluctuations (28) become

$$\begin{aligned} \mathbf{D}^-_{\text{HLLEM}}(\mathbf{Q}_L, \mathbf{Q}_R) &= -\frac{s_L}{s_R - s_L}\left[\mathbf{f}_R - \mathbf{f}_L + \tilde{\mathbf{B}}\left(\mathbf{Q}_L, \mathbf{Q}_*\right)\left(\mathbf{Q}_* - \mathbf{Q}_L\right) + \tilde{\mathbf{B}}\left(\mathbf{Q}_*, \mathbf{Q}_R\right)\left(\mathbf{Q}_R - \mathbf{Q}_*\right)\right], \\ \mathbf{D}^+_{\text{HLLEM}}(\mathbf{Q}_L, \mathbf{Q}_R) &= -\frac{s_L}{s_R - s_L}\left[\mathbf{f}_R - \mathbf{f}_L + \tilde{\mathbf{B}}\left(\mathbf{Q}_L, \mathbf{Q}_*\right)\left(\mathbf{Q}_* - \mathbf{Q}_L\right) + \tilde{\mathbf{B}}\left(\mathbf{Q}_*, \mathbf{Q}_R\right)\left(\mathbf{Q}_R - \mathbf{Q}_*\right)\right]. \end{aligned} \tag{43}$$

Using eqn. (41) one obtains for the term in square brackets

$$\mathbf{f}_R - \mathbf{f}_L + \tilde{\mathbf{B}}\left(\mathbf{Q}_L, \mathbf{Q}_*\right)\left(\mathbf{Q}_* - \mathbf{Q}_L\right) + \tilde{\mathbf{B}}\left(\mathbf{Q}_*, \mathbf{Q}_R\right)\left(\mathbf{Q}_R - \mathbf{Q}_*\right) = \begin{pmatrix} 0 \\ \frac{1}{2}g(h_R^2 - h_L^2) + \frac{1}{2}g(b_R - b_L)(h_R + h_L) \\ 0 \\ 0 \end{pmatrix} = 0, \tag{44}$$

since

$$\frac{1}{2}g(h_R^2 - h_L^2) + \frac{1}{2}g(b_R - b_L)(h_R + h_L) = \frac{1}{2}g\left(\overbrace{(h_R + b_R)}^{\eta} - \overbrace{(h_L + b_L)}^{\eta}\right)(h_R + h_L) = 0,$$

hence

$$\mathbf{D}^-_{\text{HLLEM}}(\mathbf{Q}_L, \mathbf{Q}_R) = \mathbf{D}^+_{\text{HLLEM}}(\mathbf{Q}_L, \mathbf{Q}_R) = 0. \tag{45}$$

The path-conservative HLLEM scheme is therefore *exactly well-balanced* for the lake-at-rest for arbitrary choices of the bottom topography and the signal speeds.

Numerical verification of the exact C-property. In the following, the well-balanced property is also verified numerically by using the classical test problem of LeVeque [62], consisting in a small perturbation of a free surface at rest over a smoothly varying bottom topography. The computational domain is given by $\Omega = [0, 2]$ and the initial condition is $u(x, 0) = 0$,

$$\eta(x, 0) = \begin{cases} 1 + \epsilon & \text{if} \quad 1.1 \le x \le 1.2, \\ 1 & \text{else.} \end{cases}$$

The bottom topography is defined as

$$b(x) = \begin{cases} 0.25\left(\cos(10\pi(x - 1.5)) + 1\right) & \text{if} \quad 1.4 \le x \le 1.6, \\ 0 & \text{else.} \end{cases}$$

All simulations are carried out on a mesh with 200 equidistant cells and using a CFL number of 0.9. Reconstruction is *not* performed in terms of the conservative variables h, $h\mathbf{v}$ and b, but in the variables η, $h\mathbf{v}$ and b, as suggested in [25, 37], in order to keep also the reconstruction well-balanced. First, the *exact* well-balanced property is verified using $\epsilon = 0$. The results are reported for various machine precisions in the left column of Table 1, confirming that the scheme is able to maintain the water at rest solution up to machine precision. Next, the free surface is perturbed by using $\epsilon = 0.2$ in the first case, and $\epsilon = 10^{-3}$ in the second one. In Figures 1 the numerical results obtained with the new HLLEM RS scheme are compared with a reference solution computed on a very fine mesh of 10000 cells using a well-balanced second order TVD finite volume scheme based on a path-conservative Rusanov scheme [37]. Overall, a good agreement of the two solutions can be noted, confirming that the present scheme is able to simulate accurately small perturbations of a steady state without introducing spurious oscillations in the presence of a variable bottom topography. Similar results have been obtained very recently also with a high order accurate semi-implicit discontinuous Galerkin finite element scheme on staggered grids, see [39, 85].

Table 1: Numerical verification of the exact C-property (well-balancedness) for different machine precisions. The L_∞ errors are reported for the single layer shallow water equations (left column), the two-layer shallow water equations (middle column) and for the Pitman and Le model (right column). They refer to the L_∞ norm of the flow velocity vectors $\mathbf{v}$ (shallow water equations), $\mathbf{v}_1$ (two-layer shallow water equations) and $\mathbf{v}_s$ Pitman and Le model).

Case	L_∞ single layer shallow water	L_∞ two-layer shallow water	L_∞ Pitman & Le
Single precision	$7.8134161\ 10^{-7}$	$7.5865739\ 10^{-7}$	$3.3436726\ 10^{-7}$
Double precision	$1.1255465\ 10^{-15}$	$1.4511592\ 10^{-15}$	$4.7206307\ 10^{-16}$
Quadruple precision	$3.7348994\ 10^{-31}$	$1.1662217\ 10^{-33}$	$9.0952771\ 10^{-34}$

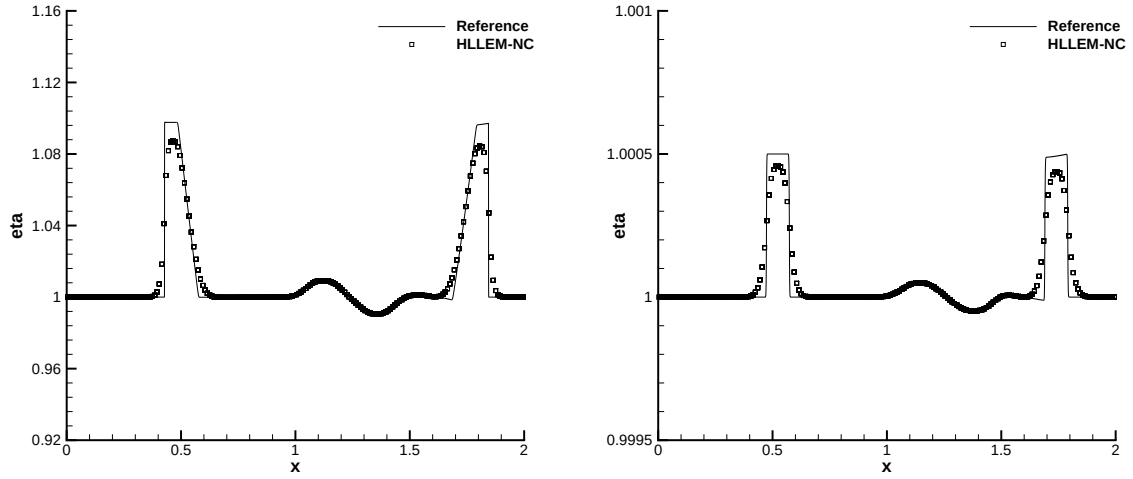

Figure 1: Reference solution and numerical solution for the free-surface perturbation test problem of LeVeque [62] at $t = 0.2$ using the path-conservative HLLEM scheme presented in this article. Left: large perturbation ($\epsilon = 0.2$). Right: small perturbation ($\epsilon = 10^{-3}$).

3.1.2. Riemann problems

In the following we solve four Riemann problems using the new path-conservative HLLEM scheme proposed in this paper. The initial conditions are defined in Table 2. We use 100 equidistant grid cells, set the CFL number to 0.9 and the gravity acceleration is defined as $g = 9.81$. The results of our new path-conservative HLLEM scheme for general non-conservative hyperbolic systems (denoted by HLLEM-NC) are compared with the exact solutions of the Riemann problem provided by Toro [89] and by Bernetti et al. [18]. The same Riemann problems have also been solved previously by using the path-conservative Osher scheme proposed by Dumbser and Toro in [44].

The first Riemann problem RP0 consists in a *flat free surface* and two superimposed stationary jump discontinuities, namely a bottom jump and a shear wave, hence the water is *not* globally at rest here. From the top row of Fig. 2 one can observe that the new HLLEM scheme is able to resolve these steady intermediate waves *exactly*, as expected, without adding any spurious numerical diffusion. The absolute value of the normal velocity was always of the order of machine accuracy ($|u| < 4.0 \cdot 10^{-15}$).

Riemann problem RP1 is a classical dam–break over an empty half–space, first solved by Ritter in [75]. The other Riemann problems contain a jump in the bottom topography and have been taken from [18]. The numerical results are depicted in Fig. 2. In RP1 we observe that the HLLEM scheme is able to deal robustly with the dry bed case. The numerical solutions obtained for the remaining Riemann problems with bottom jump agree very well with the exact solution provided by Bernetti et al. [18]. Very similar results have also been reported in [44] using the path-conservative Osher scheme.

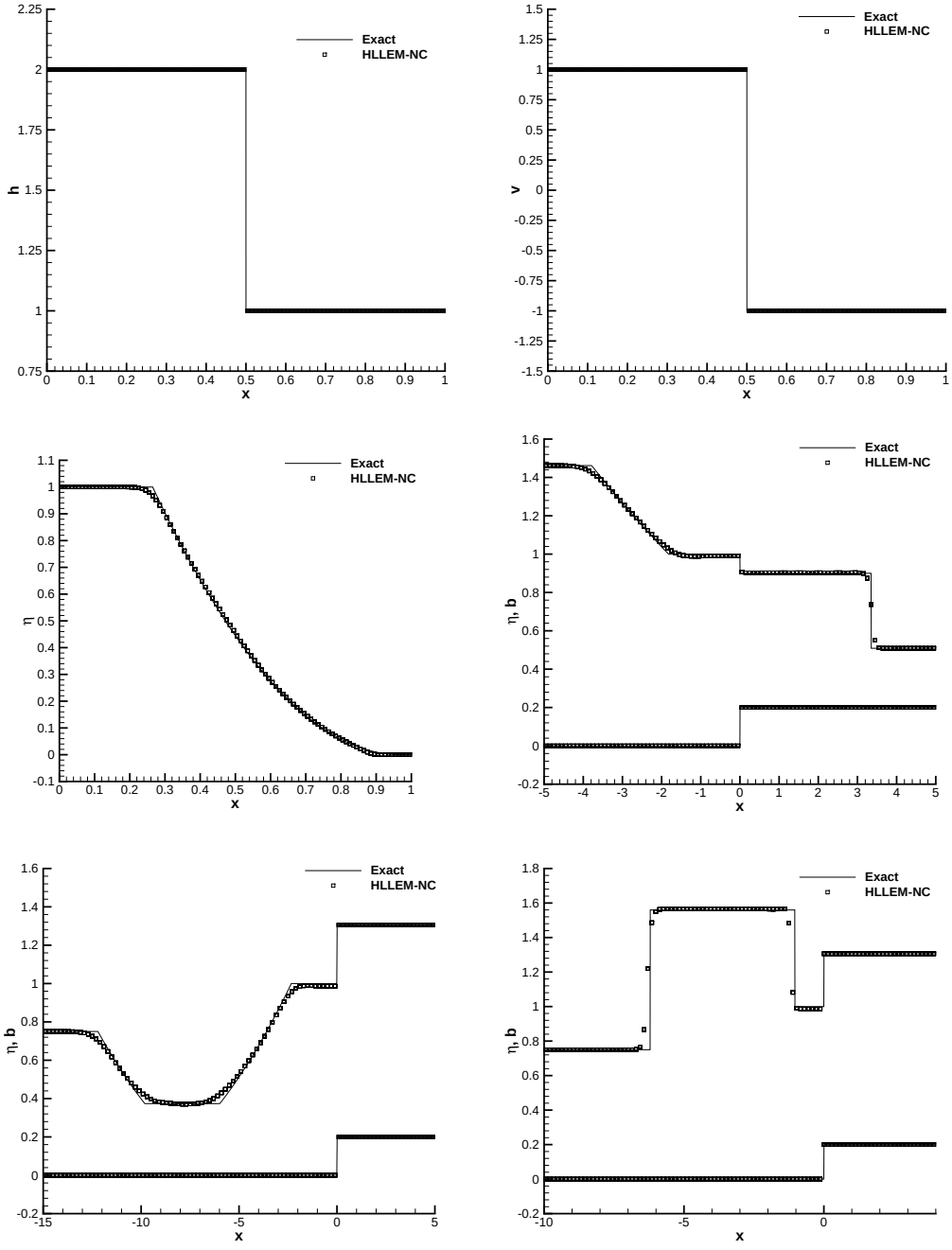

Figure 2: Computational results for the single layer shallow water equations. Top row: Riemann problem RP0 that contains two stationary, linearly degenerate intermediate waves (bottom jump and shear wave). Middle row: Riemann problems RP1 (left) and RP2 (right) . Bottom row: Riemann problems RP3 (left) and RP4 (right). The variable $\eta = h + b$ denotes the free surface location.

Table 2: Single-layer shallow water equations: left and right initial states (water depth h, velocity components u and v, bottom height b), final output times (t_{end}), computational domain $\Omega = [x_L, x_R]$ and initial position of the discontinuity (x_c).

Case	h_L	u_L	v_L	b_L	h_R	u_R	v_R	b_R	t_{end}	x_L	x_R	x_c
RP0	2.0	0.0	1.0	0.0	1.0	0.0	-1.0	1.0	1.0	0.0	1.0	0.5
RP1	1.0	0.0	0.0	0.0	10^{-14}	0.0	0.0	0.0	0.075	0.0	1.0	0.5
RP2	1.46184	0.0	0.0	0.0	0.30873	0.0	0.0	0.2	1.0	-5.0	5.0	0.0
RP3	0.75	-9.49365	0.0	0.0	1.10594	-4.94074	0.0	0.2	1.0	-15.0	5.0	0.0
RP4	0.75	-1.35624	0.0	0.0	1.10594	-4.94074	0.0	0.2	1.0	-10.0	4.0	0.0

3.2. Two-layer shallow water equations

In one space dimension the two-layer shallow water equations with transverse flow velocities can be cast into the quasi-linear form (2) with the state vector $\mathbf{Q} = (h_1, h_1u_1, h_1v_1, h_2, h_2u_2, h_2v_2, b)^T$ and the system matrix

$$\mathbf{A}(\mathbf{Q}) = \begin{pmatrix} 0 & 1 & 0 & 0 & 0 & 0 & 0 \\ -u_1^2 + gh_1 & 2u_1 & 0 & gh_1 & 0 & 0 & gh_1 \\ -u_1v_1 & v_1 & u_1 & 0 & 0 & 0 & 0 \\ 0 & 0 & 0 & 0 & 1 & 0 & 0 \\ \rho gh_2 & 0 & 0 & -u_2^2 + gh_2 & 2u_2 & 0 & gh_2 \\ 0 & 0 & 0 & -u_2v_2 & v_2 & u_2 & 0 \\ 0 & 0 & 0 & 0 & 0 & 0 & 0 \end{pmatrix}, \tag{46}$$

where h_k is the water depth, u_k is the normal velocity and v_k is the transverse velocity of layer number $k \in \{1, 2\}$; $b = b(x)$ is again the bottom topography and g denotes the gravity acceleration; the symbol $\rho = \rho_1/\rho_2$ denotes the density ratio of the upper fluid ($k = 1$) and the lower fluid ($k = 2$). In the following, we will also use the total free surface height $\eta = \eta_1 = b + h_2 + h_1$ and the free surface elevation of the interior layer $\eta_2 = b + h_2$. We will also denote the velocity vector of layer k by $\mathbf{v}_k = (u_k, v_k)$. The lake-at-rest solution for this PDE system is given by

$$h_1 = const., \qquad \eta = h_1 + h_2 + b = const., \qquad u_1 = u_2 = v_1 = v_2 = 0, \tag{47}$$

This system contains three linearly degenerate inner fields: i) a stationary wave, associated with the bottom jump, and ii) two shear waves, associated with the transverse flow velocities v_k. The eigenvalues of these three linearly degenerate inner fields, together with the associated left and right eigenvectors are given by

$$\mathbf{\Lambda}_* = \begin{pmatrix} 0 & 0 & 0 \\ 0 & u_1 & 0 \\ 0 & 0 & u_2 \end{pmatrix}, \qquad \mathbf{R}_* = \begin{pmatrix} e_0c_1^2u_2^2 & -v_1 & 0 \\ 0 & 0 & 0 \\ e_0v_1c_1^2u_2^2 & 1 & 0 \\ e_0c_2^2e_1 & 0 & -v_2 \\ 0 & 0 & 0 \\ e_0v_2^2c_2^2e_1 & 0 & 1 \\ e_0e_2 & 0 & 0 \end{pmatrix}, \qquad \mathbf{L}_* = \begin{pmatrix} 0 & 0 & 0 & 0 & 0 & 0 & e_0 \\ 0 & 0 & 1 & 0 & 0 & 0 & 0 \\ 0 & 0 & 0 & 0 & 0 & 1 & 0 \end{pmatrix}, \tag{48}$$

with the abbreviations

$$c_1^2 = gh_1, \qquad c_2^2 = gh_2, \qquad e_1 = (\rho - 1)c_1^2 + u_1^2, \qquad e_2 = -c_2^2e_1 + u_2^2(u_1^2 - c_1^2). \tag{49}$$

The normalization constant e_0 of the first pair of eigenvectors is given by

$$e_0 = \frac{1}{\sqrt{e_2}}. \tag{50}$$

3.2.1. Well-balancing / C-property

Here, we validate the C-property of the HLLEM scheme in the context of the two-layer shallow water equations. For this purpose, a slightly modified version of the test case proposed by Leveque [62] is solved in the following. The initial conditions for the total free surface elevation and for the bottom topography are the same as the ones used for the single layer shallow water equations before, i.e. $\eta(x,0)$ is given by (46) and $b(x)$ is defined according to (46). The velocity of both layers is set to zero, $\mathbf{v}_1 = \mathbf{v}_2 = 0$, and the initial free surface elevation of the intermediate layer is fixed as $\eta_2(x,0) = 0.65$. The final computational time is chosen as $t = 0.2$; the density ratio is given by $\rho = 0.8$, the computational grid is composed of 400 cells and the CFL number has been set to 0.9. First, we set the perturbation of the total free surface elevation to $\epsilon = 0$, in order to verify whether the scheme is able to conserve the lake at rest solution exactly. The obtained computational results are reported in the middle column of Table 1 for single, double and quadruple precision. We find that the scheme is exactly well-balanced up to machine precision. Next, we apply a large and a small perturbation to the free surface, as in the single layer shallow water case. The computational results obtained with the path-conservative HLLEM scheme are reported in Fig. 3 and are compared against a simple well-balanced path-conservative Rusanov scheme [37], running the same problem on a very fine mesh of 10,000 cells. We can note a very good agreement between the path-conservative HLLEM results and the fine grid reference solution.

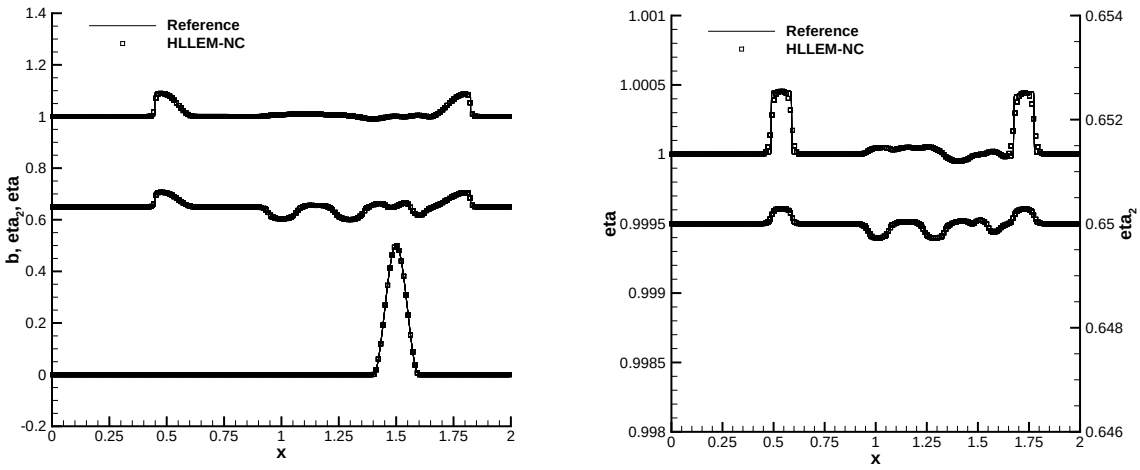

Figure 3: Reference solution and numerical solution for the small perturbation test problem adopted for the two-layer shallow water equations at $t = 0.2$ using the path-conservative HLLEM scheme presented in this article. Left: large perturbation ($\epsilon = 0.2$). Right: small perturbation ($\epsilon = 10^{-3}$).

3.2.2. Riemann problems

In the following we solve three Riemann problems for the two-layer shallow water equations, where in all cases $\rho = 0.8$ has been used. The initial data are summarized in Table 3.

Similar to the single layer shallow water equations, the first Riemann problem RP0 consists in three stationary jump discontinuities in the linearly degenerate intermediate fields, i.e. the initial data contain a superposition of a bottom jump and a shear wave in each layer. The computational results are compared against the exact solution in Fig. 4, where one can easily observe that the path-conservative HLLEM scheme presented in this paper is able to resolve all stationary intermediate waves exactly, as expected, without adding any spurious numerical dissipation. We have explicitly verified that the normal velocity remained of the order of machine accuracy ($|u_k| < 10^{-15}$) for both layers for all times.

In the second problem, see also [37], the bottom is flat, while the third problem contains a jump in the bottom. For RP0 and RP1 we use the path-conservative HLLEM scheme on 200 cells, while the second Riemann problem is solved using an equidistant grid of 400 elements. In Fig. 5 the computational results for RP1 and RP2 are compared

Table 3: Two-layer shallow water equations: left and right initial states, final output times (t_{end}), computational domain $\Omega = [x_L, x_R]$ and initial position of the discontinuity (x_c).

Case	h_1	u_1	v_1	h_2	u_2	v_2	b	t_{end}	x_L	x_R	x_c
RP0 L:	0.5	0.0	0.5	0.8	0.0	-0.2	0.2	1.0	-5.0	+5.0	0.0
R:	0.5	0.0	-0.5	0.2	0.0	+0.2	0.8				
RP1 L:	0.4	0.0	0.0	0.6	0.0	0.0	0.0	1.25	-5.0	+5.0	0.0
R:	0.6	0.0	0.0	0.4	0.0	0.0	0.0				
RP2 L:	1.0	0.0	0.0	1.0	0.0	0.0	0.0	1.0	-5.0	+5.0	0.0
R:	0.5	0.0	0.0	0.5	0.0	0.0	0.5				

against a fine-grid reference solution obtained with a standard path-conservative Rusanov method [37, 27] on a very fine mesh of 10,000 elements.

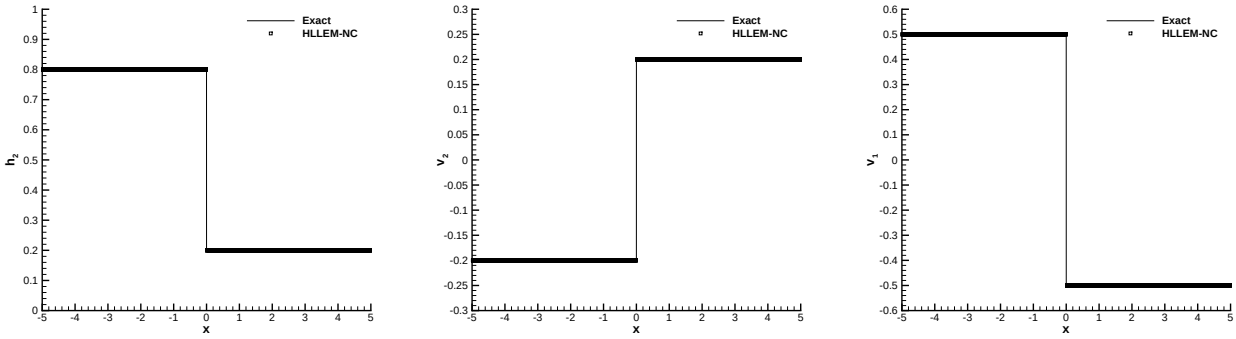

Figure 4: Exact and numerical solution at time $t = 1.0$ for Riemann problem RP0 of the two-layer shallow water model using the path-conservative HLLEM scheme presented in this article. Left: depth of the bottom layer h_2. Middle: transverse velocity v_2 of the bottom layer. Right: transverse velocity v_1 of the upper layer.

3.3. The multi-phase debris flow model of Pitman & Le

The Pitman & Le multi-phase debris flow model [72] in the formulation of Pelanti et al. [71] can be written in one space dimension (including transverse flow velocities) under the form of PDE system (2) with the state vector $\mathbf{Q} = (h_s, h_s u_s, h_s v_s, h_f, h_f u_f, h_f v_f, b)^T$ and the system matrix

$$\mathbf{A}(\mathbf{Q}) = \begin{bmatrix} 0 & 1 & 0 & 0 & 0 & 0 & 0 \\ \frac{1}{2}(T_1^{xx} + T_2^{xx}) - u_s^2 + \rho g h_s & 2u_s & 0 & \frac{1}{2}T_1^{xx} + g\rho h_s & 0 & 0 & T_1^{xx} + \rho g h_s \\ \frac{1}{2}(T_1^{xy} + T_2^{xy}) - u_s v_s & v_s & u_s & \frac{1}{2}T_1^{xy} & 0 & 0 & T_1^{xy} \\ 0 & 0 & 0 & 0 & 1 & 0 & 0 \\ g h_f & 0 & 0 & -u_f^2 + g h_f & 2u_f & 0 & g h_f \\ 0 & 0 & 0 & -u_f v_f & v_f & u_f & 0 \\ 0 & 0 & 0 & 0 & 0 & 0 & 0 \end{bmatrix}, \tag{51}$$

with the two abbreviations

$$T_1^{ij} = a_{ij} g(1-\rho) h_s, \qquad T_2^{ij} = a_{ij} g(1-\rho)(h_s + h_f), \tag{52}$$

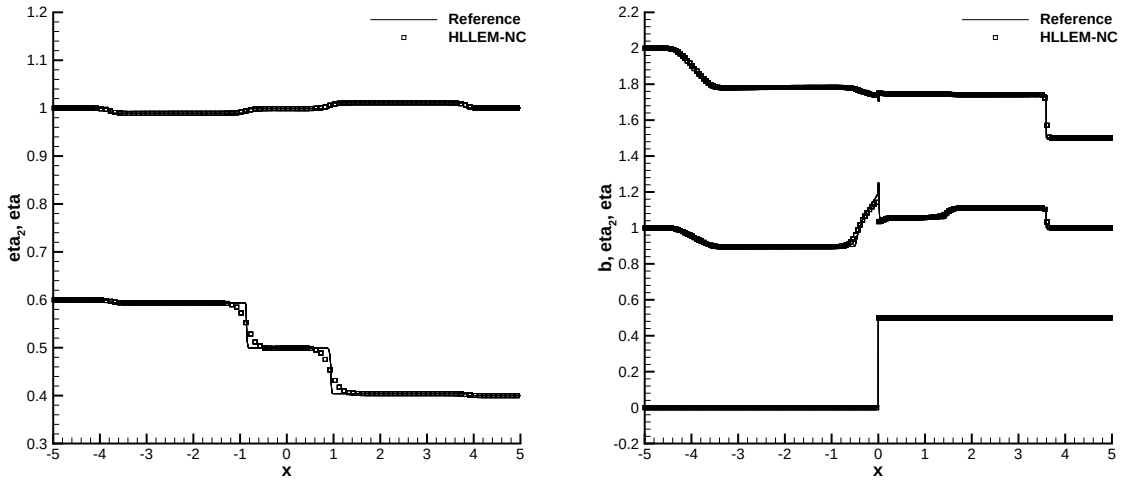

Figure 5: Reference solution and numerical solution for the Riemann problems RP1 and RP2 of the two-layer shallow water model using the path-conservative HLLEM scheme presented in this article. Left: Riemann problem RP1 at time $t = 1.25$. Right: Riemann problem RP2 at time $t = 1.0$.

where i and j denote either x or y. Here, h_k is the water depth, u_k is the normal velocity and v_k is the transverse velocity with $k \in \{s, f\}$ of the solid layer s and the fluid layer f, respectively; $b = b(x)$ is again the bottom topography and g denotes the gravity acceleration; the symbol $\rho = \rho_f/\rho_s$ denotes the density ratio of the fluid and the solid. In the following, we also use the total free surface height $\eta = b + h_s + h_f$ and the free surface elevation of the solid layer $\eta_s = b + h_s$. The model of Pitman and Le has many similarities with the two-layer shallow water model discussed previously. The lake-at-rest solution for this system is given by the following relations:

$$\phi = \frac{h_s}{h_s + h_f} = const., \qquad \eta = h_s + h_f + b = const., \qquad u_s = v_s = u_f = v_f = 0, \tag{53}$$

In the following we will assume $a_{xy} = 0$. This system contains three linearly degenerate inner fields: a stationary wave, associated with the bottom jump, and two shear waves, associated with the transverse flow velocities v_k. The eigenvalues of these three linearly degenerate inner fields, together with the associated left and right eigenvectors are given by

$$\mathbf{\Lambda}_* = \begin{pmatrix} 0 & 0 & 0 \\ 0 & u_s & 0 \\ 0 & 0 & u_f \end{pmatrix}, \qquad \mathbf{R}_* = \begin{pmatrix} e_0 e_1 & -v_s & 0 \\ 0 & 0 & 0 \\ e_0 e_1 v_s & 1 & 0 \\ e_0 e_2 & 0 & -v_f \\ 0 & 0 & 0 \\ e_0 e_2 v_f & 0 & 1 \\ e_0 e_3 & 0 & 0 \end{pmatrix}, \qquad \mathbf{L}_* = \begin{pmatrix} 0 & 0 & 0 & 0 & 0 & 0 & e_0 \\ 0 & 0 & 1 & 0 & 0 & 0 & 0 \\ 0 & 0 & 0 & 0 & 0 & 1 & 0 \end{pmatrix}, \tag{54}$$

with the abbreviations

$$e_1 = \left((2u_f^2 - g h_f) T_1^{xx} + 2 u_f^2 \rho g h_s \right), \qquad e_2 = g h_f \left(T_1^{xx} - T_2^{xx} + 2 u_s^2 \right)$$

and

$$e_3 = \left((2u_s^2 - 2\rho g h_s - T_1^{xx} - T_2^{xx}) u_f^2 + g h_f (T_2^{xx} - 2u_s^2) \right), \qquad e_0 = \frac{1}{\sqrt{e_3}}.$$

In the following, we will set the model constants $a_{xx} = a_{yy} = 1$.

3.3.1. Well-balancing / C-property

The C-property of the HLLEM scheme is validated for the two-fluid debris flow model of Pitman and Le according to the test case proposed by Pelanti et al. in [71]. The setup is again similar to the one proposed by Leveque [62]. More precisely, the bottom topography is defined by

$$b(x) = \begin{cases} 0.25\left(\cos\left(10\pi(x-\frac{1}{2})\right)+1\right) & \text{if } |x-0.5| \leq 0.1, \\ 0 & \text{else.} \end{cases} \tag{55}$$

All velocities are initially set to zero and a small perturbation is added to the free surface elevation η and the solid volume fraction ϕ:

$$\eta(x,0) = \eta_0 + \epsilon, \qquad \phi(x,0) = \phi_0 - \epsilon \qquad \text{for} \quad -0.6 \leq x \leq -0.5. \tag{56}$$

For this test problem, we use $\eta_0 = 1$, $\phi_0 = 0.6$, $g = 1$ and $\rho = 0.5$. The computational domain is $\Omega = [-1.2; 1.2]$, which is slightly larger than the one used in [71]. The path-conservative HLLEM scheme is employed on a uniform grid with 400 cells and the CFL number is set to 0.9. First, we solve this problem without any perturbation of the free surface ($\epsilon = 0$) in order to verify the exact well-balancedness of our scheme. The results are reported for various machine precisions in the right column of Table 1, showing that the new path-conservative HLLEM scheme is exactly well-balanced also for the Pitman and Le model up to machine precision. Next, we add a small perturbation to the free surface by choosing $\epsilon = 10^{-3}$. A fine-grid reference solution is obtained using a classical path-conservative Rusanov scheme [37] on 10,000 cells. A comparison of the path-conservative HLLEM scheme with the reference solution is depicted in Fig. 6, where a very good agreement can be observed.

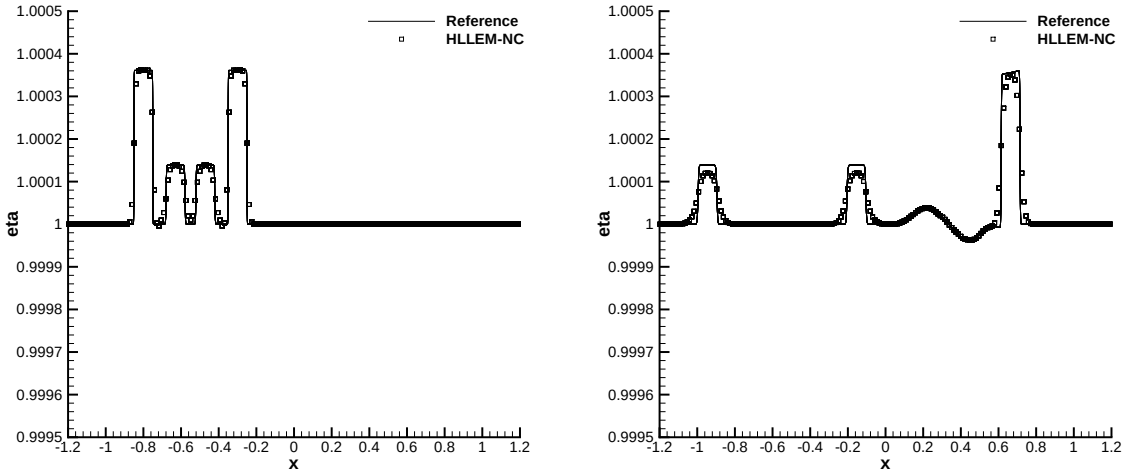

Figure 6: Reference solution and numerical solution for the small surface perturbation test problem [71, 37] adopted for the Pitman and Le model at $t = 0.5$ (left) and at $t = 1.25$ (right) using the path-conservative HLLEM scheme presented in this article.

3.3.2. Riemann problems

In the following three Riemann problems we set $\rho = 0.5$ and $g = 9.8$. The initial data are summarized in Table 4. In all cases we use the path-conservative HLLEM scheme on 200 cells, setting the CFL number to 0.9. We first solve a Riemann problem denoted by RP0, which contains the superposition of three stationary jump discontinuities in the linearly degenerate fields. The free surface is flat ($\eta = 2$), with a bottom jump and a jump in the depths of the solid and the fluid, coupled with two shear waves in the solid and the fluid, respectively. The solid volume fraction $\phi = 0.75$ is constant in this test problem. The computational results are compared against the exact solution in Fig. 7, where one can note a perfect match, due to the capability of the HLLEM scheme to resolve all stationary intermediate fields exactly. The normal velocities u_s and u_f have remained always at the order of machine zero throughout the entire simulation.

Table 4: Two-fluid model of Pitman and Le: left and right initial states, final output times (t_{end}), computational domain $\Omega = [x_L, x_R]$ and initial position of the discontinuity (x_c).

Case	h_s	u_s	v_s	h_f	u_f	v_f	b	t_{end}	x_L	x_R	x_c
RP0 L:	1.5	0.0	+0.2	0.5	0.0	-0.5	0.0	1.0	-5.0	+5.0	0.0
R:	1.125	0.0	-0.2	0.375	0.0	+0.5	0.5				
RP1 L:	2.1	0.0	0.0	0.9	0.0	0.0	0.0	0.5	-5.0	+5.0	0.0
R:	0.8	0.0	0.0	1.2	0.0	0.0	0.0				
RP2 L:	2.1	-1.4	0.0	0.9	0.3	0.0	0.0	0.5	-5.0	+5.0	0.0
R:	0.8	-0.9	0.0	1.2	0.1	0.0	0.0				

We then solve two Riemann problems for the Pitman and Le model with flat bottom and which have already been used in [71, 37, 74] as validation benchmarks. In Fig. 8 the results obtained with the HLLEM RS are compared against a fine-grid reference solution obtained with a standard path-conservative Rusanov method [37] on a very fine mesh of 10,000 elements. A similar reference solution has also been used in [71, 37]. One can observe that the solution obtained with the path-conservative HLLEM scheme matches the reference solution very well.

3.4. The Baer-Nunziato model of compressible multi-phase flows

The Baer–Nunziato model of compressible two–phase flows has been introduced for the first time in [6] and has successively been modified and intensively studied by Saurel and Abgrall in [81]. The governing PDE system reads

$$\begin{aligned}
\frac{\partial}{\partial t}(\phi_1\rho_1) + \nabla\cdot(\phi_1\rho_1\mathbf{v}_1) &= 0,\\
\frac{\partial}{\partial t}(\phi_1\rho_1\mathbf{v}_1) + \nabla\cdot(\phi_1(\rho_1\mathbf{v}_1\mathbf{v}_1 + p_1)) - p_I\nabla\phi_1 &= 0,\\
\frac{\partial}{\partial t}(\phi_1\rho_1E_1) + \nabla\cdot(\phi_1\mathbf{v}_1(\rho_1E_1 + p_1)) + p_I\frac{\partial}{\partial t}\phi_1 &= 0,\\
\frac{\partial}{\partial t}(\phi_2\rho_2) + \nabla\cdot(\phi_2\rho_2\mathbf{v}_2) &= 0,\\
\frac{\partial}{\partial t}(\phi_2\rho_2\mathbf{v}_2) + \nabla\cdot(\phi_2(\rho_2\mathbf{v}_2\mathbf{v}_2 + p_2)) - p_I\nabla\phi_2 &= 0,\\
\frac{\partial}{\partial t}(\phi_2\rho_2E_2) + \nabla\cdot(\phi_2\mathbf{v}_2(\rho_2E_2 + p_2)) + p_I\frac{\partial}{\partial t}\phi_2 &= 0,\\
\frac{\partial}{\partial t}\phi_1 + \mathbf{v}_I\cdot\nabla\phi_1 &= 0,
\end{aligned} \tag{57}$$

where ϕ_j is the volume fraction of phase number j with $\phi_1 + \phi_2 = 1$, ρ_j is the fluid mass density, $\mathbf{v}_j = (u_j, v_j)$ the 2D velocity vector, p_j the pressure and $\rho_jE_j = \rho_je_j + \frac{1}{2}\rho_j\mathbf{v}_j^2$ the total energy density of phase number j, respectively. The model (57) is closed by the stiffened gas equations of state that links the pressure p_j to the density ρ_j and the internal energy e_j by

$$\rho_je_j = \frac{p_j + \gamma_j\pi_j}{(\gamma_j - 1)}. \tag{58}$$

Here, γ_j is the ratio of specific heats and π_j is a constant. For the EOS (58) the sound speed c_i in each phase is given by the relation

$$c_j = \sqrt{\gamma_j\frac{p_j + \pi_j}{\rho_j}}. \tag{59}$$

According to the original choice made in [6], the interface velocity $\mathbf{v}_I$ and the interface pressure p_I are given by

$$p_I = p_2, \qquad \text{and} \qquad \mathbf{v}_I = \mathbf{v}_1, \tag{60}$$

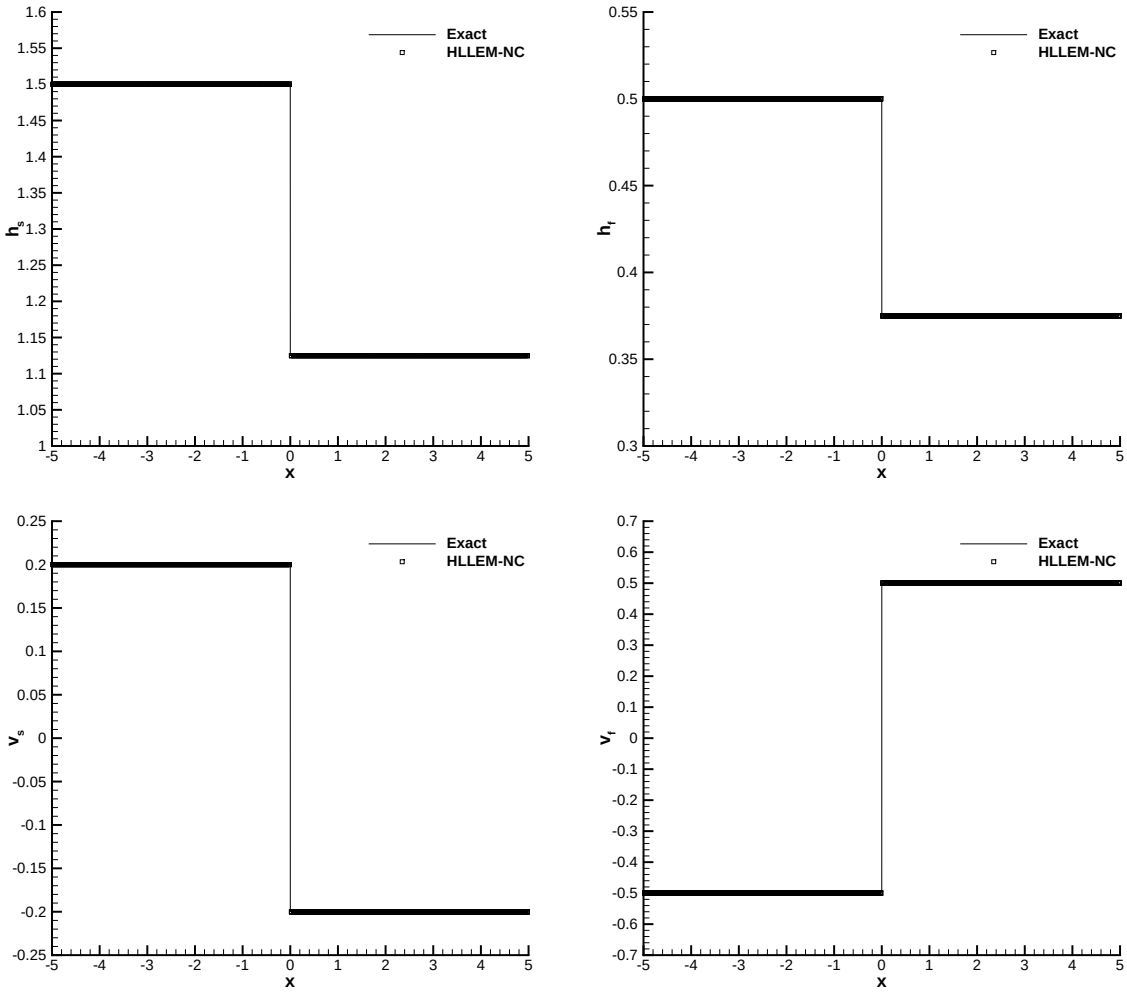

Figure 7: Exact and numerical solution at time $t = 1.0$ for Riemann problem RP0 of the Pitman & Le debris flow model using the path-conservative HLLEM scheme presented in this article. Top row: solid depth (left) and fluid depth (right). Bottom row: solid transverse velocity (left) and fluid transverse velocity (right).

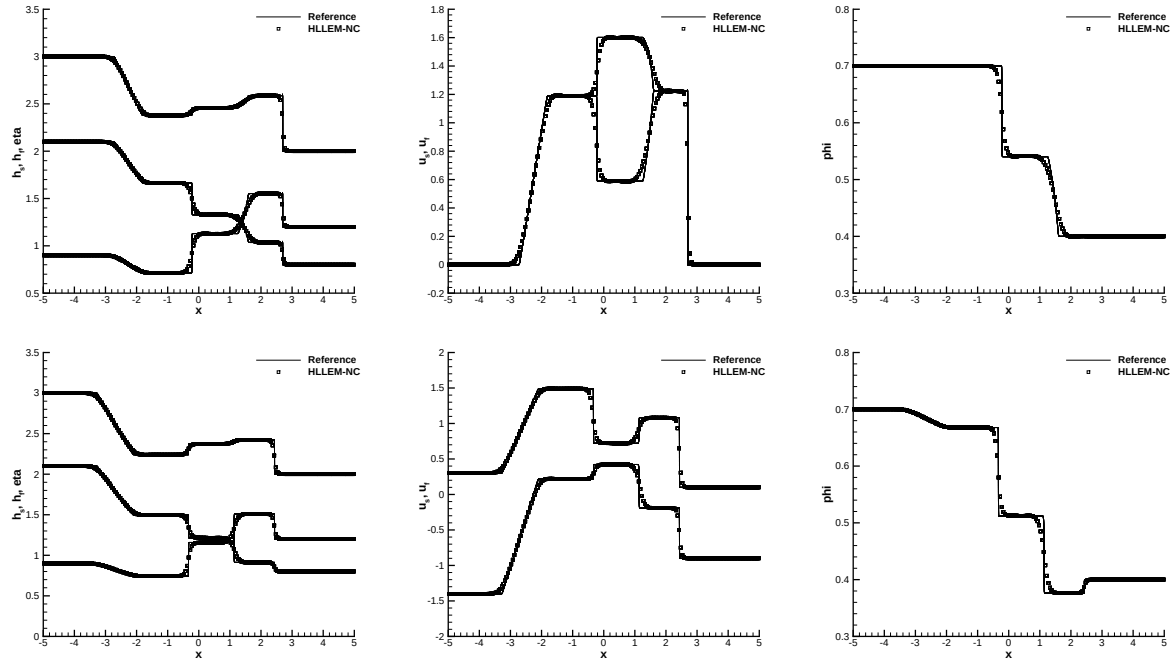

Figure 8: Reference solution and numerical solution for the Riemann problems RP1 (top) and RP2 (bottom) of the two-fluid debris flow model of Pitman & Le at time $t = 0.5$ using the path-conservative HLLEM scheme presented in this article. Left: free surface elevation η, depth functions h_s and h_f. Middle: velocities u_s and u_f of the solid and the fluid phase. Right: solid volume fraction ϕ.

which is also used here. Other choices for p_I and $\mathbf{v}_I$ are possible, see for example [81]. In the following, $j = 1 = s$ denotes the solid phase and $j = 2 = g$ the gas phase. The Baer-Nunziato model with one transverse flow velocity per phase, v_1 and v_2, respectively, contains five linearly degenerate fields, namely one entropy wave (contact discontinuity) and one shear wave within each single phase, and one material contact associated with a jump in the volume fraction ϕ_s. The associated eigenvalues and eigenvectors are

$$\mathbf{\Lambda}_* = \begin{pmatrix} u_1 & 0 & 0 & 0 & 0 \\ 0 & u_1 & 0 & 0 & 0 \\ 0 & 0 & u_1 & 0 & 0 \\ 0 & 0 & 0 & u_2 & 0 \\ 0 & 0 & 0 & 0 & u_2 \end{pmatrix}, \qquad \mathbf{L}_* = \begin{pmatrix} 0 & 0 & 1 & 0 & 0 & 0 & 0 & 0 & 0 \\ 1 & 0 & 0 & -\frac{1}{c_1^2} & 0 & 0 & 0 & 0 & \frac{p_2-p_1}{\phi_1 c_1^2} \\ 0 & 0 & 0 & 0 & 0 & 0 & 0 & 0 & \frac{\rho_2}{\phi_2\left((u_1-u_2)^2-c_2^2\right)} \\ 0 & 0 & 0 & 0 & 0 & 0 & 1 & 0 & 0 \\ 0 & 0 & 0 & 0 & 1 & 0 & 0 & -\frac{1}{c_2^2} & 0 \end{pmatrix} \frac{\partial \mathbf{V}}{\partial \mathbf{Q}}, \tag{61}$$

$$\mathbf{R}_* = \frac{\partial \mathbf{Q}}{\partial \mathbf{V}} \begin{pmatrix} 0 & 1 & 0 & 0 & 0 \\ 0 & 0 & 0 & 0 & 0 \\ 1 & 0 & 0 & 0 & 0 \\ 0 & 0 & \frac{\phi_2(p_2-p_1)\left((u_1-u_2)^2-c_2^2\right)}{\phi_1\rho_2} & 0 & 0 \\ 0 & 0 & (u_1-u_2)^2 & 0 & 1 \\ 0 & 0 & \frac{c_2^2(u_1-u_2)}{\rho_2} & 0 & 0 \\ 0 & 0 & 0 & 1 & 0 \\ 0 & 0 & c_2^2\,(u_1-u_2)^2 & 0 & 0 \\ 0 & 0 & \frac{\phi_2\left((u_1-u_2)^2-c_2^2\right)}{\rho_2} & 0 & 0 \end{pmatrix}, \qquad \frac{\partial \mathbf{V}}{\partial \mathbf{Q}} = \left(\frac{\partial \mathbf{Q}}{\partial \mathbf{V}}\right)^{-1}. \tag{62}$$

The matrix $\frac{\partial \mathbf{Q}}{\partial \mathbf{V}}$ denotes the derivative of the state vector $\mathbf{Q} = (\phi_1\rho_1, \phi_1\rho_1\mathbf{v}_1, \phi_1\rho_1 E_1, \phi_2\rho_2, \phi_2\rho_2\mathbf{v}_2, \phi_2\rho_2 E_2, \phi_1)$ with respect to the vector of primitive variables $\mathbf{V} = (\rho_1, \mathbf{v}_1, p_1, \rho_2, \mathbf{v}_2, p_2, \phi_1)$ and is given by

$$\frac{\partial \mathbf{Q}}{\partial \mathbf{V}} = \begin{pmatrix} \phi_1 & 0 & 0 & 0 & 0 & 0 & 0 & 0 & \rho_1 \\ \phi_1 u_1 & \phi_1\rho_1 & 0 & 0 & 0 & 0 & 0 & 0 & \rho_1 u_1 \\ \phi_1 v_1 & 0 & \phi_1\rho_1 & 0 & 0 & 0 & 0 & 0 & \rho_1 v_1 \\ \frac{1}{2}\phi_1\mathbf{v}_1^2 & \phi_1\rho_1 u_1 & \phi_1\rho_1 v_1 & \frac{\phi_1}{\gamma_1-1} & 0 & 0 & 0 & 0 & \frac{p_1+\gamma_1\pi_1}{\gamma_1-1} + \frac{1}{2}\rho_1\mathbf{v}_1^2 \\ 0 & 0 & 0 & 0 & \phi_2 & 0 & 0 & 0 & -\rho_2 \\ 0 & 0 & 0 & 0 & \phi_2 u_2 & \phi_2\rho_2 & 0 & 0 & -\rho_2 u_2 \\ 0 & 0 & 0 & 0 & \phi_2 v_2 & 0 & \phi_2\rho_2 & 0 & -\rho_2 v_2 \\ 0 & 0 & 0 & 0 & \frac{1}{2}\phi_2\mathbf{v}_2^2 & \phi_2\rho_2 u_2 & \phi_2\rho_2 v_2 & \frac{\phi_2}{\gamma_2-1} & -\frac{p_2+\gamma_2\pi_2}{\gamma_2-1} - \frac{1}{2}\rho_2\mathbf{v}_2^2 \\ 0 & 0 & 0 & 0 & 0 & 0 & 0 & 0 & 1 \end{pmatrix} \tag{63}$$

3.4.1. Numerical verification of the Abgrall condition

Any numerical scheme applied to the Baer-Nunziato model (57) should verify the so-called *Abgrall condition* [1, 81, 80], which states that a mixture of two phases moving with uniform velocity and pressure should exactly preserve this constant pressure and velocity field also at the discrete level.

Here, we verify the Abgrall condition numerically with a simple numerical experiment. The computational domain is $\Omega = [-0.5; +0.5]$, discretized with 400 equidistant control volumes. For the first phase (the solid phase) we use the stiffened gas EOS with $\gamma_1 = 3.0$ and $\pi_1 = 100$, whereas for the second phase (the gas phase) we simply set $\gamma_2 = 1.4$ and $\pi_2 = 0$. Initially, the pressures and velocities for both phases are $p_{1,2} = u_{1,2} = 1$. The densities are $\rho_{1,L} = 800$, $\rho_{2,L} = 2$ at the left and $\rho_{1,R} = 1000$, $\rho_{2,R} = 1$ at the right of the location $x = 0$. At the left of the discontinuity we set the solid volume fraction to $\phi_s = 0.99$, while $\phi_s = 0.01$ is used on the right. The Baer-Nunziato model is then solved with the HLLEM RS until $t = 0.25$. The results obtained for the velocities, the pressures and the solid volume fraction are depicted in Fig. 9. We find that the pressure and velocity remain constant up to machine precision (a maximum velocity error of 2.0561330410^{-13} was measured at the final time after 260 time steps).

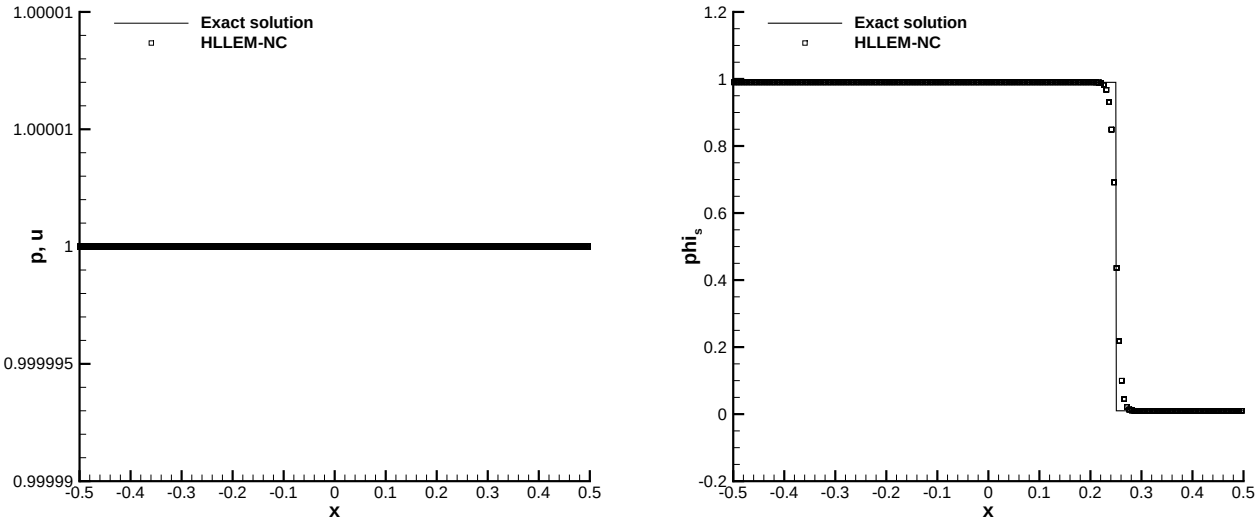

Figure 9: Numerical verification of the Abgrall condition. Left: pressures p_s, p_g and velocities u_s, u_g at the final time $t = 0.25$. Right: distribution of ϕ_s after $t = 0.25$ using the path-conservative HLLEM scheme proposed in this paper. No unphysical spurious pressure and velocity oscillations are visible.

3.4.2. Riemann problems

The first exact Riemann solver for the homogeneous Baer–Nunziato equations (57) was published by Andrianov and Warnecke in [3]. Their method was a so–called *inverse* Riemann solver that computed the initial states from a given wave–pattern of the solution. Later, direct exact Riemann solvers for the system (57) have been published by Schwendeman et al. in [83] and by Deledicque and Papalexandris in [35]. In this section, we solve six Riemann problems on the domain $\Omega = [-0.5; 0.5]$ using the path-conservative HLLEM scheme on a computational grid composed of 400 equidistant cells and using a CFL number of 0.9. Note that for the Baer-Nunziato system, it was necessary to scale all entries of the anti-diffusion matrix $\boldsymbol{\delta}$ of the HLLEM scheme by the constant factor $\varphi = 0.97$ in order to obtain stable solutions for Riemann problems RP3-RP6. The detailed initial conditions for Riemann problems RP1-RP6 are given in Table 5 and the computational results obtained with the HLLEM scheme are compared against the exact solution of the Riemann problem in Figs. 10-11. The same set of test problems has already been solved by a path-conservative FORCE method in [40] and a subset of this sequence of test problems was solved with a path-conservative extension of the Osher method in [44]. From our computational results we find overall a satisfactory agreement with the exact solution, despite some visible discrepancies. The quality of the computational results obtained with the new HLLEM scheme is comparable with the one obtained with other schemes presented in the literature for the Baer-Nunziato system, see [3, 83, 40, 44]. Very recently, a HLLC-type Riemann solver for the Baer-Nunziato system has been proposed by Tokareva and Toro in [87]. At this point we would like to underline that for general, complex hyperbolic PDE systems it is not always straightforward to construct such HLLC-type schemes, while the reformulated HLLEM–type Riemann solver presented in this paper is *automatic* for general conservative and non-conservative systems, as long as the eigenvalues and eigenvectors of intermediate linearly degenerate characteristic fields are known.

To conclude the discussion on the discretization of non-conservative hyperbolic PDE systems with the new HLLEM scheme, we run Riemann problem RP3 for the Baer-Nunziato model again, but using this time an increasing number of cells. The aim is to show that although path-conservative schemes are *formally consistent* with the definition of weak solutions in the sense of Dal Maso, Le Floch and Murat [63], the final result may still be dominated by the *numerical viscosity* present in the scheme. The computational results for this last test are depicted in Fig. 12, where one can easily observe that the method seems to converge to a solution that is only *close* to the exact solution, but still exhibits visible discrepancies. For a more detailed discussion on this topic, the reader is referred to [26].

3.5. The equations of magnetohydrodynamics (MHD)

In this section we solve the equations of classical, ideal magnetohydrodynamics (MHD). The augmented PDE system including the hyperbolic divergence–correction term proposed by Dedner et al. [33] reads

$$\frac{\partial}{\partial t}\begin{pmatrix} \rho \\ \rho\mathbf{v} \\ \rho E \\ \mathbf{B} \\ \psi \end{pmatrix} + \nabla\cdot\begin{pmatrix} \rho\mathbf{v} \\ \rho\mathbf{v}\mathbf{v} + p_m\mathbf{I} - \frac{1}{4\pi}\mathbf{B}\mathbf{B} \\ \mathbf{B}(\rho E + p_m) - \frac{1}{4\pi}\mathbf{B}(\mathbf{v}\cdot\mathbf{B}) \\ \mathbf{v}\mathbf{B} - \mathbf{B}\mathbf{v} + \psi\mathbf{I} \\ c_h^2\mathbf{B} \end{pmatrix} = 0, \tag{64}$$

with

$$p = (\gamma - 1)(\rho E - \frac{1}{2}\rho\mathbf{v}^2 - \frac{1}{8\pi}\mathbf{B}^2), \qquad p_m = p + \frac{1}{8\pi}\mathbf{B}^2. \tag{65}$$

Here, ρ is the gas density, $\mathbf{v} = (u, v, w)$ is the velocity vector, $\mathbf{B} = (B_x, B_y, B_z)$ is the vector of the magnetic field, not to be confounded with the matrix $\mathbf{B}(\mathbf{Q})$ of the non-conservative product in (1), which is zero in the case of the MHD equations (64). p is the gas pressure, p_m is the sum of the gas and the magnetic pressure, ρE is the total energy and γ is the ratio of specific heats. $\mathbf{I}$ is the identity matrix and the notation $\mathbf{x}_1\mathbf{x}_2 = \mathbf{x}_1 \otimes \mathbf{x}_2$ is a short hand notation for the dyadic product of two vectors. The scalar ψ is used for divergence cleaning, see [33], to satisfy the constraint $\nabla\cdot\mathbf{B} = 0$ approximately in multiple space dimensions. In one dimension, this constraint simply reduces to $\partial B_x/\partial x = 0$. For a detailed discussion on the origin of the divergence errors that arise in numerical discretizations of the MHD system, see [60, 61].

To our knowledge, this is the first time that a HLLEM Riemann solver is applied to the system of the ideal MHD equations (64). With our general formulation (28), the fluctuations follow very naturally once the eigenvalues and

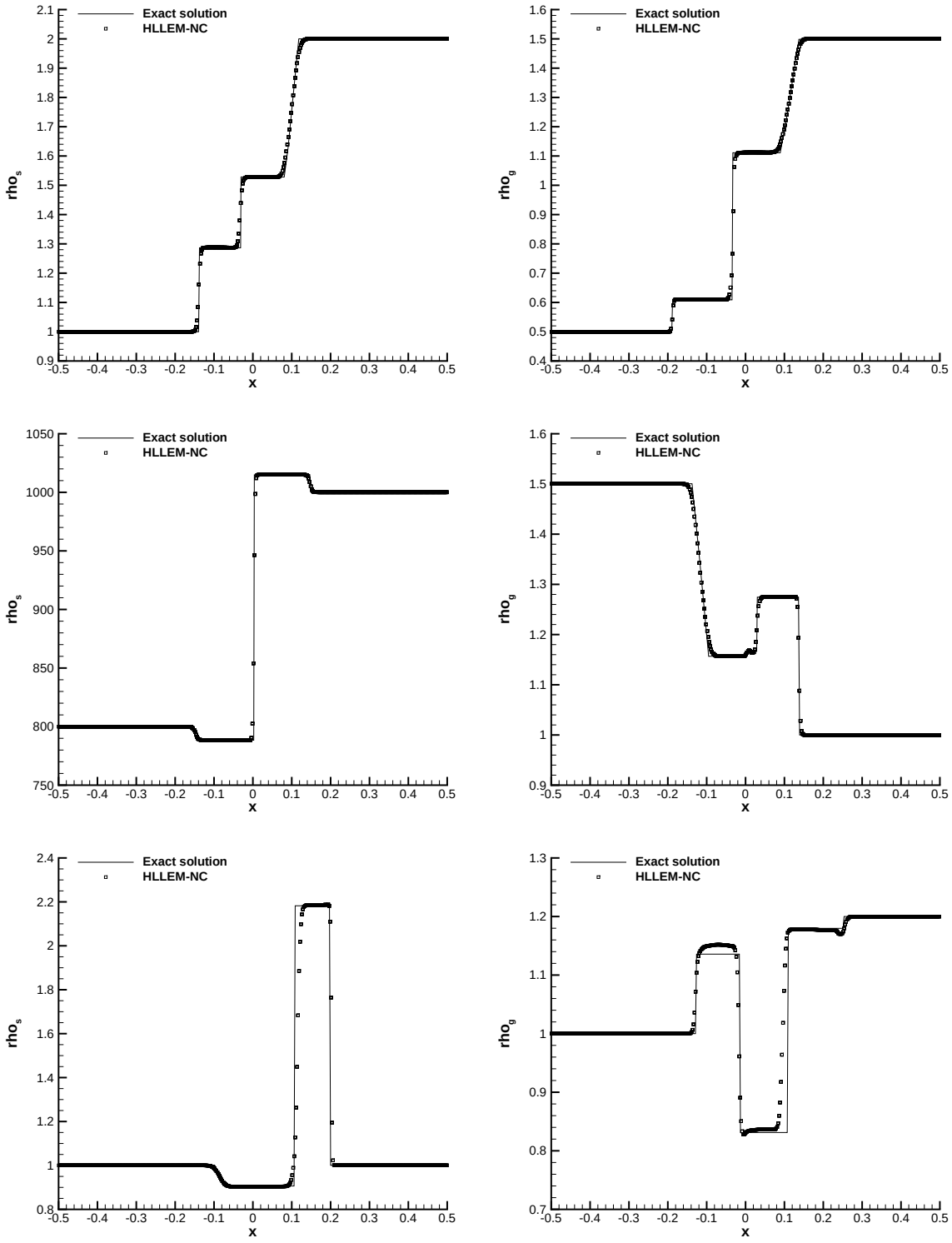

Figure 10: Computational results obtained for the Riemann problems RP1-RP3 (from top to bottom) with the path-conservative HLLEM scheme for the Baer-Nunziato model. Left: solid density ρ_s. Right: gas density ρ_g.

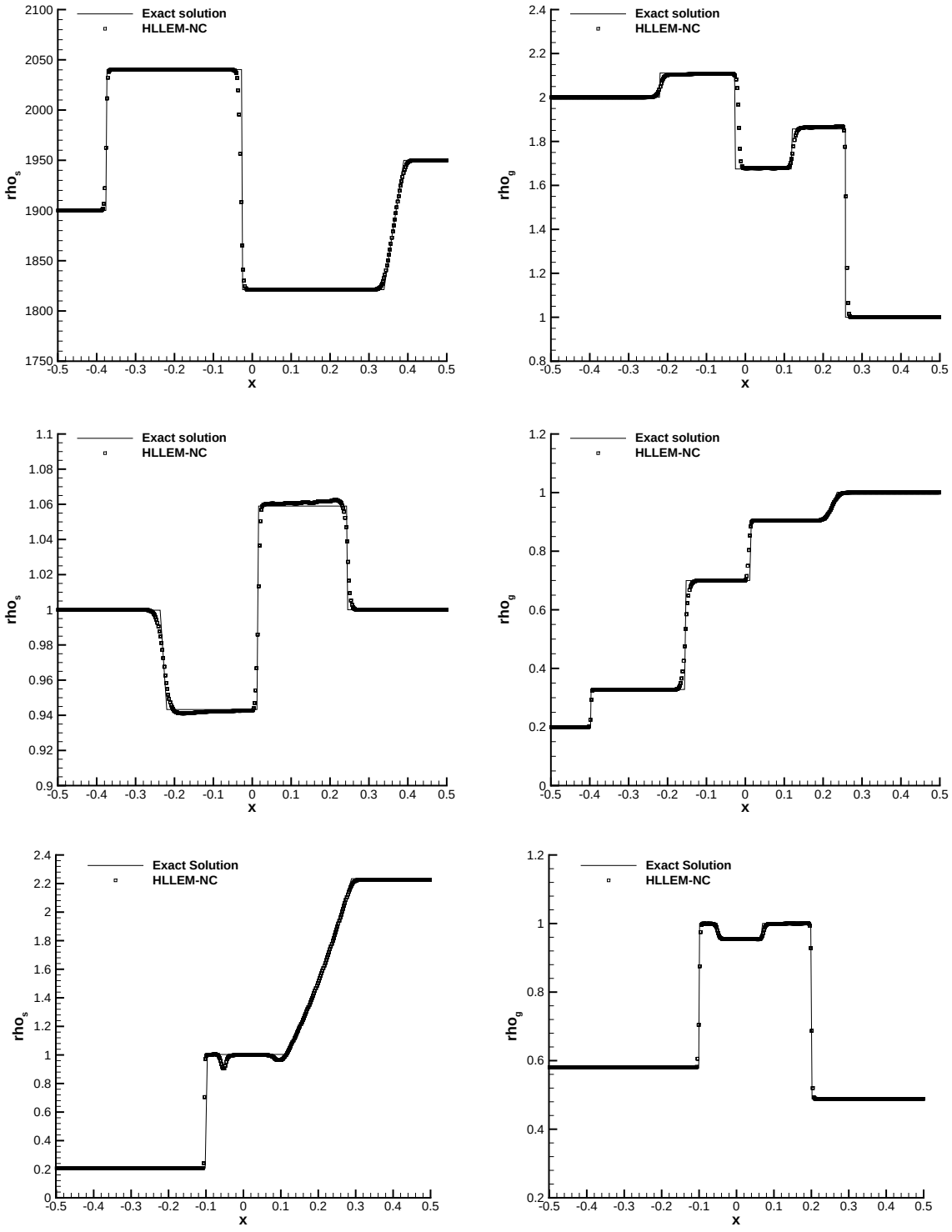

Figure 11: Computational results obtained for the Riemann problems RP4-RP6 (from top to bottom) with the path-conservative HLLEM scheme for the Baer-Nunziato model. Left: solid density ρ_s. Right: gas density ρ_g.

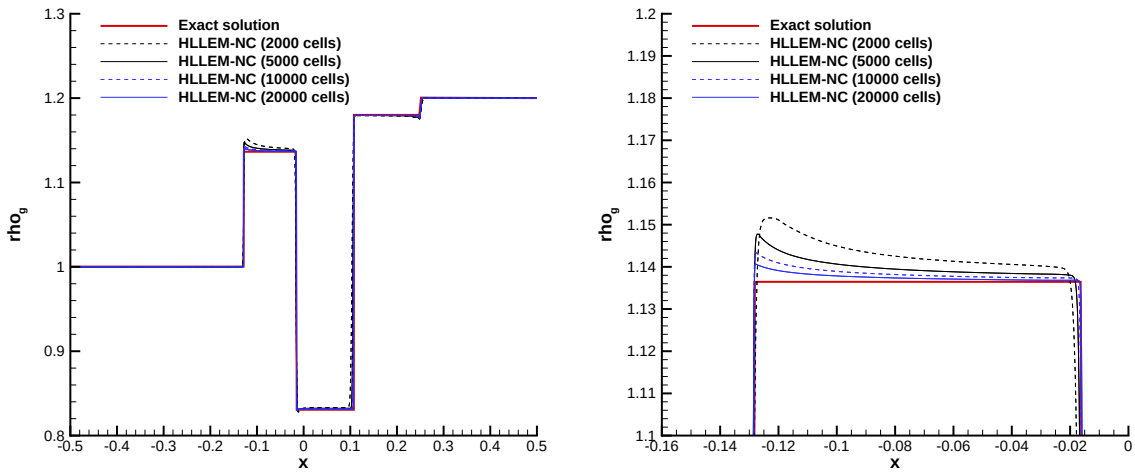

Figure 12: Computational results obtained for the Riemann problem RP3 with the path-conservative HLLEM scheme for the Baer-Nunziato model using an increasing number of cells. Left: gas density ρ_g. Right: zoom into the same results for $x < 0$.

the eigenvectors of the intermediate fields are known. For the MHD equations, the analytical eigenstructure has been published in the seminal paper of Roe and Balsara [77], hence our generalized HLLEM formulation (28) is immediately available also for this system. For the MHD equations, we decide to include *all* intermediate waves in $\mathbf{\Lambda}_*$, $\mathbf{R}_*$ and $\mathbf{L}_*$, also the slow magnetosonic waves, hence in this case the HLLEM scheme becomes a *complete* Riemann solver.

Table 5: Initial states left (L) and right (R) for the Riemann problems solved in 2D and 3D with the Baer-Nunziato model. Values for γ_i, π_i and the final time t_e are also given.

	ρ_s	u_s	p_s	ρ_g	u_g	p_g	ϕ_s	t_e
RP1 [35]:	$\gamma_s = 1.4$,	$\pi_s = 0$,	$\gamma_g = 1.4$,	$\pi_g = 0$				
L	1.0	0.0	1.0	0.5	0.0	1.0	0.4	0.10
R	2.0	0.0	2.0	1.5	0.0	2.0	0.8	
RP2 [35]:	$\gamma_s = 3.0$,	$\pi_s = 100$,	$\gamma_g = 1.4$,	$\pi_g = 0$				
L	800.0	0.0	500.0	1.5	0.0	2.0	0.4	0.10
R	1000.0	0.0	600.0	1.0	0.0	1.0	0.3	
RP3 [35]:	$\gamma_s = 1.4$,	$\pi_s = 0$,	$\gamma_g = 1.4$,	$\pi_g = 0$				
L	1.0	0.9	2.5	1.0	0.0	1.0	0.9	0.10
R	1.0	0.0	1.0	1.2	1.0	2.0	0.2	
RP4 [83]:	$\gamma_s = 3.0$,	$\pi_s = 3400$,	$\gamma_g = 1.35$,	$\pi_g = 0$				
L	1900.0	0.0	10.0	2.0	0.0	3.0	0.2	0.15
R	1950.0	0.0	1000.0	1.0	0.0	1.0	0.9	
RP5 [83]:	$\gamma_s = 1.4$,	$\pi_s = 0$,	$\gamma_g = 1.4$,	$\pi_g = 0$				
L	1.0	0.0	1.0	0.2	0.0	0.3	0.8	0.20
R	1.0	0.0	1.0	1.0	0.0	1.0	0.3	
RP6 [3]:	$\gamma_s = 1.4$,	$\pi_s = 0$,	$\gamma_g = 1.4$,	$\pi_g = 0$				
L	0.2068	1.4166	0.0416	0.5806	1.5833	1.375	0.1	0.10
R	2.2263	0.9366	6.0	0.4890	-0.70138	0.986	0.2	

Table 6: Initial states left and right for the density ρ, velocity vector $\mathbf{v} = (u, v, w)$, the pressure p and the magnetic field vector $\mathbf{B} = (B_x, B_y, B_z)$ for the ideal classical MHD equations. The final output times, ($t_{\rm end}$) and the initial position of the discontinuity (x_d) are also given.

Case	ρ	u	v	w	p	B_x	B_y	B_z	$t_{\rm end}$, x_d
RP1a L:	1.0	0.0	0.0	0.0	1.0	1.0	0.0	0.0	0.25
R:	0.1	0.0	0.0	0.0	1.0	1.0	0.0	0.0	0.0
RP1b L:	$\frac{1}{4\pi}$	-1.0	+1.0	-1.0	1.0	1.0	-1.0	+1.0	0.25
R:	$\frac{1}{4\pi}$	-1.0	-1.0	-1.0	1.0	1.0	1.0	+1.0	0.0
RP2 L:	1.0	0.0	0.0	0.0	1.0	$\frac{3}{4}\sqrt{4\pi}$	$\sqrt{4\pi}$	0.0	0.1
R:	0.125	0.0	0.0	0.0	0.1	$\frac{3}{4}\sqrt{4\pi}$	$-\sqrt{4\pi}$	0.0	0.0
RP3 L:	1.08	1.2	0.01	0.5	0.95	2.0	3.6	2.0	0.2
R:	0.9891	-0.0131	0.0269	0.010037	0.97159	2.0	4.0244	2.0026	-0.1
RP4 L:	0.15	21.55	1.0	1.0	0.28	0.05	-2.0	-1.0	0.04
R:	0.1	-26.45	0.0	0.0	0.1	0.05	2.0	1.0	0.0
RP5 L:	1.0	0.0	0.0	0.0	1.0	$1.3\sqrt{4\pi}$	$\sqrt{4\pi}$	0.0	0.16
R:	0.4	0.0	0.0	0.0	0.4	$1.3\sqrt{4\pi}$	$-\sqrt{4\pi}$	0.0	0.0
RP6 L:	1.0	36.87	-0.115	-0.0386	1.0	4.0	4.0	1.0	0.03
R:	1.0	-36.87	0.0	0.0	1.0	4.0	4.0	1.0	0.0
RP7 L:	1.7	0.0	0.0	0.0	1.7	3.899398	3.544908	0.0	0.15
R:	0.2	0.0	0.0	-1.496891	0.2	3.899398	2.785898	2.192064	-0.1

In the following, we apply our approach to a set of Riemann problems already used for the validation of the Osher-type scheme [45]. The initial conditions for the shock tube problems are listed in Table 6 and the ratio of specific heats is $\gamma = \frac{5}{3}$ for all cases apart for RP1a and RP1b, where it is $\gamma = 1.4$. We solve all shock–tube problems on a mesh of 400 equidistant cells, apart from RP1, where only 200 zones are used. The computational results obtained with the second order version of our generalized HLLEM scheme (28) and those obtained with a classical HLL method (23) are depicted in Figs. 13 and 14, together with the exact solution. Riemann problems RP1a and RP1b consist in a steady contact wave and an isolated steady Alfvén wave. Both steady waves are perfectly well captured with the new generalized HLLEM scheme, while there is visible smearing present due to excessive numerical dissipation in the case of the standard HLL scheme. This result is expected, since the HLLEM methods accounts for all linearly degenerate intermediate waves using a piecewise linear representation of the intermediate HLL state (26), while the original HLL scheme does not. The exact Riemann solver for MHD has kindly been provided by S.A.E.G. Falle [48]. For an alternative exact Riemann solver of the MHD equations, see also [92].

3.6. Euler Equations of Compressible Gas Dynamics with general EOS

In the following, we consider the augmented Euler equations of compressible gasdynamics with transverse velocity

$$\frac{\partial}{\partial t}\begin{pmatrix}\rho\\ \rho u\\ \rho v\\ \rho E\end{pmatrix}+\frac{\partial}{\partial x}\begin{pmatrix}\rho u\\ \rho u^2+p\\ \rho uv\\ u(\rho E+p)\end{pmatrix}=0, \tag{66}$$

where, ρ denotes the fluid density, $\mathbf{v} = (u, v)$ is the velocity vector, $\rho E = \rho e + \frac{1}{2}\rho\mathbf{v}^2$ is the total energy density, e is the specific internal energy and p is the fluid pressure. Furthermore, we will use the specific total enthalpy $h = (\rho E + p)/\rho$ and the fluid temperature T. The system (66) is closed by a general equation of state (EOS) of the form

$$p = p(\rho, e), \qquad T = T(\rho, e). \tag{67}$$

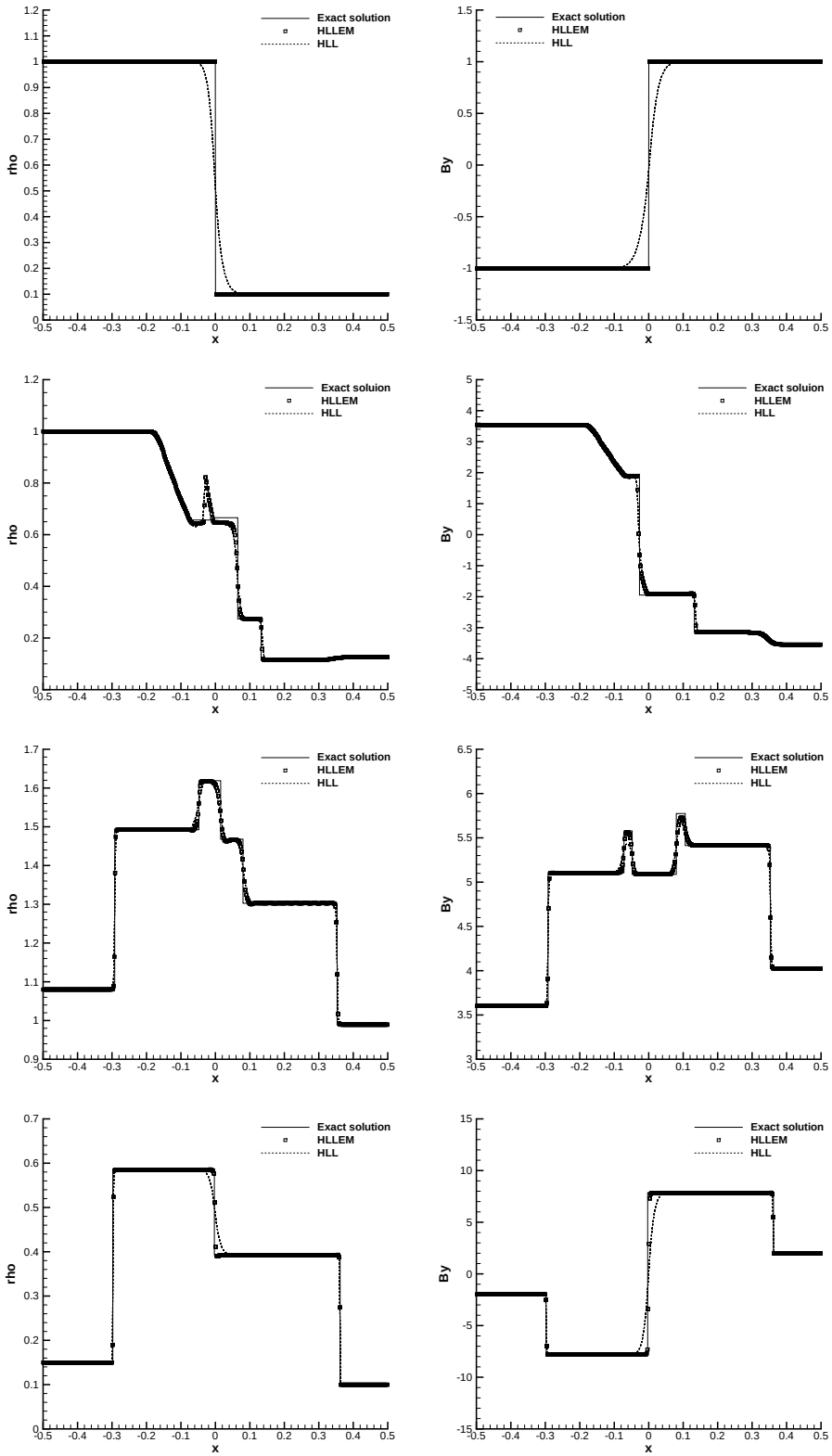

Figure 13: Riemann problems RP1-RP4 (from top to bottom) for the ideal classical MHD equations. Left: mass density. Right: Magnetic field component B_y.

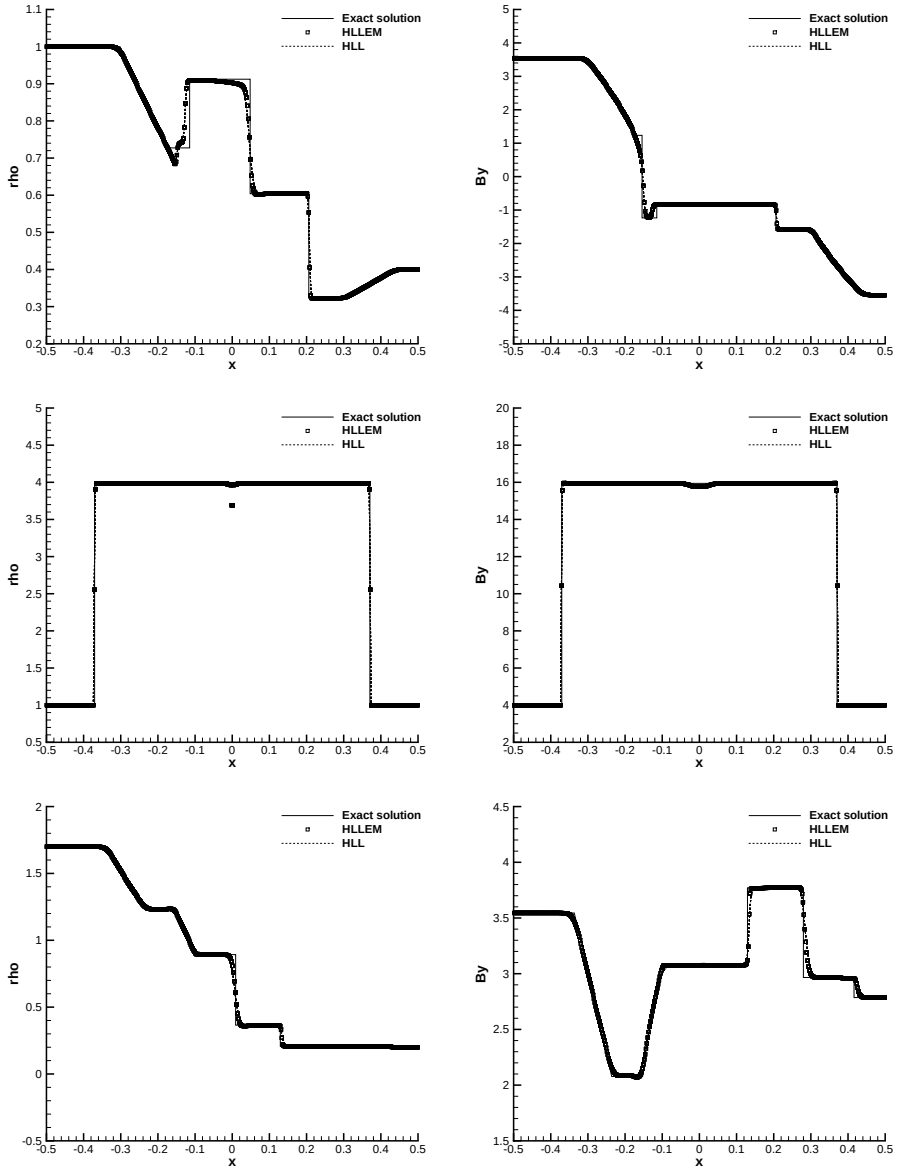

Figure 14: Riemann problems RP5-RP7 (from top to bottom) for the ideal classical MHD equations. Left: mass density. Right: Magnetic field component B_y.

In the case of a general EOS (67), the sound speed in the fluid is given by

$$c = \sqrt{\frac{\partial p}{\partial \rho} + \frac{p}{\rho^2}\frac{\partial p}{\partial e}}. \tag{68}$$

In this paper, we consider explicit Godunov-type finite volume schemes based on the HLLEM Riemann solver. For recent developments on alternative semi-implicit finite volume methods for compressible gas dynamics with general equation of state, the reader is referred to [41, 38].

The Euler system has two linear degenerate waves, both moving with velocity u. The first one is the entropy wave (contact discontinuity), the second one is the shear wave associated with jumps in the transverse velocity v. Since these two are the only intermediate fields of the compressible Euler equations, the HLLEM method becomes a *complete* Riemann solver in this case. The eigenvalues and eigenvectors associated with these linearly degenerate fields are

$$\mathbf{\Lambda}_* = \begin{pmatrix} u & 0 \\ 0 & u \end{pmatrix}, \qquad \mathbf{R}_* = \begin{pmatrix} 1 & 0 \\ u & 0 \\ 0 & 1 \\ \alpha & v \end{pmatrix}, \qquad \mathbf{L}_* = \frac{1}{\beta}\begin{pmatrix} \mathbf{v}^2 - h & -u & -v & 1 \\ v(u^2-\alpha) & -uv & \alpha - h & v \end{pmatrix}, \tag{69}$$

where we have used the abbreviations $\alpha = \rho E/\rho - \rho\frac{\partial p}{\partial \rho}/\frac{\partial p}{\partial e} - v^2$ and $\beta = -(\rho\frac{\partial p}{\partial \rho}/\frac{\partial p}{\partial e} + p/\rho)$.

3.6.1. Ideal gas EOS

In the case of an ideal gas, the EOS is given by the simple relation

$$p(\rho, e) = (\gamma - 1)\rho e, \tag{70}$$

with the ratio of specific heats γ. In this paragraph, we therefore use first the simple ideal gas EOS (70) with $\gamma = 1.4$, solving a well–known set of shock–tube problems that has been proposed and explained by Toro in great detail in [90]. In this reference, also all the necessary information about the exact solution of the Riemann problem is provided. The left and right initial states for the Riemann problems are summarized in Table 7. The computational domain is $\Omega = [-\frac{1}{2}; \frac{1}{2}]$ and is discretized with 200 equidistant cells. In Figs. 15 and 16 we present the exact solution of Riemann problems RP0–RP6 together with the computational results obtained with the new generalized HLLEM scheme (28). For comparison, we also plot the numerical solution obtained with the standard HLL method (23) The Riemann problem RP0 consists of a simple stationary contact discontinuity, onto which a shear wave is superimposed. From the computational results of this test problem depicted in 15 we can conclude that the HLLEM method properly resolves stationary shear and contact waves, while the HLL method does not (as expected). For the other test cases we note that the new generalized HLLEM flux is robust, even for RP2, where very low densities are produced. For a detailed discussion on this topic, see the original papers on the HLLEM scheme by Einfeldt et al. [46, 47]. Also note that the HLLEM scheme does *not* produce the well-known sonic glitch for RP1, unlike the original Riemann solver of Roe [76].

3.6.2. Complex EOS of real fluids

After the validation on the simple ideal gas EOS, we can now move to a complex equation of state for a real fluid. In particular, we consider the EOS of n-heptane, which has been provided by Span and Wagner in [84]. In order to evaluate the complex EOS in a computationally efficient manner, we use the L_2-projection technique of the EOS $(\rho, e) \rightarrow (T, p)$ onto piecewise high order polynomials in combination with adaptive mesh refinement (AMR) and Cartesian cut-cells in phase-space proposed by Dumbser et al. in [42]. In this reference, also a quasi-exact Riemann solver for general EOS including phase transition was presented. In the following, we solve three of the Riemann problems for n-heptane proposed in [42], from where we have also taken the numbering of the problems. The detailed initial conditions are summarized in Table 8.

Note that in the case of phase-transition, the equation of state $(\rho, e) \rightarrow (T, p)$ is *not* invertible inside the wet steam region, since there the pressure and the temperature are no longer independent variables, but they are directly coupled by the relation $p = p_{\text{sat}}(T)$, where $p_{\text{sat}}(T)$ is the saturation pressure for a given temperature T. Within the

Table 7: Initial states left and right for the density ρ, velocity u and the pressure p for the compressible Euler equations. The final output times, (t_{end}) and the initial position of the discontinuity (x_d) are also given.

Case	ρ_L	u_L	v_L	p_L	ρ_R	u_R	v_R	p_R	t_{end}	x_d
RP0	1.0	0.0	1.0	1.0	0.1	0.0	2.0	1.0	0.5	0.0
RP1	1.0	0.75	0.0	1.0	0.125	0.0	0.0	0.1	0.2	-0.1
RP2	1.0	-2.0	0.0	0.4	1.0	2.0	0.0	0.4	0.15	0.0
RP3	1.0	0.0	0.0	1000	1.0	0.0	0.0	0.01	0.012	0.1
RP4	5.99924	19.5975	0.0	460.894	5.99242	-6.19633	0.0	46.095	0.035	-0.2
RP5	1.0	-19.59745	0.0	1000.0	1.0	-19.59745	0.0	0.01	0.012	0.3
RP6	1.0	2.0	0.0	0.1	1.0	-2.0	0.0	0.1	0.8	0.0

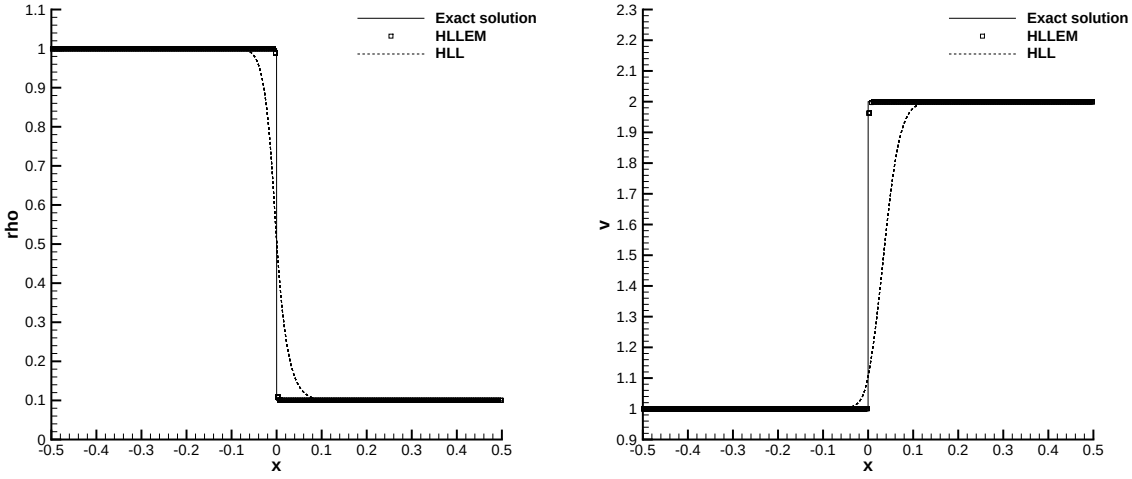

Figure 15: Riemann problem RP0 for the Euler equations of compressible gas dynamics with ideal gas EOS. Second order results for the density ρ (left) and the transverse velocity v (right), obtained on 200 equidistant cells.

wet steam region, a new independent parameter is therefore needed to fully characterize the physical state of the fluid. This parameter is the vapor mass fraction μ, from which density and internal energy can be computed for a given temperature T as

$$\frac{1}{\rho} = \frac{1-\mu}{\rho_l} + \frac{\mu}{\rho_v}, \qquad e = (1-\mu)e_l + \mu\, e_v, \tag{71}$$

where $\rho_l = \rho_l(T)$ is the liquid density and $\rho_v = \rho_v(T)$ is the vapour density of the mixture. $e_l = e_l(T)$ and $e_v = e_v(T)$ denote the liquid and vapour internal energy, respectively, and the pressure is given by $p = p_{\text{sat}}(T)$. See any standard textbook on thermodynamics on this subject [5].

Riemann problem RP-H3:. This test problem is a very stringent one, with a pressure jump over three orders of magnitude and where the solution of the Riemann problem crosses the entire wet–steam region, i.e. the vapour mass fraction μ takes all values from zero to one. The left state of this test case is pure liquid ($\mu = 0$) while the right state is pure vapor ($\mu = 1$). The quasi-exact solution for the intermediate states in the star region is given in [42]. The wet–steam region is crossed within the left–running rarefaction fan. There, one observes an interesting physical effect that is known to happen in flows with phase transition. As soon as the vapor pressure is reached, the speed of sound significantly drops over two orders of magnitude. In our case here from $c \approx 711.55$ to $c \approx 3.755$. This causes the

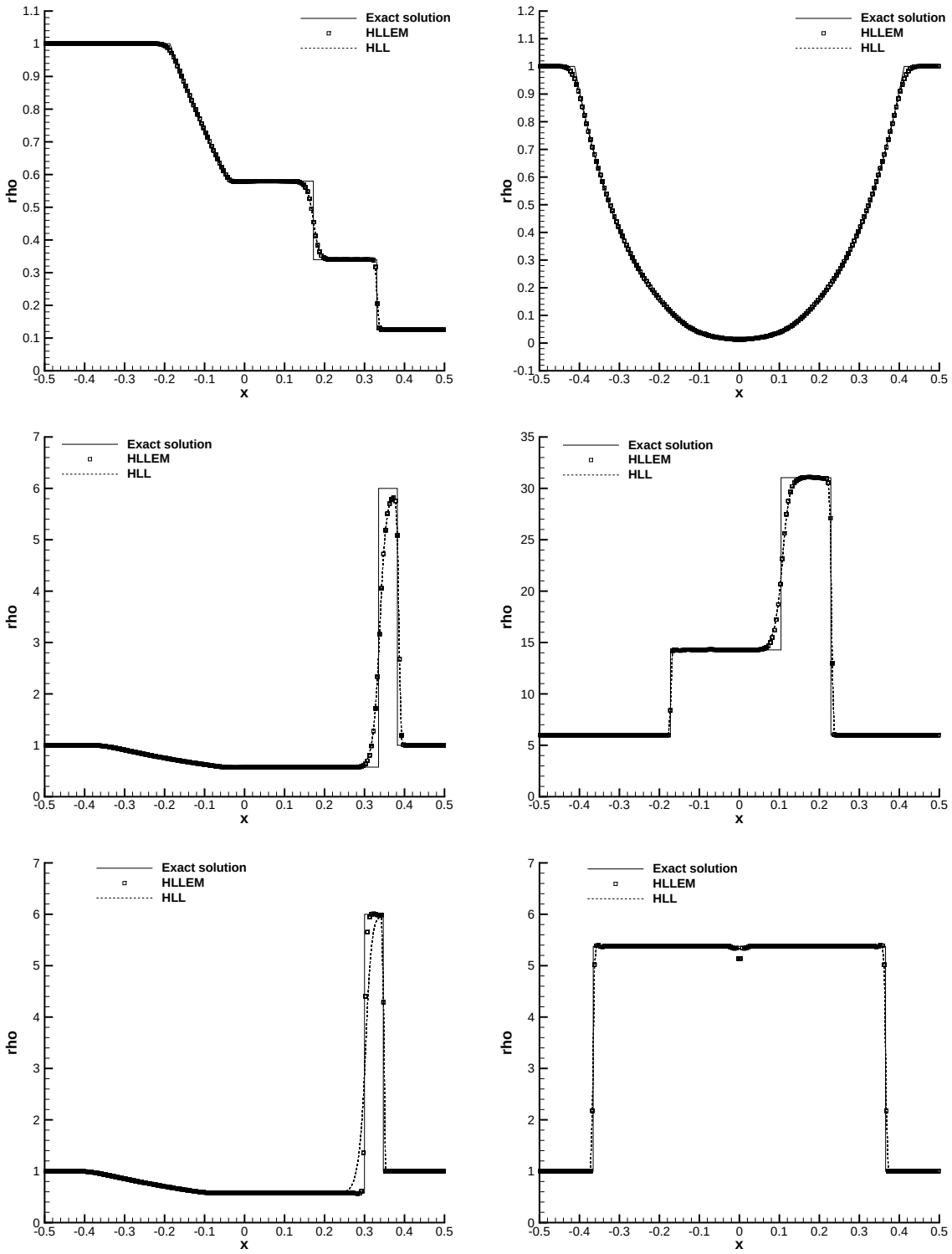

Figure 16: Riemann problems RP1-RP6 (from top left to bottom right) for the Euler equations of compressible gas dynamics with ideal gas EOS. Second order results for the density ρ, obtained on 200 equidistant cells.

rarefaction fan to be *split* into two pieces. One part is the rarefaction inside the pure liquid region with a fast sound speed and the other part is inside the wet–steam region with a very low speed of sound. The discontinuity in c causes the coordinate $\xi = x/t = u - c$ to jump instantaneously from the tail characteristic of the first part of the rarefaction fan inside the liquid region to the head–characteristic of the second part of the same rarefaction fan in the wet–steam region, see the sketch of the structure of the Riemann problem in Fig. 17 in the $x - t$–plane. For a more detailed discussion of this phenomenon, the reader is referred to [31, 68, 42]. In this test problem, the wet–steam region is left at the contact discontinuity, where the vapor pressure rises significantly due to the increased temperature and hence the fluid fully evaporates ($\mu = 1$). These phenomena are correctly captured in our numerical simulations shown in Fig. 18. The wave pattern agrees *qualitatively* with the one found by Saurel et al. in [82] (see Figure 10 in reference [82]) based on a non-equilibrium PDE model. Despite the complex wave structure of this Riemann problem, the agreement between the quasi–exact solution and the numerical results obtained with the HLLEM RS is excellent. Note that it was not possible to solve this problem with the generalized Osher-type Riemann solver [45].

Riemann problem RP-H5:. In this Riemann problem the initial data consist of pure liquid, subject to a strongly divergent flow. This causes two rarefaction waves which lead to a significant drop of the pressure so that the vapor pressure is reached and hence a *cavitation bubble* is produced. As in the shock tube problem RP-H3, the sudden drop of the speed of sound in the wet–steam region causes the rarefaction waves to split and two new intermediate zones $\tilde{Q}_L$ and $\tilde{Q}_R$ appear, see Fig. 19. Due to the symmetry of the problem, there is only one state in the star region. The computational results obtained with the second order order finite volume method based on the HLLEM RS are compared with the quasi–exact reference solution [42] in Fig. 20. Like in the previous test problem, we find a good agreement between the two solutions. The same wave pattern has been found by Saurel et al. for a similar problem in [82] (see reference [82], Figures 15 and 17).

Riemann problem RP-H6:. The initial states of this shock tube problem consist of wet–steam on the left and pure vapor on the right. The initial vapor mass fractions are given by $\mu_L = 0.25$ and $\mu_R = 1.0$. The wave pattern of this test problem is a classical one with a left–moving rarefaction, an intermediate contact and a right–moving shock. The quasi–exact solution is depicted in Fig. 21 and is compared against the numerical solution obtained by the HLLEM Riemann solver. Overall, we note a very good agreement.

3.7. The Equations of Nonlinear Elasticity

In this last section we consider the equations of nonlinear hyper-elasticity (NLE) as derived by Godunov and Romenski in Eulerian coordinates in [52, 53, 54]. This very interesting system has been studied numerically for example in [86, 36, 45], where either simple centered–type numerical fluxes or a new, universal formulation of the Osher Riemann solver have been used. Exact solutions for the Riemann problem of the nonlinear elasticity equations have first been presented in [86, 15]. In this article we apply the HLLEM Riemann solver for the first time to these

Table 8: Initial data of three Riemann problems for n–heptane taken from [42]. The initial location of the discontinuity x_c and the final simulation time t_e are also listed for each problem.

	ρ	u	p	e	T	μ
RP-H3: left state liquid, right state vapor. $x_c = 0.0$, $t_e = 1.0 \cdot 10^{-3}$						
Left	600.0	0.0	$1.0 \cdot 10^7$	$-1.0827852 \cdot 10^5$	406.63151	0.0
Right	0.25	0.0	$1.0 \cdot 10^4$	$3.3981878 \cdot 10^5$	482.98821	1.0
RP-H5: initially liquid, cavitation by rarefaction. $x_c = 0.0$, $t_e = 1.0 \cdot 10^{-3}$						
Left	550.0	-100.0	$2.0 \cdot 10^6$	$-1.4080779 \cdot 10^4$	437.31057	0.0
Right	550.0	+100.0	$2.0 \cdot 10^6$	$-1.4080779 \cdot 10^4$	437.31057	0.0
RP-H6: left state wet–steam, right state vapor. $x_c = -0.5$, $t_e = 2.0 \cdot 10^{-3}$						
Left	115.414555	0.0	$1.0119333 \cdot 10^6$	$1.4965669 \cdot 10^5$	475.0	0.25
Right	0.5	0.0	$1.5 \cdot 10^4$	$8.8179442 \cdot 10^4$	364.49192	1.0

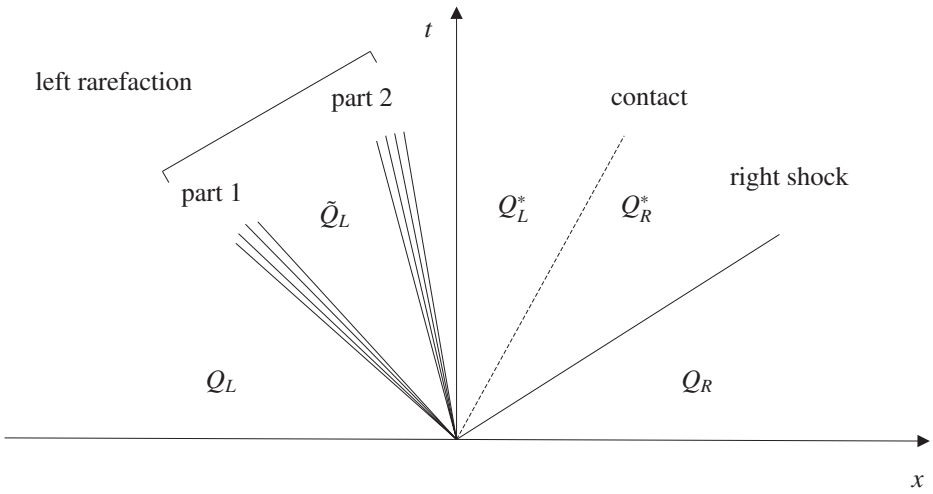

Figure 17: Sketch of the wave pattern of Riemann problem RP-H3. The left rarefaction fan is split into two parts ([68, 31]) due to the instantaneous drop of the speed of sound as soon as the wet–steam region is reached. A new region with piecewise constant intermediate state $\tilde{Q}_L$ appears.

complex equations. We follow the notation of Titarev et al. [86] and Barton et al. [15], hence the governing PDE system reads

$$\begin{aligned}
\frac{\partial \rho}{\partial t} + \frac{\partial (\rho u_k)}{\partial x_k} &= 0, \\
\frac{\partial \rho u_i}{\partial t} + \frac{\partial (\rho u_i u_k - \sigma_{ik})}{\partial x_k} &= 0, \\
\frac{\partial \rho F_{ij}}{\partial t} + \frac{\partial (\rho F_{ij} u_k - \rho F_{kj} u_i)}{\partial x_k} &= 0, \\
\frac{\partial \rho E}{\partial t} + \frac{\partial (\rho u_k E - u_i \sigma_{ik})}{\partial x_k} &= 0.
\end{aligned} \tag{72}$$

Here ρ is the density u_i is the velocity vector, F_{ij} is the deformation gradient and σ_{ik} is the stress tensor. The density equation and one of the equations for ρF_{ij} are redundant. In order to guarantee exact mass conservation, we therefore prefer to use the equation for density, which replaces one equation for the deformation gradient, say ρF_{11}. This procedure has been adopted in [86], which we follow in this paper. The total energy density is defined as usual as $\rho E = \rho(e + \frac{1}{2} u_i u_i)$. The stress tensor σ_{ij} is a complicated nonlinear function of the deformation gradient F_{ij} and depends on the equation of state (EOS) that is needed to close the system. The EOS defines the internal energy e as a function of the the deformation gradient F_{ij} and entropy S as $e = e(F_{ij}, S)$. Then, the following definitions for density ρ, strain tensor g_{ij}, stress tensor σ_{ij} and temperature T hold:

$$\rho = \frac{\rho_0}{\det(F)}, \quad G = g_{ij} = F^{-T} F^{-1}, \quad \sigma_{ik} = \rho F_{ij} \frac{\partial e}{\partial F_{kj}} = -2\rho g_{ij} \frac{\partial e}{\partial g_{jk}}, \quad T = \frac{\partial e}{\partial S}, \tag{73}$$

where ρ_0 is a constant reference density. In an isotropic medium, the internal energy e is a function of three invariants of the strain tensor g_{ij}:

$$e(I_1, I_2, I_3) = \frac{K_0}{2\alpha^2} \left(I_3^{\alpha/2} - 1 \right)^2 + c_V T_0 I_3^{\gamma/2} \left(e^{S/c_V} - 1 \right) + \frac{B_0}{2} I_3^{\beta/2} \left(\frac{1}{3} I_1^2 - I_2 \right), \tag{74}$$

with the invariants

$$I_1 = \operatorname{tr}\left(g_{ij}\right) = g_{11} + g_{22} + g_{33}, \quad I_3 = \det\left(g_{ij}\right) = \left(\frac{\rho}{\rho_0} \right)^2,$$

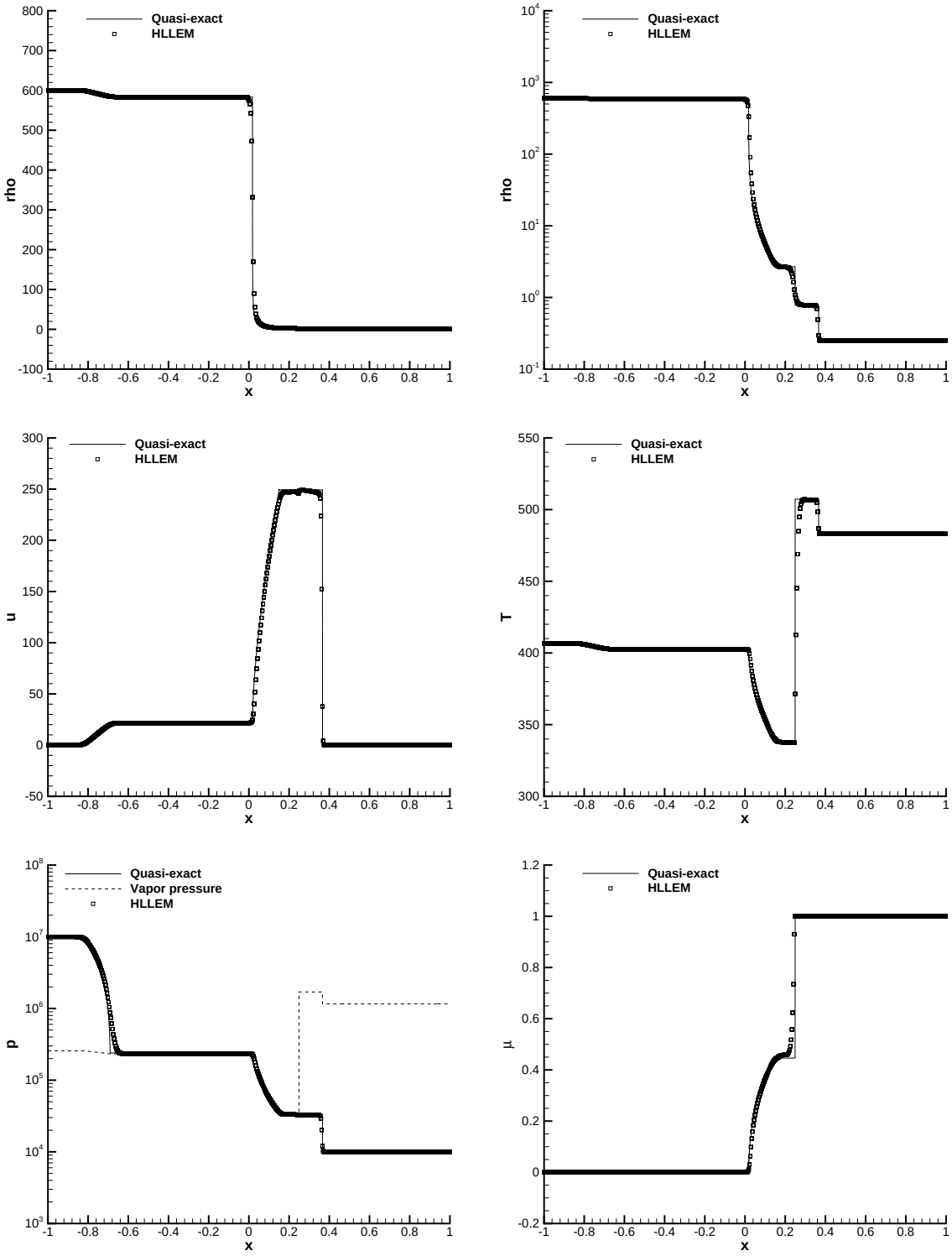

Figure 18: Quasi–exact solution and second order results obtained with the new formulation of the HLLEM Riemann solver on 500 grid points at time $t = 1.0 \cdot 10^{-3}$ for density, velocity, temperature, pressure and vapor mass fraction of the Riemann problem RP-H3 for n–heptane.

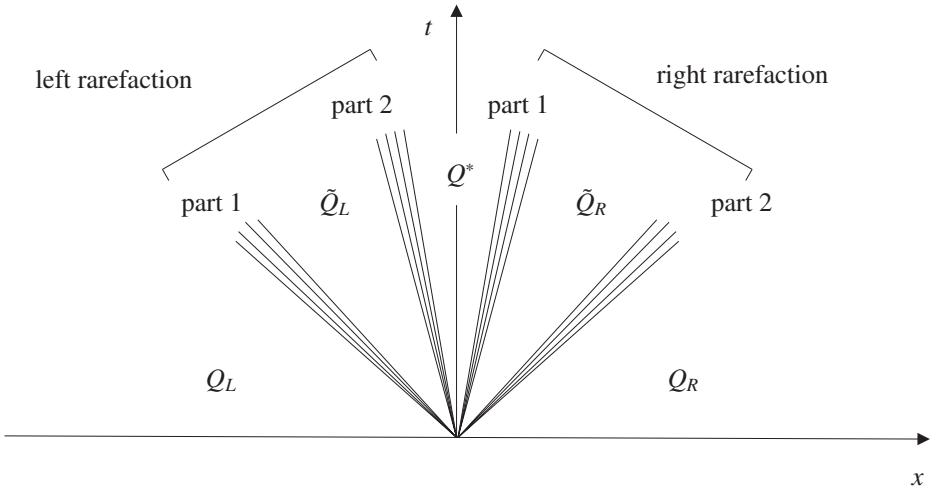

Figure 19: Sketch of the wave pattern of Riemann problem RP-H5. In this symmetric problem the left and right rarefaction are split [31, 68] into two parts due to the instantaneous drop of the speed of sound in the wet–steam region. Two new intermediate regions with piecewise constant states $\tilde{Q}_L$ and $\tilde{Q}_R$ appear. Due to the symmetry of the problem, there is only one state Q^* in the star region.

$$I_2 = (g_{11}g_{22} - g_{12}g_{21}) + (g_{22}g_{33} - g_{23}g_{32}) + (g_{33}g_{11} - g_{31}g_{13}) \,. \tag{75}$$

According to [86], K_0 and B_0 are the squared speed of the pressure and the shear wave, respectively, c_V is the heat capacity at constant volume, T_0 is the reference temperature and α, β and γ are constants characterizing the non-linearities in the EOS. For the details on the eigenstructure of this system, see [15].

We solve two of the one-dimensional shock tube problems proposed in [86] using the new generalized HLLEM flux (30). The material properties for copper are chosen as in [86], i.e. we use $\rho_0 = 8.9$, $K_0 = c_0^2 - \frac{4}{3}b_0^2$, $B_0 = b_0^2$, $c_0 = 4.6$, $b_0 = 2.1$, $T_0 = 300$ and $c_v = 0.4 \cdot 10^{-3}$. We set furthermore $\alpha = 1$, $\beta = 3$ and $\gamma = 2$. The computational domain is chosen as $\Omega = [0; 1]$ using 200 cells. Transmissive boundaries are imposed in x-direction. The initial condition consists of two piecewise constant states, separated by a discontinuity at $x = 0.5$. The initial states for all test cases are given in terms of the primitive variables in Table 9.

The first problem RP0 consists of an isolated, steady contact discontinuity, which is almost perfectly well resolved by the new HLLEM Riemann solver, while it is significantly smeared by a standard HLL RS, even in the context of the second order TVD finite volume scheme that has been applied here. RP1 corresponds to the three-wave shock tube problem and test case RP2 corresponds to the five-wave shock tube problem described in [86]. The second test case consists of two pieces of material that have been subject to different strain conditions and that are subsequently attached to each other. Dr. Titarev kindly provided us with the exact solution of the three-wave shock tube problem and with the numerical reference solution of the five-wave shock tube problem, as published in [86]. The numerical results obtained with the new HLLEM RS are compared against the reference solution for all test cases in Fig. 22. For comparison, also the results obtained with a classical HLL RS are shown. As expected, the HLLEM Riemann solver behaves much better compared to the simple HLL flux, in particular at the slowly-moving inner waves.

3.8. Ideal Relativistic MHD Equations (RMHD)

The ideal relativistic MHD equations (RMHD) form an extremely challenging nonlinear hyperbolic PDE system, since they have the additional difficulty with respect to the previous PDE that the primitive variables needed for expressing the flux $\mathbf{F}(\mathbf{Q})$ can *not* be expressed analytically in terms of the conserved quantities $\mathbf{Q}$. Instead, iterative procedures are necessary to compute $\mathbf{F}(\mathbf{Q})$ for a given state vector $\mathbf{Q}$, see e.g. [7, 95]. More details about this very interesting hyperbolic system can be found in [7, 95, 50, 58, 64, 65, 96, 73, 4]. The RMHD system reads

$$\frac{\partial \mathbf{Q}}{\partial t} + \nabla \cdot \mathbf{F}(\mathbf{Q}) = 0, \tag{76}$$

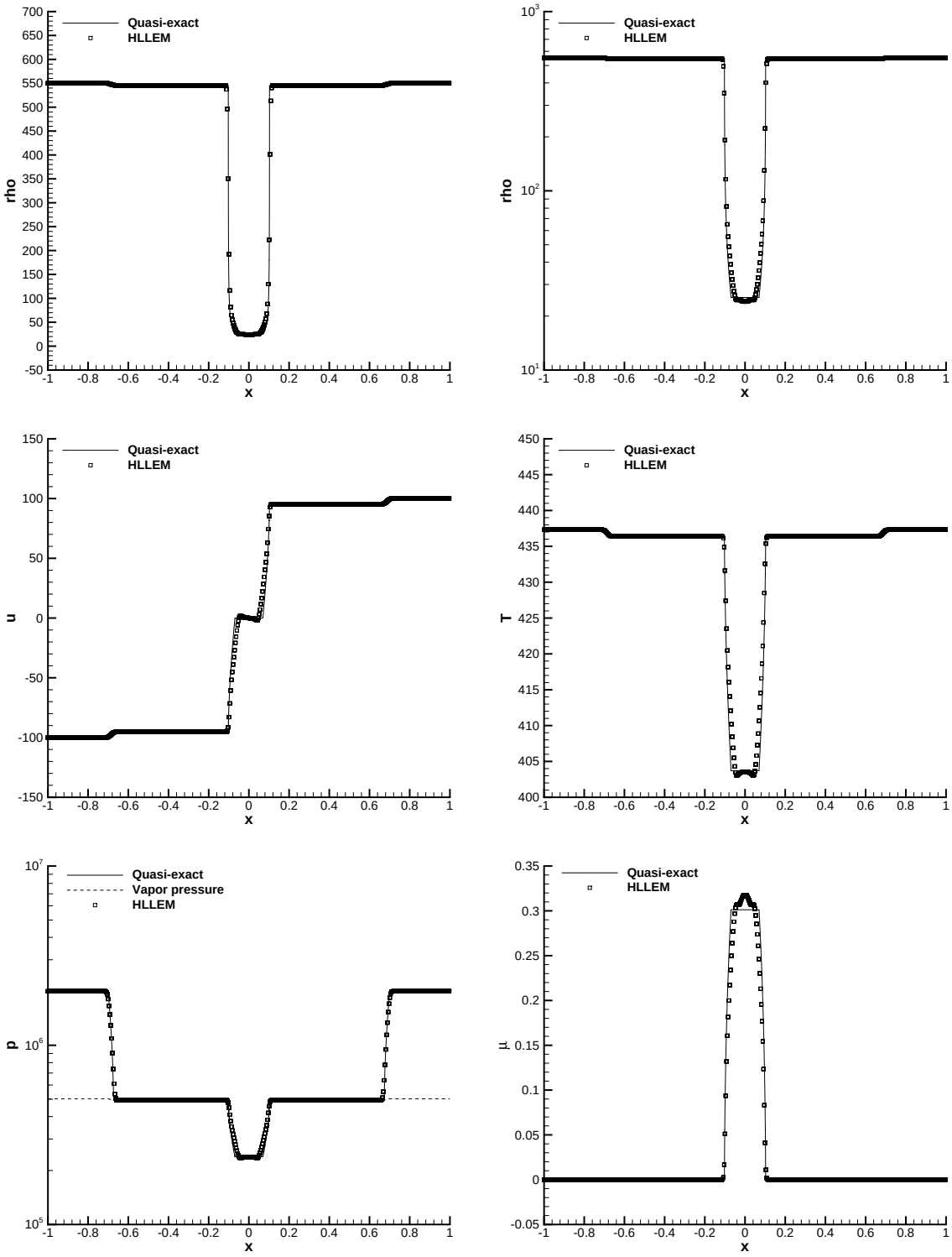

Figure 20: Quasi–exact solution and second order results obtained with the new formulation of the HLLEM Riemann solver on 2000 grid points at time $t = 1.0 \cdot 10^{-3}$ for density, velocity, temperature, pressure and vapour volume fraction of the Riemann problem RP-H5 for n–heptane.

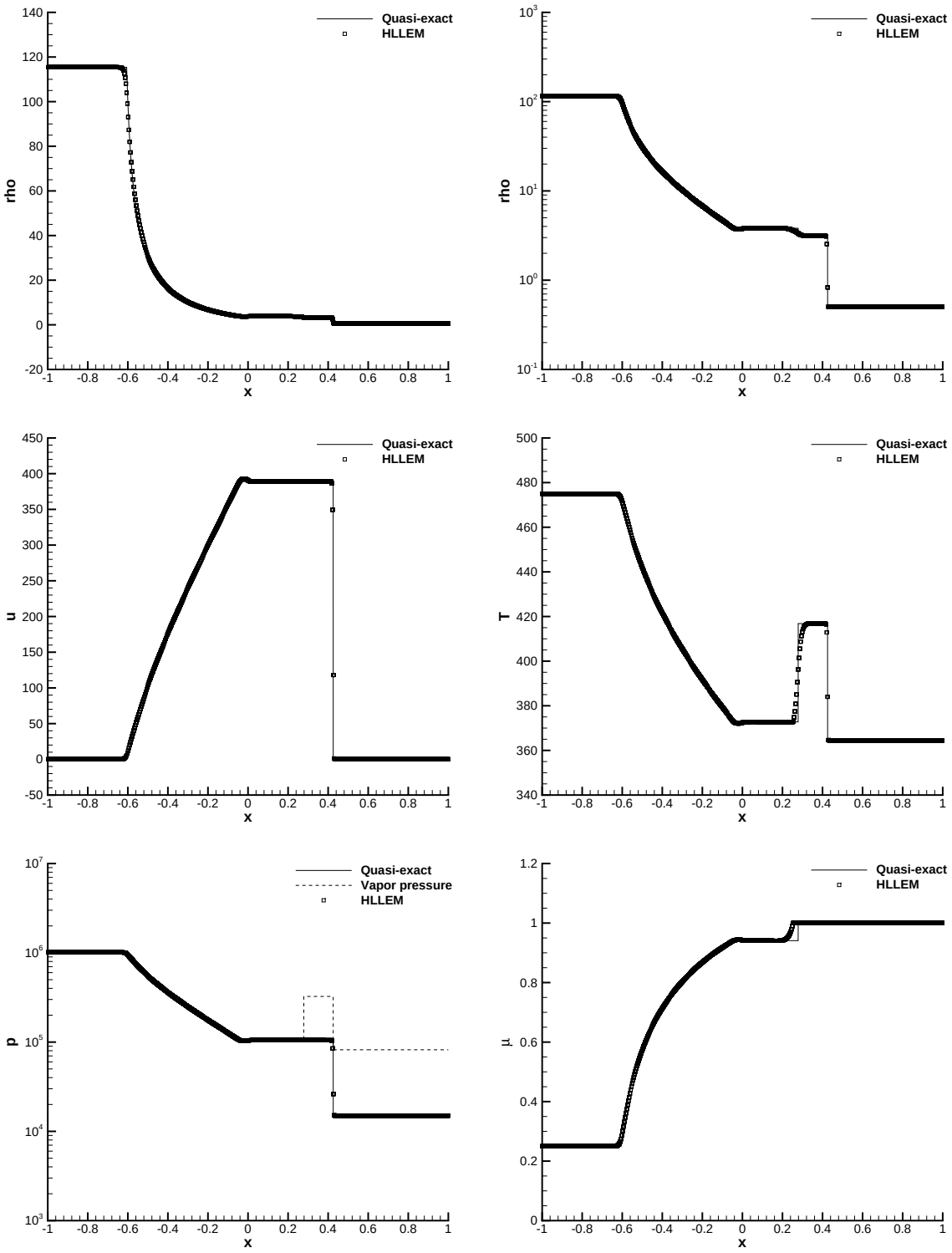

Figure 21: Quasi–exact solution and second order results obtained with the new formulation of the HLLEM Riemann solver on 500 grid points at time $t = 2.0 \cdot 10^{-3}$ for density, velocity, temperature, pressure and vapour volume fraction of the Riemann problem RP-H6 for n–heptane.

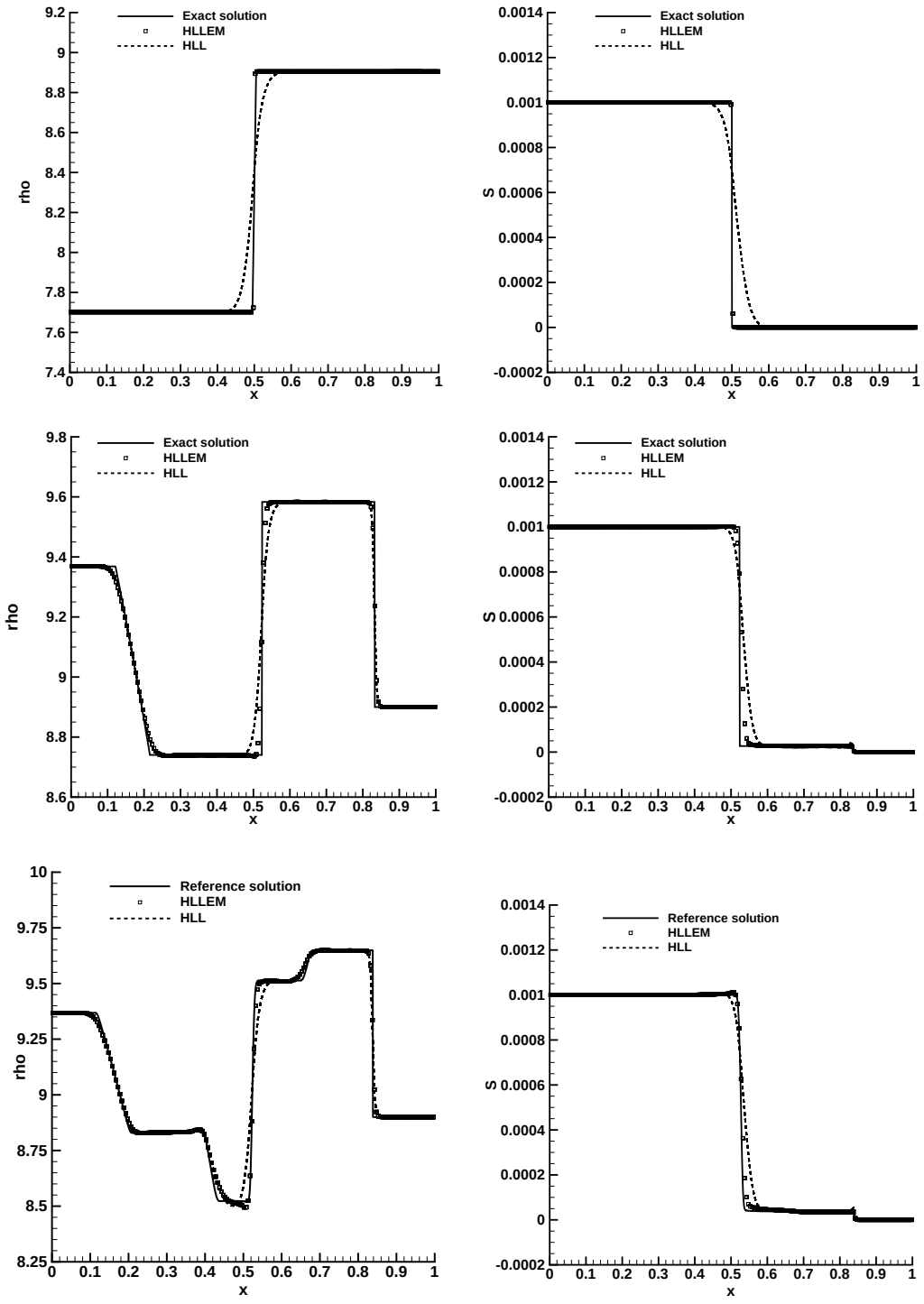

Figure 22: Numerical solution obtained with the HLLEM solver applied to the equations of nonlinear hyper-elasticity for Riemann problems RP0–RP2 (top to bottom). RP0 is a stationary contact wave, RP1 contains only three waves and RP2 contains five different waves.

Table 9: Initial states left (L) and right (R) for the Riemann problems for the nonlinear hyperelasticity model of Godunov and Romenski [52] and final output times t_e.

Case	u	v	F_{11}	F_{12}	F_{21}	F_{22}	S	t_e
RP0 L:	0.0	0.0	1.156276	0.034688	0.093191	1.002196	0.001	0.2
RP0 R:	0.0	0.0	1.0	0.03	0.02	1.0	0.0	
RP1 L:	0.0	0.0	0.95	0.0	0.0	1.0	0.001	0.06
RP1 R:	0.0	0.0	1.0	0.0	0.0	1.0	0.0	
RP2 L:	0.0	1.0	0.95	0.0	0.05	1.0	0.001	0.06
RP2 R:	0.0	0.0	1.0	0.0	0.0	1.0	0.0	

with the vector of conserved quantities

$$\mathbf{Q} = \begin{pmatrix} D \\ \mathbf{M} \\ E \\ \mathbf{B} \\ \psi \end{pmatrix} = \begin{pmatrix} \gamma\rho \\ \gamma w_{\text{tot}}\mathbf{v} - b^0\mathbf{b} \\ \gamma^2 w_{\text{tot}} - b^0 b^0 - p_{\text{tot}} \\ \mathbf{B} \\ \psi \end{pmatrix}, \tag{77}$$

and the flux tensor

$$\mathbf{F}(\mathbf{Q}) = \begin{pmatrix} \gamma\rho\mathbf{v}, \\ \gamma^2 w_{\text{tot}}\mathbf{v}\mathbf{v} - \mathbf{v}\mathbf{b} + p_{\text{tot}}\mathbf{I}, \\ \gamma^2 w_{\text{tot}}\mathbf{v} - b^0\mathbf{b} \\ \mathbf{v}\mathbf{B} - \mathbf{B}\mathbf{v} + \psi\mathbf{I} \\ c_h^2\mathbf{B} \end{pmatrix}. \tag{78}$$

The equation of state is

$$e = \rho + \frac{p}{\Gamma - 1}, \tag{79}$$

the Lorentz factor, denoted as γ in this section, is defined by

$$\gamma = \frac{1}{\sqrt{1 - \vec{v}^2}}, \tag{80}$$

further quantities appearing in (77) and (78) are given by

$$b^0 = \gamma\mathbf{v}\cdot\mathbf{B}, \quad \mathbf{b} = \frac{\mathbf{B}}{\gamma} + \gamma\mathbf{v}, \quad |b|^2 = \frac{\mathbf{B}^2}{\gamma^2} + (v_k B_k)^2, \tag{81}$$

from which total enthalpy and total pressure are defined as

$$w_{\text{tot}} = e + p + |b|^2, \qquad p_{\text{tot}} = p + \frac{1}{2}|b|^2. \tag{82}$$

Here, the speed of light is set to unity. The computation of the primitive variables ρ, $\mathbf{v}$ and p from the vector $\mathbf{Q}$ of conserved quantities is very complicated. It can not be done analytically but requires necessarily the use of iterative techniques. A very robust and efficient conservative to primitive variable transformation that uses the exact roots of a third degree polynomial in combination with the solution of a single nonlinear scalar equation is given in [95]. The exact solution of the Riemann problem has been published in [50, 73] and the eigenstructure has been made available in [7] and [4]. This allows us immediately to apply our new HLLEM Riemann solver (30) even to the RMHD system

Table 10: Initial states left (L) and right (R) for the RMHD shock tube problems and final times t_e.

Case	ρ	p	u	v	w	B_y	B_z	B_x	t_e
1L	1.0	1.0	0.0	0.0	0.0	1.0	0.0	0.5	0.4
1R	0.125	0.1	0.0	0.0	0.0	-1.0	0.0	0.5	
2L	1.0	30.0	0.0	0.0	0.0	6.0	6.0	5.0	0.4
2R	1.0	1.0	0.0	0.0	0.0	0.7	0.7	5.0	
3L	1.0	1000.0	0.0	0.0	0.0	7.0	7.0	10.0	0.4
3R	1.0	0.1	0.0	0.0	0.0	0.7	0.7	10.0	
4L	1.0	0.1	0.999	0.0	0.0	7.0	7.0	10.0	0.4
4R.	1.0	0.1	-0.999	0.0	0.0	-7.0	-7.0	10.0	
5L	1.08	0.95	0.4	0.3	0.2	0.3	0.3	2.0	0.55
5R	1.0	1.0	-0.45	-0.2	0.2	-0.7	0.5	2.0	

(76) – (78). Like for the classical MHD case, we include *all* intermediate waves (also the slow magnetosonic waves), making thus the HLLEM Riemann solver *a complete* Riemann solver. We emphasize that the construction of the present HLLEM solver (30) is *simple* and *automatic*, even for such complex hyperbolic PDE systems like the RMHD equations, while the design of HLLC and HLLD Riemann solvers needs to be done case by case for each system again.

The computational domain is chosen as $\Omega = [0; 1]$ and the initial condition consists of two piecewise constant states, separated by a discontinuity located at $x = 0.5$. The initial data are summarized in Table 10. In all test cases we use $\Gamma = 5/3$, except for the first test case, where $\Gamma = 2$, see [7]. For all test problems, reconstruction is performed in *primitive* variables and *not* componentwise in conservative variables. The numerical results obtained with our new HLLEM Riemann solver are shown in Figs. 23 - 27. We use 400 elements in all test cases, except for RP3, where 800 elements have been used. The CFL number is set to CFL = 0.9 in all problems, except for RP3 and RP4, where we use CFL = 0.5. For all Riemann problems we note a good agreement between the numerical solution obtained with the new HLLEM flux and the exact reference solution.

4. Conclusions

This is the first time that the one-dimensional HLLEM Riemann solver has been extended to non-conservative hyperbolic systems and to *general* nonlinear hyperbolic systems of conservation laws. The proposed approach is surprisingly *simple* and *universal*. In the original papers of Einfeldt [46] and Einfeldt, Munz et al. [47] the HLLEM method has been developed for the Euler equations of compressible gas dynamics and the scaling factor δ has been derived only for this very particular system. In the present paper we have extended the HLLEM method to general nonlinear hyperbolic PDE and where an *arbitrary* number of intermediate characteristic fields can be included. This is achieved by a generalization of the scaling factor δ to the scaling matrix $\boldsymbol{\delta}_*$, for which a simple and general expression has been derived. Since our new formulation of the HLLEM scheme can in principle accommodate as many intermediate characteristic fields as one wishes, the method could be alternatively named **HLLI** Riemann solver, where 'I' stands for the intermediate characteristic fields that can be accounted for.

This new Riemann solver inherits many of the good positivity properties that are built into the HLL Riemann solver. Entropy enforcement at rarefaction fans is built-in by design. Inclusion of the intermediate waves ensures that slowly-moving linearly degenerate inner characteristic fields are well-preserved. This can usually be done with very little additional cost. Furthermore, retention of the intermediate waves ensures that a well-balanced scheme can be obtained in the case of shallow-water-type systems. Most importantly, by using similarity variables, the Riemann solver can be derived in a straightforward manner. The range of test problems in this paper includes compressible gas dynamics with ideal and real equation of state, multiphase flow, shallow water-type equations, magnetohydrodynamics (MHD & RMHD) and nonlinear elasticity. Given the range of problems that can be handled by the new HLLEM RS, it

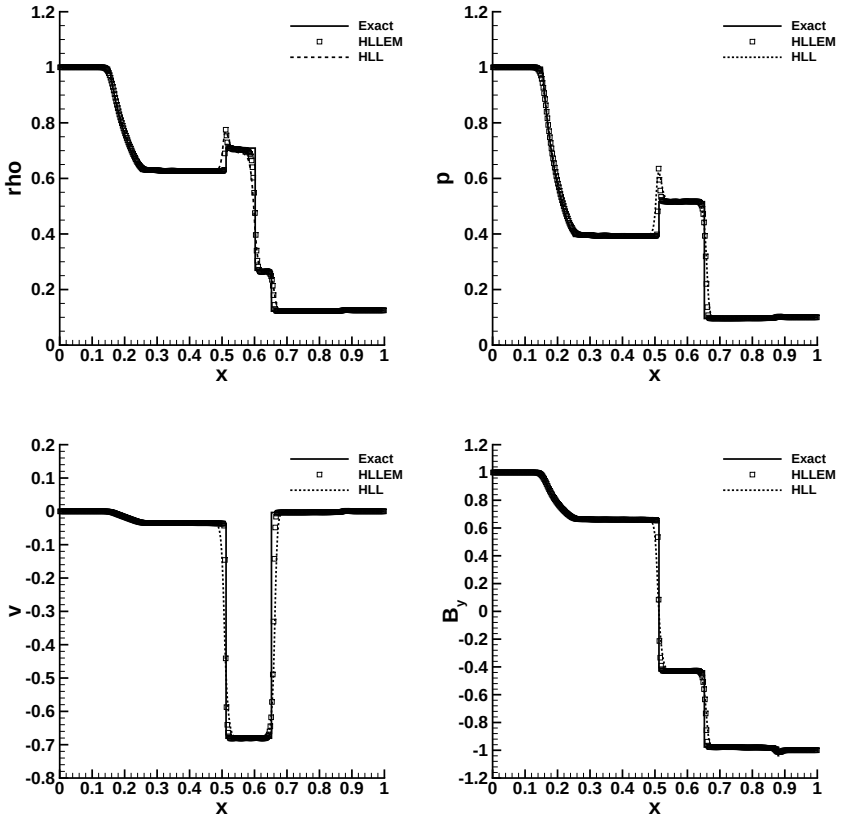

Figure 23: Numerical results obtained with the new HLLEM RS for the RMHD Riemann problem 1 at $t = 0.4$ using 400 elements.

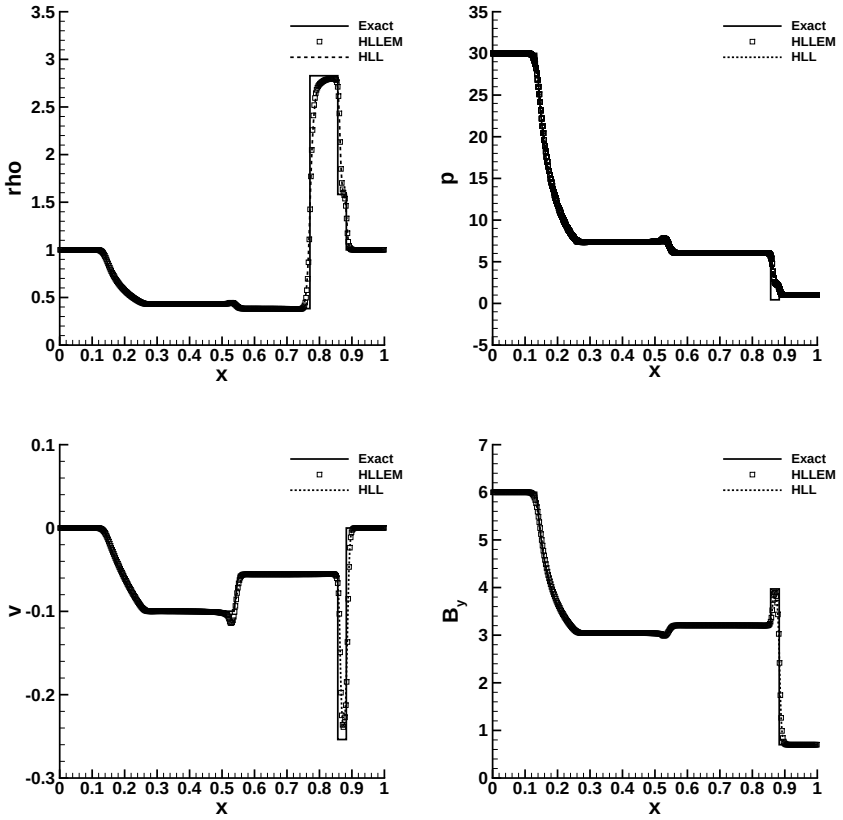

Figure 24: Numerical results obtained with the new HLLEM RS for the RMHD Riemann problem 2 at $t = 0.4$ using 400 elements.

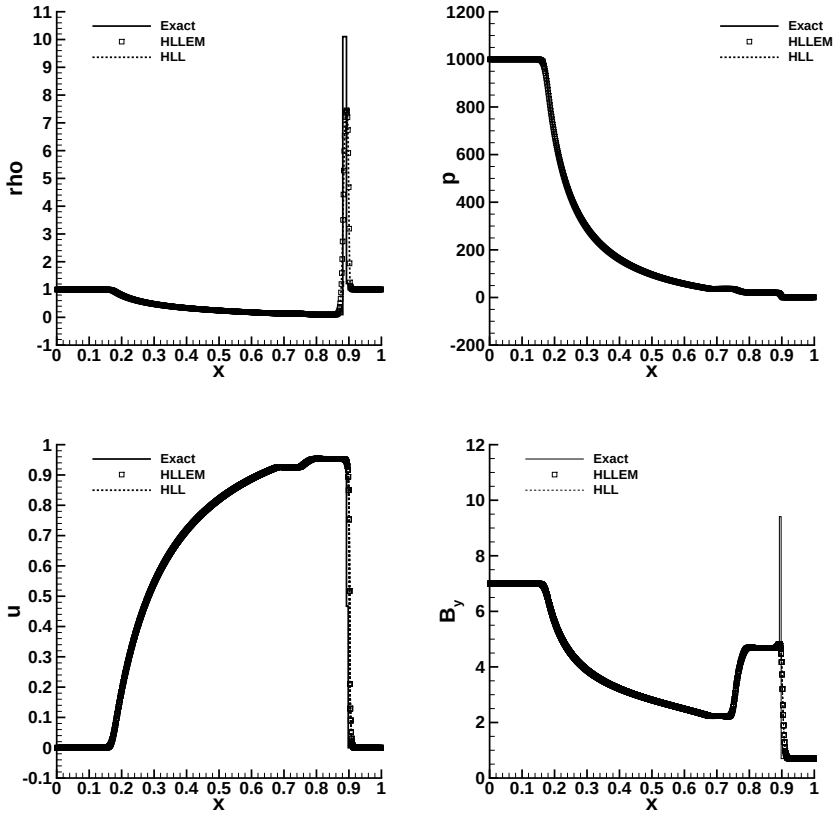

Figure 25: Numerical results obtained with the new HLLEM RS for the RMHD Riemann problem 3 at $t = 0.4$ using 800 elements.

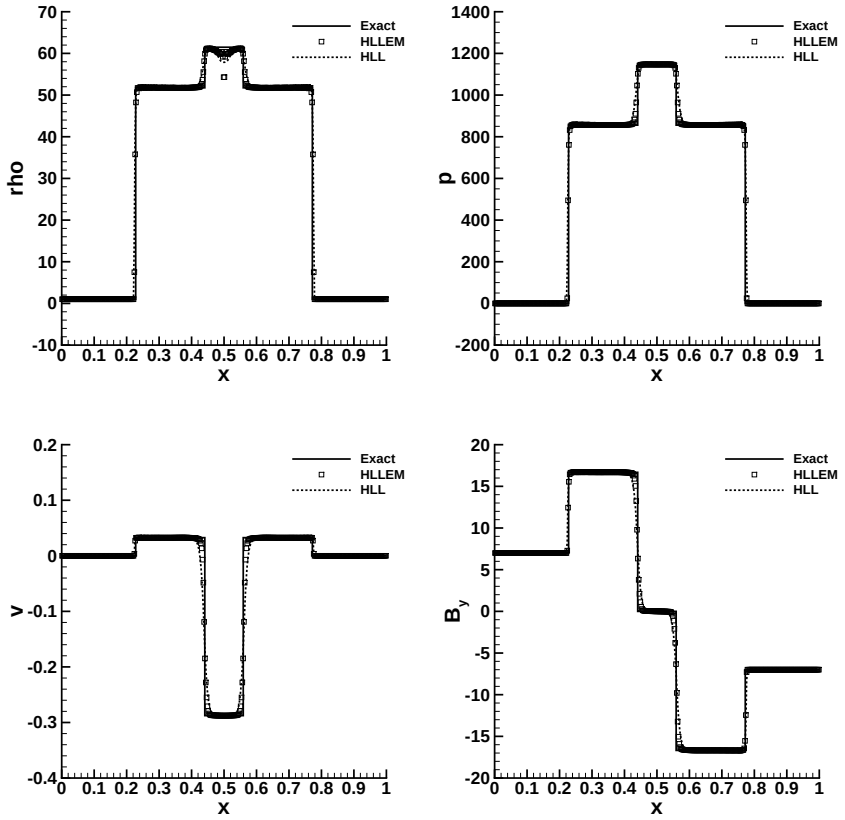

Figure 26: Numerical results obtained with the new HLLEM RS for the RMHD Riemann problem 4 at $t = 0.4$ using 400 elements.

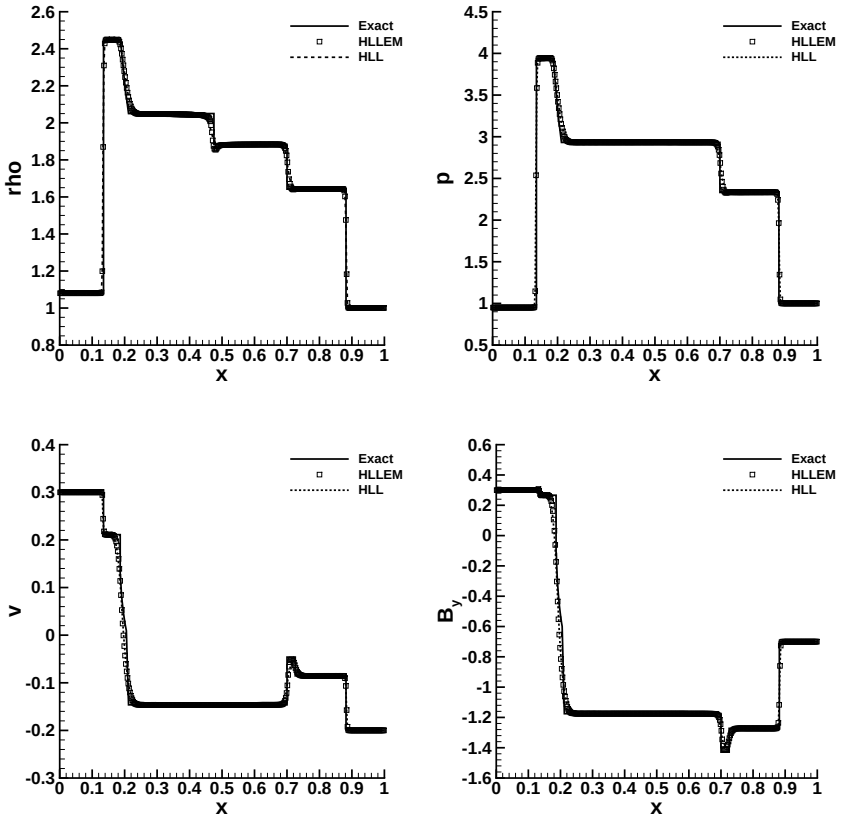

Figure 27: Numerical results obtained with the new HLLEM RS for the RMHD Riemann problem 5 at $t = 0.55$ using 400 elements.

is shown to be a versatile performer and a very valuable, accurate but low-cost addition to the computational scientist's toolkit.

The present HLLEM RS has a computational complexity that is closer to the HLL RS, while offering performance that is closer to that of a complete RS, like the Roe-type or Osher-type Riemann solvers. Like the DOT RS of Dumbser and Toro [44, 45], it can even operate in situations where the Roe matrices are not analytically available. While the DOT RS requires the evaluation of the full eigenstructure of the characteristic matrix along multiple points on the path that connects the left and right states, the HLLEM RS bypasses this very expensive step, since only one evaluation of intermediate eigenvalues and eigenvectors is required. The intermediate eigenvectors are usually very easy and inexpensive to construct. The present HLLEM RS, therefore, outperforms the DOT RS by a wide margin while retaining the full versatility of DOT and providing similar solution quality. Two further interesting observations should be made. First, notice that the HLLEM RS is also amenable to a high order quadrature-free formulation in ADER-WENO finite volume schemes (Dumbser et al. [43]) if the signal speeds and the viscosity matrix are frozen for each element interface. Second, Morales de Luna et al. [32] have recently presented a formulation for analyzing the viscosity of any Riemann solver in terms of a polynomial expansion. Given the practical thrust of this paper, we do not carry out a PVM analysis of the HLLEM RS, but we do point out that such a study is worthwhile. The self-similar formulation developed in Balsara [9, 10, 11, 12], Balsara, Dumbser & Abgrall [14] and Balsara & Dumbser [13] has been shown in this paper to be an important paradigm for designing Riemann solvers. Our eventual goal is also to use the one-dimensional HLLEM RS as a building block for multidimensional Riemann solvers of the HLL and HLLEM type for non-conservative hyperbolic systems. Please notice, therefore, that our somewhat detailed description of the inclusion of substructure in the one-dimensional Riemann solver is also intended to give us some clues about the inclusion of corresponding multidimensional sub-structure in the multidimensional Riemann solver. This will be developed in a subsequent paper.

Acknowledgments

MD has been financed by the European Research Council (ERC) under the European Union's Seventh Framework Programme (FP7/2007-2013) with the research project *STiMulUs*, ERC Grant agreement no. 278267.

DSB acknowledges support via NSF grants NSF-AST-1009091 , NSF-ACI-1307369 and NSF-DMS-1361197. DSB also acknowledges support via NASA grants from the Fermi program as well as NASA-NNX 12A088G.

The authors would like to cordially thank the two anonymous referees for their helpful comments and for the suggestion of valuable additional test cases, which helped to improve the quality of this paper.

[1] R. Abgrall. How to prevent pressure oscillations in multicomponent flow calculations: A quasi conservative approach. *Journal of Computational Physics*, 125:150–160, 1996.

[2] R. Abgrall and S. Karni. A comment on the computation of non-conservative products. *Journal of Computational Physics*, 229:2759–2763, 2010.

[3] N. Andrianov and G. Warnecke. The Riemann problem for the Baer-Nunziato two-phase flow model. *Journal of Computational Physics*, 212:434–464, 2004.

[4] L. Antón, J. A. Miralles, J. M. Martí, J. M. Ibáñez, M. A. Aloy, and P. Mimica. Relativistic magnetohydrodynamics: renormalized eigenvectors and full wave decomposition Riemann solver. *Astrophys. J. Suppl.*, 188:1–31, May 2010.

[5] H.D. Baehr and S. Kabelac. *Thermodynamik*. Springer Berlin Heidelberg, 14th edition edition, 2009.

[6] M.R. Baer and J.W. Nunziato. A two-phase mixture theory for the deflagration-to-detonation transition (DDT) in reactive granular materials. *J. Multiphase Flow*, 12:861–889, 1986.

[7] D. Balsara. Total variation diminishing scheme for relativistic magneto-hydrodynamics. *The Astrophysical Journal Supplement Series*, 132:83–101, 2001.

[8] D. S. Balsara. Self-adjusting, positivity preserving high order schemes for hydrodynamics and magnetohydrodynamics. *Journal of Computational Physics*, 231:7504–7517, September 2012.

[9] D.S. Balsara. Multidimensional HLLE Riemann solver: Application to Euler and magnetohydrodynamic flows. *Journal of Computational Physics*, 229:1970–1993, 2010.

[10] D.S. Balsara. A two-dimensional HLLC Riemann solver for conservation laws: Application to Euler and magnetohydrodynamic flows. *Journal of Computational Physics*, 231:7476–7503, 2012.

[11] D.S. Balsara. Multidimensional Riemann problem with self-similar internal structure Part I Application to hyperbolic conservation laws on structured meshes. *Journal of Computational Physics*, 277:163–200, 2014.

[12] D.S. Balsara. Three dimensional HLL Riemann solver for conservation laws on structured meshes; Application to Euler and magnetohydrodynamic flows. *Journal of Computational Physics*, 295:1–23, 2015.

[13] D.S. Balsara and M. Dumbser. Multidimensional Riemann problem with self-similar internal structure Part II Application to hyperbolic conservation laws on unstructured meshes. *Journal of Computational Physics*, 287:269–292, 2015.
[14] D.S. Balsara, M. Dumbser, and R. Abgrall. Multidimensional HLLC Riemann solver for unstructured meshes - with application to Euler and MHD flows. *Journal of Computational Physics*, 261:172–208, 2014.
[15] P.T. Barton, D. Drikakis, E. Romenski, and V.A. Titarev. Exact and approximate solutions of Riemann problems in non-linear elasticity. *Journal of Computational Physics*, 228:7046–7068, 2009.
[16] P. Batten, N. Clarke, C. Lambert, and D.M. Causon. On the choice of wavespeeds for the HLLC Riemann solver. *SIAM J. Sci. Comput.*, 18:1553–1570, 1997.
[17] A. Bermúdez and M.E. Vázquez. Upwind methods for hyperbolic conservation laws with source terms. *Computers and Fluids*, 23:1049–1071, 1994.
[18] R. Bernetti, V.A. Titarev, and E.F. Toro. Exact solution of the Riemann problem for the shallow water equations with discontinuous bottom geometry. *Journal of Computational Physics*, 227:3212–3243, 2008.
[19] S.J. Billett and E.F. Toro. On WAF-type schemes for multidimensional hyperbolic conservation laws. *Journal of Computational Physics*, 130:1–24, 1997.
[20] A. Canestrelli, A. Siviglia, M. Dumbser, and E.F. Toro. Well-balanced high-order centered schemes for non-conservative hyperbolic systems. applications to shallow water equations with fixed and mobile bed. *Advances in Water Resources*, 32:834–844, 2009.
[21] M.J. Castro and E. Fernández-Nieto. A class of computationally fast first order finite volume solvers: PVM methods. *SIAM Journal of Scientific Computing*, 34:A2173–A2196, 2012.
[22] M.J. Castro, E.D. Fernández-Nieto, T. Morales de Luna, G. Narbona-Reina, and C. Parés. A HLLC scheme for nonconservative hyperbolic problems. Application to turbidity currents with sediment transport. *ESAIM: Mathematical Modelling and Numerical Analysis*, 47:1–32, 2013.
[23] M.J. Castro, J.M. Gallardo, J.A. López, and C. Parés. Well-balanced high order extensions of Godunov's method for semilinear balance laws. *SIAM Journal of Numerical Analysis*, 46:1012–1039, 2008.
[24] M.J. Castro, J.M. Gallardo, and A. Marquina. Approximate Osher–Solomon schemes for hyperbolic systems. *Applied Mathematics and Computation*, 2015. DOI: 10.1016/j.amc.2015.06.104.
[25] M.J. Castro, J.M. Gallardo, and C. Parés. High-order finite volume schemes based on reconstruction of states for solving hyperbolic systems with nonconservative products. applications to shallow-water systems. *Mathematics of Computation*, 75:1103–1134, 2006.
[26] M.J. Castro, P.G. LeFloch, M.L. Muñoz-Ruiz, and C. Parés. Why many theories of shock waves are necessary: Convergence error in formally path-consistent schemes. *Journal of Computational Physics*, 227:8107–8129, 2008.
[27] M.J. Castro, A. Pardo, C. Parés, and E.F. Toro. On some fast well-balanced first order solvers for nonconservative systems. *Mathematics of Computation*, 79:1427–1472, 2010.
[28] A.J. Chorin. Random choice solution of hyperbolic systems. *Journal of Computational Physics*, 22:517–533, 1976.
[29] P. Colella. A direct Eulerian MUSCL scheme for gas dynamics. *SIAM J. Sci. Statist. Comput.*, 6:104–117, 1985.
[30] P. Colella and P.R. Woodward. The piecewise parabolic method (PPM) for gas-dynamical simulations. *Journal of Computational Physics*, 54(1):174–201, 1984.
[31] J.M. Correia, P.G. LeFloch, and M.D. Thanh. Hyperbolic conservation laws with Lipschitz continuous flux-functions. The Riemann problem. *Bol. Soc. Bras. Mat.*, 32:271–301, 2001.
[32] T. Morales de Luna, M.J. Castro, and C. Parés. Relation between PVM schemes and simple Riemann solvers. *Numerical Methods for Partial Differential Equations*, 30:1315–1341, 2014.
[33] A. Dedner, F. Kemm, D. Kröner, C.-D. Munz, T. Schnitzer, and M. Wesenberg. Hyperbolic divergence cleaning for the MHD equations. *Journal of Computational Physics*, 175:645–673, 2002.
[34] P. Degond, P. F. Peyrard, G. Russo, and P. Villedieu. Polynomial upwind schemes for hyperbolic systems. *C. R. Acad. Sci. Paris, Ser I*, 328:479–483, 1999.
[35] V. Deledicque and M.V. Papalexandris. An exact Riemann solver for compressible two-phase flow models containing non-conservative products. *Journal of Computational Physics*, 222:217–245, 2007.
[36] M. Dumbser, D. S. Balsara, E. F. Toro, and C.-D. Munz. A unified framework for the construction of one-step finite volume and discontinuous Galerkin schemes on unstructured meshes. *Journal of Computational Physics*, 227:8209–8253, September 2008.
[37] M. Dumbser, M. Castro, C. Parés, and E.F. Toro. ADER schemes on unstructured meshes for non-conservative hyperbolic systems: Applications to geophysical flows. *Computers and Fluids*, 38:1731–1748, 2009.
[38] M. Dumbser and V. Casulli. A conservative, weakly nonlinear semi-implicit finite volume method for the compressible Navier-Stokes equations with general equation of state. *Applied Mathematics and Computation*, 0:0, 0. in press. DOI: 10.1016/j.amc.2015.08.042.
[39] M. Dumbser and V. Casulli. A staggered semi-implicit spectral discontinuous Galerkin scheme for the shallow water equations. *Applied Mathematics and Computation*, 219:8057–8077, 2013.
[40] M. Dumbser, A. Hidalgo, M. Castro, C. Parés, and E.F. Toro. FORCE schemes on unstructured meshes II: Non–conservative hyperbolic systems. *Computer Methods in Applied Mechanics and Engineering*, 199:625–647, 2010.
[41] M. Dumbser, U. Iben, and M. Ioriatti. An efficient semi-implicit finite volume method for axially symmetric compressible flows in compliant tubes. *Applied Numerical Mathematics*, 89:24–44, 2015.
[42] M. Dumbser, U. Iben, and C.D. Munz. Efficient implementation of high order unstructured WENO schemes for cavitating flows. *Computers and Fluids*, 86:141–168, 2013.
[43] M. Dumbser, M. Käser, V.A Titarev, and E.F. Toro. Quadrature-free non-oscillatory finite volume schemes on unstructured meshes for nonlinear hyperbolic systems. *Journal of Computational Physics*, 226:204–243, 2007.
[44] M. Dumbser and E. F. Toro. A simple extension of the Osher Riemann solver to non-conservative hyperbolic systems. *Journal of Scientific Computing*, 48:70–88, 2011.
[45] M. Dumbser and E.F. Toro. On universal Osher–type schemes for general nonlinear hyperbolic conservation laws. *Communications in Computational Physics*, 10:635–671, 2011.

[46] B. Einfeldt. On Godunov-type methods for gas dynamics. *SIAM J. Numer. Anal.*, 25:294–318, 1988.
[47] B. Einfeldt, P. L. Roe, C. D. Munz, and B. Sjogreen. On Godunov-type methods near low densities. *Journal of Computational Physics*, 92:273–295, February 1991.
[48] S.A.E.G. Falle. On the inadmissibility of non-evolutionary shocks. *Journal of Plasma Physics*, 65:29–58, 2001.
[49] J.M. Gallardo, C. Parés, and M.J. Castro. On a well-balanced high-order finite volume scheme for shallow water equations with topography and dry areas. *Journal of Computational Physics*, 227:574–601, 2007.
[50] B. Giacomazzo and L. Rezzolla. The exact solution of the Riemann problem in relativistic magnetohydrodynamics. *Journal of Fluid Mechanics*, 562:223–259, 2006.
[51] S.K. Godunov. Finite difference methods for the computation of discontinuous solutions of the equations of fluid dynamics. *Mathematics of the USSR - Sbornik*, 47:271–306, 1959.
[52] S.K. Godunov and E.I. Romenski. Nonstationary equations of the nonlinear theory of elasticity in Euler coordinates. *Journal of Applied Mechanics and Technical Physics*, 13:868–885, 1972.
[53] S.K. Godunov and E.I. Romenski. Thermodynamics, conservation laws, and symmetric forms of differential equations in mechanics of continuous media. In *Computational Fluid Dynamics Review 95*, pages 19–31. John Wiley, NY, 1995.
[54] S.K. Godunov and E.I. Romenski. *Elements of Continuum Mechanics and Conservation Laws*. Kluwer Academic/ Plenum Publishers, 2003.
[55] L. Gosse. A well-balanced flux-vector splitting scheme designed for hyperbolic systems of conservation laws with source terms. *Comput. Math. Appl.*, 39:135–159, 2000.
[56] L. Gosse. A well-balanced scheme using non-conservative products designed for hyperbolic systems of conservation laws with source terms. *Math Models Methods Appl Sci*, 11:339–365, 2001.
[57] A. Harten, P.D. Lax, and B. van Leer. On upstream differencing and godunov-type schemes for hyperbolic conservation laws. *SIAM Review*, 25(1):35–61, 1983.
[58] V. Honkkila and P. Janhunen. HLLC solver for ideal relativistic MHD. *Journal of Computational Physics*, 223:643–656, 2007.
[59] E. Isaacson and B. Temple. Nonlinear resonance in systems of conservation laws. *SIAM J. Appl. Math*, 52:1260–1278, 1992.
[60] F. Kemm. On the origin of divergence errors in MHD simulations and consequences for numerical schemes. *Communications in Applied Mathematics and Computational Science*, 8(1):1–38, 2013.
[61] F. Kemm. Roe-type schemes for shallow water magnetohydrodynamics with hyperbolic divergence cleaning. *Applied Mathematics and Computation*, 2015. in press. DOI:10.1016/j.amc.2015.05.079.
[62] R. J. LeVeque. Balancing source terms and flux gradients in high-resolution godunov methods: The quasi-steady wavepropagation algorithm. *Journal of Computational Physics*, 146:346–365, 1998.
[63] G. Dal Maso, P.G. LeFloch, and F. Murat. Definition and weak stability of nonconservative products. *J. Math. Pures Appl.*, 74:483–548, 1995.
[64] A. Mignone and G. Bodo. An HLLC Riemann solver for relativistic flows - I. Hydrodynamics. *Mon. Not. R. Astron. Soc.*, 364:126–136, November 2005.
[65] A. Mignone and G. Bodo. An HLLC Riemann solver for relativistic flows - II. Magnetohydrodynamics. *Mon. Not. R. Astron. Soc.*, 368:1040–1054, May 2006.
[66] M.L. Muñoz and C. Parés. Godunov method for nonconservative hyperbolic systems. *Mathematical Modelling and Numerical Analysis*, 41:169–185, 2007.
[67] L.O. Müller, C. Parés, and E.F. Toro. Well-balanced high-order numerical schemes for one-dimensional blood flow in vessels with varying mechanical properties. *Journal of Computational Physics*, 242:53–85, 2013.
[68] S. Müller and A. Voss. The Riemann problem for the Euler equations with nonconvex and nonsmooth equation of state: Construction of wave curves. *SIAM Journal on Scientific Computing*, 28:651–681, 2006.
[69] S. Osher and F. Solomon. Upwind difference schemes for hyperbolic conservation laws. *Math. Comput.*, 38:339–374, 1982.
[70] C. Parés. Numerical methods for nonconservative hyperbolic systems: a theoretical framework. *SIAM Journal on Numerical Analysis*, 44:300–321, 2006.
[71] M. Pelanti, F. Bouchut, and A. Mangeney. A Roe-type scheme for two-phase shallow granular flows over variable topography. *Mathematical Modelling and Numerical Analysis*, 42:851–885, 2008.
[72] E.B. Pitman and L. Le. A two-fluid model for avalanche and debris flows. *Phil. Trans. R. Soc. A*, 363:1573–1601, 2005.
[73] L. Rezzolla and O. Zanotti. An improved exact Riemann solver for relativistic hydrodynamics. *Journal of Fluid Mechanics*, 449:395–411, 2001.
[74] S. Rhebergen, O. Bokhove, and J.J.W. van der Vegt. Discontinuous Galerkin finite element methods for hyperbolic nonconservative partial differential equations. *Journal of Computational Physics*, 227:1887–1922, 2008.
[75] A. Ritter. Die fortpflanzung der Wasserwellen. *Zeitschrift des Vereins deutscher Ingenieure*, 36:947–954, 1892.
[76] P.L. Roe. Approximate Riemann solvers, parameter vectors, and difference schemes. *Journal of Computational Physics*, 43:357–372, 1981.
[77] P.L. Roe and D.S. Balsara. Notes on the eigensystem of magnetohydrodynamics. *SIAM Journal on Applied Mathematics*, 56:57–67, 1996.
[78] V. V. Rusanov. Calculation of Interaction of Non–Steady Shock Waves with Obstacles. *J. Comput. Math. Phys. USSR*, 1:267–279, 1961.
[79] C. Sánchez-Linares, T. Morales de Luna, and M.J. Castro. A HLLC scheme for Ripa model. *Applied Mathematics and Computation*, 2015. DOI: 10.1016/j.amc.2015.05.137.
[80] R. Saurel and R. Abgrall. A simple method for compressible multifluid flows. *SIAM Journal on Scientific Computing*, 21:1115–1145, 1999.
[81] R. Saurel and R. Abgrall. A multiphase Godunov method for compressible multifluid and multiphase flows. *Journal of Computational Physics*, 150:425–467, 1999.
[82] R. Saurel, F. Petitpas, and R. Abgrall. Modelling phase transition in metastable liquids: application to cavitating and flashing flows. *Journal of Fluid Mechanics*, 607:313–350, 2008.
[83] D.W. Schwendeman, C.W. Wahle, and A.K. Kapila. The Riemann problem and a high-resolution Godunov method for a model of compressible two-phase flow. *Journal of Computational Physics*, 212:490–526, 2006.
[84] R. Span and W. Wagner. Equations of state for technical applications. II. Results for nonpolar fluids. *Int. J. Thermophys.*, 24:135–142, 2003.

[85] M. Tavelli and M. Dumbser. A high order semi-implicit discontinuous Galerkin method for the two dimensional shallow water equations on staggered unstructured meshes. *Applied Mathematics and Computation*, 234:623–644, 2014.
[86] V.A. Titarev, E.I. Romenski, and E.F. Toro. MUSTA-type upwind fluxes for non-linear elasticity. *International Journal for Numerical Methods in Engineering*, 73:897–926, 2008.
[87] S.A. Tokareva and E.F. Toro. HLLC–type Riemann solver for the Baer–Nunziato equations of compressible two–phase flow. *Journal of Computational Physics*, 229:3573–3604, 2010.
[88] E. F. Toro, M. Spruce, and W. Speares. Restoration of the contact surface in the HLL-Riemann solver. *Shock Waves*, 4:25–34, 1994.
[89] E.F. Toro. *Shock-Capturing Methods for Free-Surface Shallow Flows*. John Wiley & Sons, 2001.
[90] E.F. Toro. *Riemann Solvers and Numerical Methods for Fluid Dynamics*. Springer, third edition, 2009.
[91] E.F. Toro and S. J. Billet. Centered TVD schemes for hyperbolic conservation laws. *IMA Journal of Numerical Analysis*, 20:44–79, 2000.
[92] M. Torrilhon. Non-uniform convergence of finite volume schemes for Riemann problems of ideal magnetohydrodynamics. *Journal of Computational Physics*, 192:73–94, 2003.
[93] I. Toumi. A weak formulation of Roe's approximate Riemann solver. *Journal of Computational Physics*, 102:360–373, 1992.
[94] B. van Leer. Towards the ultimate conservative difference scheme. v. a second-order sequel to godunov's method. *Journal of Computational Physics*, 32(1):101 – 136, 1979.
[95] L. Del Zanna, N. Bucciantini, and P. Londrillo. An efficient shock-capturing central-type scheme for multidimensional relativistic flows II. magnetohydrodynamics. *Astronomy and Astrophysics*, 400:397–413, 2003.
[96] L. Del Zanna, O. Zanotti, N. Bucciantini, and P. Londrillo. ECHO: an Eulerian conservative high order scheme for general relativistic magnetohydrodynamics and magnetodynamics. *Astronomy and Astrophysics*, 473:11–30, 2007.

Appendix A. A fully consistent HLLEM formulation in the non-conservative case

In the HLLEM scheme (28) we have assumed that the piecewise linear variation of the wave structure has *no* influence on the resulting HLL state $\mathbf{Q}_*$. While this is always true for conservation laws, it is a simplifying assumption in the case of general non-conservative hyperbolic systems. Recall that the governing PDE in similarity variables (4) reads

$$\mathbf{Q} - \frac{\partial(\xi\mathbf{Q})}{\partial\xi} + \frac{\partial\mathbf{f}}{\partial\xi} + \mathbf{B}(\mathbf{Q})\frac{\partial\mathbf{Q}}{\partial\xi} = 0, \tag{A.1}$$

while for the HLLEM scheme we assume the following internal structure of the solution of the Riemann problem,

$$\mathbf{Q}(\xi) = \begin{cases} \mathbf{Q}_L, & \text{if} \quad \xi \le s_L, \\ \mathbf{Q}_* + \varphi\mathbf{R}_*(\bar{\mathbf{Q}})\,2\delta_*(\bar{\mathbf{Q}})\,\mathbf{L}_*(\bar{\mathbf{Q}})\frac{\mathbf{Q}_R-\mathbf{Q}_L}{s_R-s_L}\left(\xi - \frac{1}{2}(s_L+s_R)\right), & \text{if} \quad s_L < \xi < s_R, \\ \mathbf{Q}_R, & \text{if} \quad \xi \ge s_R, \end{cases} \tag{A.2}$$

with $\bar{\mathbf{Q}} = \frac{1}{2}(\mathbf{Q}_L + \mathbf{Q}_R)$. This piecewise linear structure of the Riemann problem leads to two jump discontinuities at the extremal wave speeds s_L and s_R. Taking the limits from the left and the right, respectively, we obtain:

$$\lim_{\xi\to s_L^-}\mathbf{Q}(\xi) = \mathbf{Q}_L, \qquad \lim_{\xi\to s_L^+}\mathbf{Q}(\xi) = \mathbf{Q}_L^* = \mathbf{Q}_* - \varphi\mathbf{R}_*(\bar{\mathbf{Q}})\delta_*(\bar{\mathbf{Q}})\,\mathbf{L}_*(\bar{\mathbf{Q}})\,(\mathbf{Q}_R - \mathbf{Q}_L)\,, \tag{A.3}$$

$$\lim_{\xi\to s_R^+}\mathbf{Q}(\xi) = \mathbf{Q}_R, \qquad \lim_{\xi\to s_R^-}\mathbf{Q}(\xi) = \mathbf{Q}_R^* = \mathbf{Q}_* + \varphi\mathbf{R}_*(\bar{\mathbf{Q}})\delta_*(\bar{\mathbf{Q}})\,\mathbf{L}_*(\bar{\mathbf{Q}})\,(\mathbf{Q}_R - \mathbf{Q}_L)\,, \tag{A.4}$$

with jumps between $\mathbf{Q}_L$ and $\mathbf{Q}_L^*$ at the left speed s_L and between $\mathbf{Q}_R^*$ and $\mathbf{Q}_R$ at the right speed s_R. Integrating (A.1) and using (A.2) we obtain the following fully consistent relation for the star state $\mathbf{Q}_*$ in the case of the HLLEM method for non-conservative systems:

$$\mathbf{Q}_* = \frac{1}{(s_R - s_L)}\left[(\mathbf{Q}_R s_R - \mathbf{Q}_L s_L) - (\mathbf{f}_R - \mathbf{f}_L) - \left(\tilde{\mathbf{B}}\,(\mathbf{Q}_L, \mathbf{Q}_L^*)\,(\mathbf{Q}_L^* - \mathbf{Q}_L) + \tilde{\mathbf{B}}\,(\mathbf{Q}_L^*, \mathbf{Q}_R^*)\,(\mathbf{Q}_R^* - \mathbf{Q}_L^*) + \tilde{\mathbf{B}}\,(\mathbf{Q}_R^*, \mathbf{Q}_R)\,(\mathbf{Q}_R - \mathbf{Q}_R^*)\right)\right], \tag{A.5}$$

with the states $\mathbf{Q}_L^*$ and $\mathbf{Q}_R^*$ given by (A.3) and (A.3), and the Roe matrices $\tilde{\mathbf{B}}$ given by (13). The final HLLEM fluctuations are still given by (28). Despite being fully consistent with the assumed wave structure (A.2) the relation for the intermediate HLL state $\mathbf{Q}_*$ given by (A.5) is more complex than the one given in (14). The more consistent relation (A.5) furthermore did not lead to significantly improved computational results for the PDE systems under consideration here. In particular for the Baer-Nunziato model, the use of Eqn. (A.5) leads to a significant increase in the necessary number of iterations for the quasi-Newton algorithm for the iterative solution of (A.5), and eventually also to numerical instabilities. For the shallow water systems, the more sophisticated relation (A.5) yielded very similar results compared with the simple formulation (14).

Appendix B. Derivation of the diagonal matrix δ_* in the general HLLEM method

In this section we give all the necessary details to derive the expression for matrix $\boldsymbol{\delta}_*(\bar{\mathbf{Q}})$ in the HLLEM RS (28). The present study closely follows the work of Einfeldt [46], who considered the resulting viscosity matrix of the final scheme in order to choose the scaling factor δ, which in the case of the Euler equations of gas dynamics was only a scalar. In the following, we carry out the study for the case of a conservation law, hence assuming $\mathbf{B}(\mathbf{Q}) = 0$, since we are only interested in the numerical viscosity of the resulting HLLEM scheme. For that purpose, we need to cast the HLLEM flux (30) into the canonical form

$$\mathbf{f}_{\text{HLLEM}} = \frac{1}{2}\left(\mathbf{f}_R + \mathbf{f}_L\right) - \frac{1}{2}\boldsymbol{\Theta}\left(\mathbf{Q}_R - \mathbf{Q}_L\right), \tag{B.1}$$

where $\boldsymbol{\Theta}$ is the viscosity matrix, which will then be the object of our further analysis. Starting from the numerical flux (30) without the flattener, i.e. using $\varphi = 1$, we have

$$\mathbf{f}_{\text{HLLEM}} = \frac{s_R\mathbf{f}_L - s_L\mathbf{f}_R}{s_R - s_L} + \frac{s_L s_R}{s_R - s_L}\left(\mathbf{Q}_R - \mathbf{Q}_L\right) - \frac{s_R s_L}{s_R - s_L}\mathbf{R}_*(\bar{\mathbf{Q}})\,\boldsymbol{\delta}_*(\bar{\mathbf{Q}})\,\mathbf{L}_*(\bar{\mathbf{Q}})\,\left(\mathbf{Q}_R - \mathbf{Q}_L\right). \tag{B.2}$$

The first term on the right hand side can then be rewritten as

$$\begin{aligned}\frac{s_R\mathbf{f}_L - s_L\mathbf{f}_R}{s_R - s_L} &= \frac{1}{2}\frac{s_R\mathbf{f}_L - s_L\mathbf{f}_L}{s_R - s_L} + \frac{1}{2}\frac{s_R\mathbf{f}_R - s_L\mathbf{f}_R}{s_R - s_L} + \frac{1}{2}\frac{s_L\mathbf{f}_L - s_R\mathbf{f}_R + s_R\mathbf{f}_L - s_L\mathbf{f}_R}{s_R - s_L} \\ &= \frac{1}{2}\left(\mathbf{f}_L + \mathbf{f}_R\right) - \frac{1}{2}\frac{s_R + s_L}{s_R - s_L}\left(\mathbf{f}_R - \mathbf{f}_L\right) = \frac{1}{2}\left(\mathbf{f}_L + \mathbf{f}_R\right) - \frac{1}{2}\frac{s_R + s_L}{s_R - s_L}\tilde{\mathbf{A}}(\mathbf{Q}_L, \mathbf{Q}_R)\left(\mathbf{Q}_R - \mathbf{Q}_L\right),\end{aligned} \tag{B.3}$$

where $\tilde{\mathbf{A}}(\mathbf{Q}_L, \mathbf{Q}_R) = \mathbf{A}(\tilde{\mathbf{Q}})$ is the Roe-matrix of the system (1) and $\tilde{\mathbf{Q}} = \tilde{\mathbf{Q}}(\mathbf{Q}_L, \mathbf{Q}_R)$ denotes the Roe-averaged state between the left state $\mathbf{Q}_L$ and the right state $\mathbf{Q}_R$, so that $\tilde{\mathbf{A}}(\mathbf{Q}_L, \mathbf{Q}_R)\left(\mathbf{Q}_R - \mathbf{Q}_L\right) = \mathbf{f}_R - \mathbf{f}_L$. With (B.3) the viscosity matrix $\boldsymbol{\Theta}$ of the HLLEM flux (B.2) can be written as

$$\boldsymbol{\Theta} = \frac{s_R + s_L}{s_R - s_L}\tilde{\mathbf{A}}(\mathbf{Q}_L, \mathbf{Q}_R) - 2\frac{s_R s_L}{s_R - s_L}\mathbf{I} + 2\frac{s_R s_L}{s_R - s_L}\mathbf{R}_*(\bar{\mathbf{Q}})\,\boldsymbol{\delta}_*(\bar{\mathbf{Q}})\,\mathbf{L}_*(\bar{\mathbf{Q}}). \tag{B.4}$$

According to [46] the method is stable if the diagonal matrix $\boldsymbol{\Sigma}$ of the eigenvalues of the viscosity matrix $\boldsymbol{\Theta}$ satisfies the relation

$$\boldsymbol{\Sigma} \geq \left|\boldsymbol{\Lambda}(\tilde{\mathbf{Q}})\right|, \tag{B.5}$$

where $\boldsymbol{\Lambda}(\tilde{\mathbf{Q}})$ denotes the diagonal matrix of eigenvalues of the Roe-matrix $\tilde{\mathbf{A}}$. If we choose the intermediate state of the HLLEM flux $\bar{\mathbf{Q}}$ equal to the Roe-averaged state, i.e. $\bar{\mathbf{Q}} = \tilde{\mathbf{Q}}$, then we can rewrite the part of the viscosity matrix that concerns the intermediate characteristic fields as

$$\boldsymbol{\Theta}_* = \frac{s_R + s_L}{s_R - s_L}\mathbf{R}_*(\bar{\mathbf{Q}})\,\boldsymbol{\Lambda}_*(\bar{\mathbf{Q}})\,\mathbf{L}_*(\bar{\mathbf{Q}}) - 2\frac{s_R s_L}{s_R - s_L}\mathbf{R}_*(\bar{\mathbf{Q}})\,\mathbf{I}\,\mathbf{L}_*(\bar{\mathbf{Q}}) + 2\frac{s_R s_L}{s_R - s_L}\mathbf{R}_*(\bar{\mathbf{Q}})\,\boldsymbol{\delta}_*(\bar{\mathbf{Q}})\,\mathbf{L}_*(\bar{\mathbf{Q}}). \tag{B.6}$$

From (B.6) we immediately find the following relation for the eigenvalues of $\boldsymbol{\Theta}_*$:

$$\boldsymbol{\Sigma}_* = \frac{s_R + s_L}{s_R - s_L}\boldsymbol{\Lambda}_*(\bar{\mathbf{Q}}) - 2\frac{s_R s_L}{s_R - s_L}\mathbf{I} + 2\frac{s_R s_L}{s_R - s_L}\boldsymbol{\delta}_*(\bar{\mathbf{Q}}) \geq \left|\boldsymbol{\Lambda}_*(\bar{\mathbf{Q}})\right|. \tag{B.7}$$

Thus, $\boldsymbol{\delta}_*(\bar{\mathbf{Q}})$ must satisfy the relation

$$\boldsymbol{\delta}_*(\bar{\mathbf{Q}}) \leq \mathbf{I} + \frac{1}{2}\frac{s_R - s_L}{s_R s_L}\left|\boldsymbol{\Lambda}_*(\bar{\mathbf{Q}})\right| - \frac{1}{2}\frac{s_R + s_L}{s_R s_L}\boldsymbol{\Lambda}_*(\bar{\mathbf{Q}}), \tag{B.8}$$

or, equivalently

$$\boldsymbol{\delta}_*(\bar{\mathbf{Q}}) \leq \mathbf{I} - \frac{1}{2}\frac{s_R}{s_R s_L}\left(\boldsymbol{\Lambda}_*(\bar{\mathbf{Q}}) - \left|\boldsymbol{\Lambda}_*(\bar{\mathbf{Q}})\right|\right) - \frac{1}{2}\frac{s_L}{s_R s_L}\left(\boldsymbol{\Lambda}_*(\bar{\mathbf{Q}}) + \left|\boldsymbol{\Lambda}_*(\bar{\mathbf{Q}})\right|\right). \tag{B.9}$$

With the usual abbreviation $\mathbf{\Lambda}_*^{\pm}(\bar{\mathbf{Q}}) = \frac{1}{2}\left(\mathbf{\Lambda}_*(\bar{\mathbf{Q}}) \pm \left|\mathbf{\Lambda}_*(\bar{\mathbf{Q}})\right|\right)$ we get the final relation for $\boldsymbol{\delta}_*$:

$$\boldsymbol{\delta}_*(\bar{\mathbf{Q}}) \leq \mathbf{I} - \frac{\mathbf{\Lambda}_*^-(\bar{\mathbf{Q}})}{s_L} - \frac{\mathbf{\Lambda}_*^+(\bar{\mathbf{Q}})}{s_R}. \tag{B.10}$$

The above analysis is based on the assumption that $\bar{\mathbf{Q}} = \tilde{\mathbf{Q}}$. When possible, it would be therefore be advisable to use the Roe-averaged state in order to evaluate the eigenvalues and eigenvectors of the intermediate characteristic fields in the HLLEM RS (28) and (30), as also recommended in [46, 47]. However, we also would like to justify our simplified choice $\bar{\mathbf{Q}} = \frac{1}{2}(\mathbf{Q}_L + \mathbf{Q}_R)$. Note that according to [70, 25, 40, 44, 45] the Roe matrix can also be written in terms of a path-integral along a straight line segment path $\psi(\mathbf{Q}_L, \mathbf{Q}_R, s) = \mathbf{Q}_L + s(\mathbf{Q}_R - \mathbf{Q}_L)$ as

$$\tilde{\mathbf{A}}(\mathbf{Q}_L, \mathbf{Q}_R) = \int_0^1 \mathbf{A}\left(\psi(\mathbf{Q}_L, \mathbf{Q}_R, s)\right) ds. \tag{B.11}$$

For a conservation law, the resulting matrix satisfies automatically the jump conditions $\tilde{\mathbf{A}}(\mathbf{Q}_L, \mathbf{Q}_R)(\mathbf{Q}_R - \mathbf{Q}_L) = \mathbf{f}_R - \mathbf{f}_L$. If the above path integral is now approximated by a Gaussian quadrature rule based on one single integration point (the mid-point rule), we get

$$\tilde{\mathbf{A}}(\mathbf{Q}_L, \mathbf{Q}_R) \approx \mathbf{A}\left(\bar{\mathbf{Q}}\right), \qquad \text{with} \qquad \bar{\mathbf{Q}} = \frac{1}{2}(\mathbf{Q}_L + \mathbf{Q}_R). \tag{B.12}$$

Appendix C. FORTRAN 90 sample code for the HLLEM RS

In this appendix we provide two full FORTRAN 90 sample codes of the HLLEM Riemann solver presented in this paper without flattener ($\varphi = 1$). The first one (`HLLEMNC`) implements the fluctuations (28) and applies to general conservative and non-conservative hyperbolic systems, while the second one (`HLLEMFlux`) implements eqn. (30) and provides a classical numerical flux for conservation laws in the case $\mathbf{B}(\mathbf{Q}) = 0$.

The user is supposed to provide a set of functions that compute the physical flux, the eigenvalues, the eigenstructure of the intermediate characteristic fields, the matrix $\mathbf{B}(\mathbf{Q})$ of the non-conservative product and the Roe matrix. To facilitate the reading of the codes below, these user-defined functions are highlighted in red. More precisely: the user must provide `PDEIntermediateFields`, which is a subroutine that returns for each state $\mathbf{Q}$ the diagonal matrix of the eigenvalues of the intermediate characteristic fields $\mathbf{\Lambda}_*$, and the associated right and left eigenvector matrices $\mathbf{R}_*$ and $\mathbf{L}_*$, respectively. Actually, this subroutine is the *key element* for the HLLEM scheme presented in this paper. If any of the matrices $\mathbf{R}_*$, $\mathbf{\Lambda}_*$ or $\mathbf{L}_*$ cannot be computed (production of not-a-number values due to division by zero or due to square roots of negative numbers etc.), the final result is simply set to $\mathbf{R}_* = \mathbf{\Lambda}_* = \mathbf{L}_* = 0$, hence reverting the HLLEM method back to the more robust HLL scheme in that case. The subroutine `PDEEigenvalues` must return for each state $\mathbf{Q}$ a vector of *all* eigenvalues of the PDE system (1). If the eigenvalues are not known analytically, this subroutine should at least return an *estimate* for the speeds of the two extremal left- and right-moving waves. The physical flux needs to be provided in a subroutine called `PDEFlux`. In the computation of $\boldsymbol{\delta}_*$ we add two tiny numbers in the denominators to avoid division by zero. Finally, the Roe matrix $\tilde{\mathbf{B}}(\mathbf{Q}_a, \mathbf{Q}_b)$ between two generic states $\mathbf{Q}_a$ and $\mathbf{Q}_b$ is computed exactly, or numerically via Gaussian quadrature, by a subroutine called `RoeMatrix`. A simple example algorithm for such a numerical computation of the Roe matrix is given below, where the matrix $\mathbf{B}(\mathbf{Q})$ is supposed to be provided by the user in a subroutine `PDEMatrixB`.

```
SUBROUTINE RoeMatrix(BRoe,Qa,Qb,nVar)
  IMPLICIT NONE
  INTEGER, PARAMETER :: nGP = 3      ! nGP = number of Gauss-Legendre points
  INTEGER  :: nVar, i                ! nVar = number of variables in the PDE
  REAL     :: BRoe(nVar,nVar),Qa(nVar),Qb(nVar)
  REAL     :: sGP(nGP), wGP(nGP)
  REAL     :: B(nVar,nVar), Q(nVar)
  INTENT(OUT)   :: BRoe
  INTENT(IN)    :: Qa,Qb,nVar
  ! Definition of the Gauss-Legendre quadrature rule using 3 quadrature points
  sGP = (/ 0.5-sqrt(15.)/10., 0.5, 0.5+sqrt(15.)/10.  /)
  wGP = (/ 5./18., 8./18., 5./18.  /)
  BRoe = 0.                                  ! Initialize Roe matrix with zero
  DO i = 1, nGP
    Q = Qa + sGP(i)*(Qb-Qa)                        ! Straight-line segment path
    CALL PDEMatrixB(B,Q)                              ! Evaluate matrix B(Q)
    BRoe = BRoe + wGP(i)*B ! Compute the path integral using numerical quadrature
  ENDDO
END SUBROUTINE RoeMatrix
```

```
SUBROUTINE HLLEMNC(Dm,Dp,QL,QR,nVar,nLin)
  IMPLICIT NONE
  ! Argument list declaration
  INTEGER :: nVar, nLin            ! number of variables n_q and intermediate fields n_i
  REAL    :: Dm(nVar),Dp(nVar),QL(nVar),QR(nVar)
  ! Local variable declaration
  INTEGER :: i, iHLL, MaxIter = 25 ! MaxIter=0 for classical path-conservative scheme
  REAL    :: fL(nVar), fR(nVar), QM(nVar), LL(nVar), LR(nVar), LM(nVar), AD(nVar)
  REAL    :: PathInt(nVar), QHLL(nVar), QOld(nVar), BRoe1(nVar,nVar), BRoe2(nVar,nVar)
  REAL    :: RS(nVar,nLin), LS(nLin,nVar), Lambda(nLin,nLin), Id(nLin,nLin), sL, sR
  REAL    :: Delta(nLin,nLin), Lap(nLin,nLin), Lam(nLin,nLin), tol = 1e-12, res
  INTENT(OUT)  :: Dm,Dp
  INTENT(IN)   :: QL,QR,nVar,nLin
  Id = 0; FORALL(i = 1:nLin) Id(i,i) = 1.0          ! Define the identity matrix I
  QM = 0.5*(QL+QR)                                  ! Compute the intermediate state Q̄
  CALL PDEEigenvalues(LM,QM)                        ! Compute the eigenvalues in Q̄
  CALL PDEEigenvalues(LL,QL)                        ! Compute the eigenvalues in Q̄_L
  CALL PDEEigenvalues(LR,QR)                        ! Compute the eigenvalues in Q̄_R
  sL = MIN(0.0, MINVAL(LM), MINVAL(LL) )            ! Compute the left signal speed s_L
  sR = MAX(0.0, MAXVAL(LM), MAXVAL(LR) )            ! Compute the right signal speed s_R
  CALL PDEFlux(fL,QL)                               ! Compute the flux in the left state
  CALL PDEFlux(fR,QR)                               ! Compute the flux in the right state
  CALL RoeMatrix(BRoe1,QL,QR)          ! Compute the Roe matrix (exactly or numerically)
  PathInt = MATMUL(BRoe1,QR-QL) + fR - fL     ! Compute the path integral from QL to QR
  QHLL = ( QR*sR - QL*sL - PathInt ) / (sR-sL)      ! Compute the initial guess for Q_*
  ! Simple Picard-type iteration to compute the HLL state Q_*
  DO iHLL = 1, MaxIter
    QOld = QHLL                                     ! Save the old HLL state
    CALL RoeMatrix(BRoe1,QL,QHLL)          ! Compute the Roe matrix between Q_L and Q_*
    CALL RoeMatrix(BRoe2,QHLL,QR)          ! Compute the Roe matrix between Q_* and Q_R
    PathInt = MATMUL(BRoe1,QHLL-QL) + MATMUL(BRoe2,QR-QHLL) + fR - fL
    QHLL = ( QR*sR - QL*sL - PathInt ) / (sR-sL) ! Update the HLL state according to (16)
    res = SQRT(SUM(QOld-QHLL)**2)                   ! Compute the residual
    IF(res.LT.tol) EXIT                ! Exit the loop if a tolerance has been reached
  ENDDO
  CALL PDEIntermediateFields(Lambda,RS,LS,QM)       ! Compute Λ_*, R_* and L_*
  Lap = 0.5*( Lambda + ABS(Lambda) ); Lam = 0.5*( Lambda - ABS(Lambda) )  ! Compute Λ_*^±
  Delta = Id - Lam/(sL-1e-14) - Lap/(sR+1e-14)                            ! Compute δ_*
  ! Compute the HLL fluctuations and the final HLLEM fluctuations
  Dm = -sL/(sR-sL)*PathInt + sL*sR/(sR-sL)*(QR-QL)  ! Left-moving HLL fluctuation
  Dp = +sR/(sR-sL)*PathInt - sL*sR/(sR-sL)*(QR-QL)  ! Right-moving HLL fluctuation
  ! Compute the anti-diffusive term of the HLLEM RS
  AD = sR*sL/(sR-sL)*MATMUL( RS, MATMUL(Delta,MATMUL(LS,QR-QL)) )
  Dm = Dm - AD                                      ! Left-moving HLLEM fluctuation
  Dp = Dp + AD                                      ! Right-moving HLLEM fluctuation
END SUBROUTINE HLLEMNC
```

```
SUBROUTINE HLLEMFlux(flux,QL,QR,nVar,nLin)
  IMPLICIT NONE
  ! Argument list declaration
  INTEGER :: nVar, nLin           ! number of variables n_q and intermediate fields n_i
  REAL    :: flux(nVar),QL(nVar),QR(nVar)
  ! Local variable declaration
  INTEGER :: i
  REAL    :: fL(nVar), fR(nVar), QM(nVar), LL(nVar), LR(nVar), LM(nVar), AD(nVar)
  REAL    :: QHLL(nVar)
  REAL    :: RS(nVar,nLin), LS(nLin,nVar), Lambda(nLin,nLin), Id(nLin,nLin), sL, sR
  REAL    :: Delta(nLin,nLin), Lap(nLin,nLin), Lam(nLin,nLin)
  INTENT(OUT)  :: flux
  INTENT(IN)   :: QL,QR,nVar,nLin
  Id = 0; FORALL(i = 1:nLin) Id(i,i) = 1.0          ! Define the identity matrix I
  QM = 0.5*(QL+QR)                                  ! Compute the intermediate state Q̄
  CALL PDEEigenvalues(LM,QM)                        ! Compute the eigenvalues in Q̄
  CALL PDEEigenvalues(LL,QL)                        ! Compute the eigenvalues in Q̄_L
  CALL PDEEigenvalues(LR,QR)                        ! Compute the eigenvalues in Q̄_R
  sL = MIN(0.0, MINVAL(LM), MINVAL(LL) )            ! Compute the left signal speed s_L
  sR = MAX(0.0, MAXVAL(LM), MAXVAL(LR) )            ! Compute the right signal speed s_R
  CALL PDEFlux(fL,QL)                               ! Compute the flux in the left state
  CALL PDEFlux(fR,QR)                               ! Compute the flux in the right state
  QHLL = ( QR*sR - QL*sL - (fR-fL) ) / (sR-sL)      ! Compute the HLL state Q_*
  CALL PDEIntermediateFields(Lambda,RS,LS,QM)       ! Compute Λ_*, R_* and L_*
  Lap = 0.5*( Lambda + ABS(Lambda) ); Lam = 0.5*( Lambda - ABS(Lambda) ) ! Compute Λ_*^±
  Delta = Id - Lam/(sL-1e-14) - Lap/(sR+1e-14)      ! Compute δ_*
  ! Compute the HLL flux and the final HLLEM flux
  flux = (sR*fL - sL*fR)/(sR-sL) + sL*sR/(sR-sL)*(QR-QL)   ! HLL flux
  ! Compute the anti-diffusive term of the HLLEM RS
  AD = sR*sL/(sR-sL)*MATMUL( RS, MATMUL(Delta,MATMUL(LS,QR-QL)) )
  flux = flux - AD                                  ! HLLEM flux
END SUBROUTINE HLLEMFlux
```